TÉCNICO LISBOA

Development and Control of a condensation system using Peltier Cells

António Manuel Rainha Pereira Maciel

Thesis to obtain the Master of Science Degree in

Electrical and Computer Engineering

Supervisor: Professor Leonel Augusto Pires Seabra de Sousa

Co-Supervisor: Ph.D. Ana Sofia Oliveira Henriques Moita

Examination Committee

Chairperson: Professor Nuno Cavaco Gomes Horta

Supervisor: Professor Leonel Augusto Pires Seabra de Sousa

Member of Committee: Professor Bertinho Manuel D'Andrade da Costa

April 2014

Acknowledgements

Foremost, I would like to express my sincere gratitude to my external co-supervisor Engenheiro Emanuele Teodori for his patience, motivation, enthusiasm and support. I would like to thank him for the enthusiasm when he approached me with the subject for this Master Thesis.

I would like to thank my co-supervisor Ph.D. Ana Moita, for believing in me, for all the guidance and motivation when all seemed lost. I would like to add, it was an honour to work in such a professional environment, with immense knowledge. Thank you for this opportunity.

I would like to thank my supervisor Professor Leonel Sousa, for believing in me and for accepting a Master Thesis that it was not in his area. His guidance helped me overcome the numerous complications that arose during this work. Thank you for believing in me.

A huge appreciation to all the people that gave me several counselling when complications arose: Professor Maria Beatriz Borges, Professor Paulo Branco, Professor Moises Piedade, Professor Horácio Neto, Professor António Moreira. I would like to also thank my colleagues Vânia Silvério, João Cunha, Eduard Kulchinsky and Eduardo Francisco for all the counselling given.

On a more personal quote, my experience as a student would not be the same without all my closest friends, dear places like “Casa do Povo” and “Italiana”, where many unforgettable moments happened. Thank you all.

To my family, I would like to express my gratitude for their unconditional love, support and encouragement. I would like to thank them for the values and commitment that have incepted in me. Love you all.

To finalize, the person that was always present and available for me, Sofia Trindade, who always supported and encouraged me when I thought my Master Thesis would never be finished. Thank you for sharing who you are with me.

Abstract

This work proposes the development and control of a condensation system using Peltier cells. The condensation system is used to study the feasibility of direct immersion cooling of a CPU with liquid pool boiling. The design of an efficient controller requires a good understanding of the working principles of the Peltier cells. So, a secondary objective is to characterize the Peltier cells under real working conditions, namely their internal properties and its dynamic response. This is expected to be useful to provide alternative methods and guiding values to characterize the internal properties of the cells in works focused on the application and not on the fundamental research, as these methodologies are still sparsely reported in the literature. Such characterization of the system is important for a closed-loop control and is vital to an open-loop control, so it is an important task to accomplish. A PID controller was designed to control the amount of cooling the Peltier cells provide. From the experimental procedures followed, results show that the internal properties of Peltier cells are within the range described in the literature and present the same behaviour. The study of their dynamic response allowed gaining sensibility of the limiting values and how the system responded. The PID controller showed very good results that were within the requirements previously proposed. A final test of 72 hours under 100% of CPU Load was made to study the feasibility of pool boiling cooling together with the condensation system. The results obtained show that the setup designed here, despite being a preliminary configuration is indeed feasible.

Keywords

Peltier cell, PID Controller, Direct Immersion Cooling with liquid pool boiling, CPU, Arduino, Condensation.

Resumo

Este trabalho propõe o desenvolvimento e controlo de um sistema de condensação usando células de Peltier. O sistema de condensação é usado para estudar a viabilidade do arrefecimento de um processador por imersão directa com ebulição do liquido refrigerante. Para desenvolver um controlador eficiente é necessário ter um bom conhecimento dos princípios de funcionamento das células de Peltier. Portanto, um objectivo secundário é a caracterização das células de Peltier em condições reais, nomeadamente os seus parâmetros internos e resposta dinâmica. Com este procedimento espera obter-se algum conhecimento e valores de referência que permitam caracterizar os parâmetros internos da célula numa aplicação real e não apenas através de teoria. Esta caracterização é relevante para desenhar um controlador em malha-fechado mas é principalmente importante para desenhar um controlador em malha-aberta, portanto é uma caracterização relevante que deve ser realizada. Um controlador PID foi desenvolvido para controlar o arrefecimento que as células de Peltier produziam. Através da realização dos procedimentos experimentais, obtiveram-se resultados que mostram que os parâmetros internos estão dentro da gama descrita na literatura e que têm as mesmas dependências em relação às variáveis estudadas. Além disso, a resposta dinâmica permitiu ganhar uma maior sensibilidade de alguns valores limite característicos do sistema e da sua resposta dinâmica. Os resultados do teste do controlador PID demonstram que efectivamente este consegue seguir muito fielmente a referência imposta tendo em conta os requisitos previamente definidos. Um teste final de 72 horas com a carga máxima do processador foi feito no final do trabalho para demonstrar a viabilidade do arrefecimento por imersão directa com ebulição do líquido refrigerante, juntamente com o sistema de condensação. Os resultados mostram que de facto o sistema desenvolvido neste trabalho, embora ainda numa configuração preliminar, é uma solução viável para o arrefecimento de processadores.

Palavras-chave

Células Peltier, Controlador PID, Arrefecimento Imersão directa, Processador, Arduino, Condensação

Table of Contents

List of Figures

List of Tables

List of Acronyms

CPU	Central Processing Unit
IC	Integrated Circuit
TEC	Thermoelectric Cooler
emf	Electromotive force
MTBF	Mean time between failures
C.O.P.	Coefficient of Performance
DC	Direct Current
AC	Alternate Current
PWM	Pulse-Width Modulation
PID	Proportional Integrative Derivative
PC	Personal Computer
TDP	Thermal Design Power
DAC	Digital-to-Analog Converter
SPI	Serial Peripheral Interface

List of Symbols

$\dot{q}''\ (W/m^2\ )$	heat flux
$k\ (W/(m.K))$	thermal conductivity
$\dot{Q}$	rate of heat transfer
A	area
L	thickness
$h\ (W/m^2.K)$	Convective heat transfer coefficient
T_s	Temperature of the surface
T_{fl}	Temperature of the fluid
ΔT	Temperature Difference
R_{cond}	Conduction Thermal Resistance
R_{conv}	Convective Thermal Resistance
$R_{T_{series}}$	Series Thermal Resistance
$R_{T_{parallel}}$	Parallel Thermal Resistance
T_{CPU}	Temperature of the Central Processing Unit
$T_{saturation}$	Saturation temperature of the fluid
$T_{surface}$	Temperature of the surface
I	Current
V	Voltage
h_{fg}	Latent heat of vaporization

$\dot{m}$	Mass flow
x	Axial coordinate
y	Coordinate
δ	Thickness of the condensate layer
T_w	Temperature of the wall
T_v	Temperature of the vapour
u	Velocity distribution
μ	Dynamic viscosity
dm	Rate of condensation
dx	Differential length
N_{ux}	Nusselt number
T_h	Temperature of the hot surface of the Peltier cell
T_c	Temperature of the cold surface of the Peltier cell
ΔT	Temperature difference between hot and cold surface of the Peltier cell
$\dot{Q}_c$	Heat removed by the cold surface of the Peltier cell
s	Seebeck Coefficient
ρ	Electrical conductivity
N	Number of pairs of the thermoelectric elements
G	Area/length of the thermoelectric cell
S_m	Seebeck coefficient of the cell
R_m	Internal resistance of the cell
K_m	Thermal conductance of the cell
$\dot{Q}_h$	Heat released at the hot surface of the Peltier cell

P	Power supplied to the cell
$\dot{Q}_{c_{max}}$	Maximum heat removed from the cold surface by the Peltier cell
ΔT_{max}	Maximum temperature difference between hot and cold surface of the Peltier cell
I_{max}	Maximum current that can be supplied to the Peltier cell
$\dot{Q}_{CPU}$	Heat released by the CPU
L_{liquid}	Level of liquid contained inside the pool
K_p	Proportional term of the PID Controller
K_d	Derivative term of the PID Controller
K_i	Integrative term of the PID Controller
e	Error
t	Instantaneous time
τ	Variable of integration
ΔT_c	Variation in the temperature of the cold surface of the Peltier cell
$\dot{Q}_{imp}$	Power imposed to the Peltier cell
$\dot{Q}_{cond}$	Power removed by conduction to the fan

Chapter 1

Introduction

This chapter provides a brief overview of the work, as well as the motivation and the objectives.

1.1 Overview and Motivation

Since the birth of electronic technology, the heat flux produced by electronic devices has increased and this trend is expected to continue. In 1965, co-founder of Intel Gordon E. Moore stated that the number of components in an integrated circuit (IC) would approximately double every two years [1]. This trend, which was later known as Moore's law has been confirmed by half a century and is expected to continue until 2020 according to Kanellos [2]. Moore also posed the question "*Will it be possible to remove the heat generated by tens of thousands of components in a single silicon chip?*".

Since the end of the seventies, processors have improved their performance by 35% each year [3], while the size of integrated circuits has decreased [4]. However, this led to an increase in the power dissipated by electronic devices. This approach of reducing the size and increasing the frequency of operation, thus increasing the power dissipated has been possible until 2004. From this moment, the existing architectures were unable to dissipate to heat generated, so new architectures have been adopted to continuously increase the performance while maintain the power dissipated. These architectures mainly consisted in distributing the workload across multiple less powerful processors. Computer architectures nowadays continue to find new ways to increase performance by distributing the workload and thus distributing the heat dissipation. However, the increase of heat generated by the processors is inevitable. This trend led Hennessy and Patterson [3] to state that thermal management of electronic devices would be, in the near future, the biggest limitation in the development of new processors. Additionally, constant temperature below the junction temperature is required, which is approximately 85ºC for reliable operation and increased electronic device lifespan. Bar-Cohen et al. [5] alert for the performance degradation and reliability that this increase in heat dissipation can cause. Moreover, Tonapsi et al. [6] state that an increase by 10ºC in relation to the junction temperature is enough to reduce the device life by half, while Paik et al. [7] state that an increase by 15ºC can augment time response (interconnect delay) from 10% to 15%. In line with this, the development of new techniques to cool down electronics becomes crucial. Cader et al. [8], state that the conventional air cooled systems have trouble accompanying the heat flux generated by constant increase of clock frequency and number of transistors.

In recent years, various promising techniques for electronic cooling have been studied. In this work the feasibility of Direct Immersion Cooling in a dielectric liquid is tested, which addressed the liquid phase change. Two-phase cooling techniques, in which there is a phase change of the liquid, have much potential because they have a higher convective heat transfer coefficient than conventional computer cooling techniques (e.g. air cooling and water cooling). As the name implies, the heated surface which in this case is the Central Processing Unit (CPU) is immersed in a fluid. For this to be possible the fluid must have dielectric properties. To take full advantage of this technique, the used fluid must have a lower boiling point than the heated surface temperature. At a given temperature difference between the boiling point of the fluid and the temperature of the surface, the liquid starts to boil. As will be explained later, when boiling occurs there is a phase change in which the convective heat transfer coefficient rises exponentially allowing higher heat fluxes to be removed.

However, in these techniques the boiling liquid vaporizes very fast and will be lost if it is not properly condensed. Given the particular properties that these liquids must have, the feasibility of such cooling systems strongly depends on an efficient condensation system. This way, losses of the fluid are avoided and the system can continuously work for long periods of time.

The vapour will only condense in a stable condition for a well-defined temperature difference between the boiling point of the fluid and the temperature of the surface responsible for the condensation of the fluid. However, the CPU works in transient conditions for which the heat flux dissipated may change significantly along time. It is possible that for some periods of time the CPU may work under full load and generate its Thermal Design Power (TDP). This is usually given by the manufacturer and corresponds to the maximum heat power released by the CPU.

When the heat flux generated by the CPU changes, i.e. the pace at which the fluid evaporates, the temperature of the surface responsible for condensation must also be adjusted, to assure that the temperature difference is high enough to promote the vapour condensation. Hence, the good performance of the condensation system depends on how well it can adapt the temperature of the surfaces responsible for condensation to the different heat fluxes created by the CPU during its operating period. So, the key for a good performance of the condensation system lays in the accurate control of that temperature.

In this context the main purpose of this work is to develop a controlled condensation system using Peltier cells, which can fix the temperature of the surface responsible by the condensation of the fluid, accordingly to the power supplied to them. This adjustment is made taking into account the variations in the heat dissipation associated to different CPU loads, which occur during its functioning. Despite their relatively low efficiency, Peltier cells were chosen to be included in the condensation system as they allow precise temperature control, independently of the ambient temperature which is, as aforementioned, one of the biggest limitations of conventional cooling techniques. The condensation system is integrated in a pool boiling cooling strategy. The conceptual design for the system is represented in Figure 1.1. The CPU, identified by number 1, is immersed in a pool, identified by number 2, filled with a dielectric fluid (the fluid used here is HFE-7000, as further explained). As the temperature difference between the CPU and the boiling point of HFE-7000 (34ºC) increases, boiling starts to occur and HFE-700 evaporates. The vapour is transported due to a gradient density and it comes in contact with the ceiling of the pool, which must be at a lower temperature than the HFE-7000 saturation temperature, so it can condensate. The temperature of the ceiling of the pool is fixed by the Peltier cell, identified by number 3. The Peltier cell allows to precisely fix a temperature accordingly to the current supplied to it. On top of the system is the heatsink, identified by number 4, and the fan, identified by number 5, which are responsible for dissipating the heat flux created by the CPU and the Joule effect generated by the Peltier cell.

The Peltier cells may seem useless, given that at this stage of the work they could not be completely removed from the cooling components and actually are the fans that are being used to cool the cells. As it will be explained later, in Chapters 3 and 5, the heatsink cools the CPU by conduction and the fan cools the heatsink by forced convection of the air. So, in this context we have still the

physical limitation imposed by the temperature of the ambient air. However, when this temperature is above the saturation point of the dielectric fluid, condensation will not occur. If the pool is not sealed, the fluid is lost. If the pool is sealed, the fluid is not condensed, so the pressure inside the pool may rise up to dangerous values. In addition, the boiling point of most liquids, including HFE-7000 increases with pressure, so the temperature of the liquid will increase until values which do not assure a safe temperature for the CPU to work. In this context, the Peltier cells solve both these issues, while allowing a precise control of the temperature of the condensation surface, almost independently from the ambient temperature.

Furthermore, if the control of the Peltier cells is robust enough, it may allow the system developed here to operate in any other applications requiring cooling and a precise control of the temperatures (which does not necessarily need to include condensation).

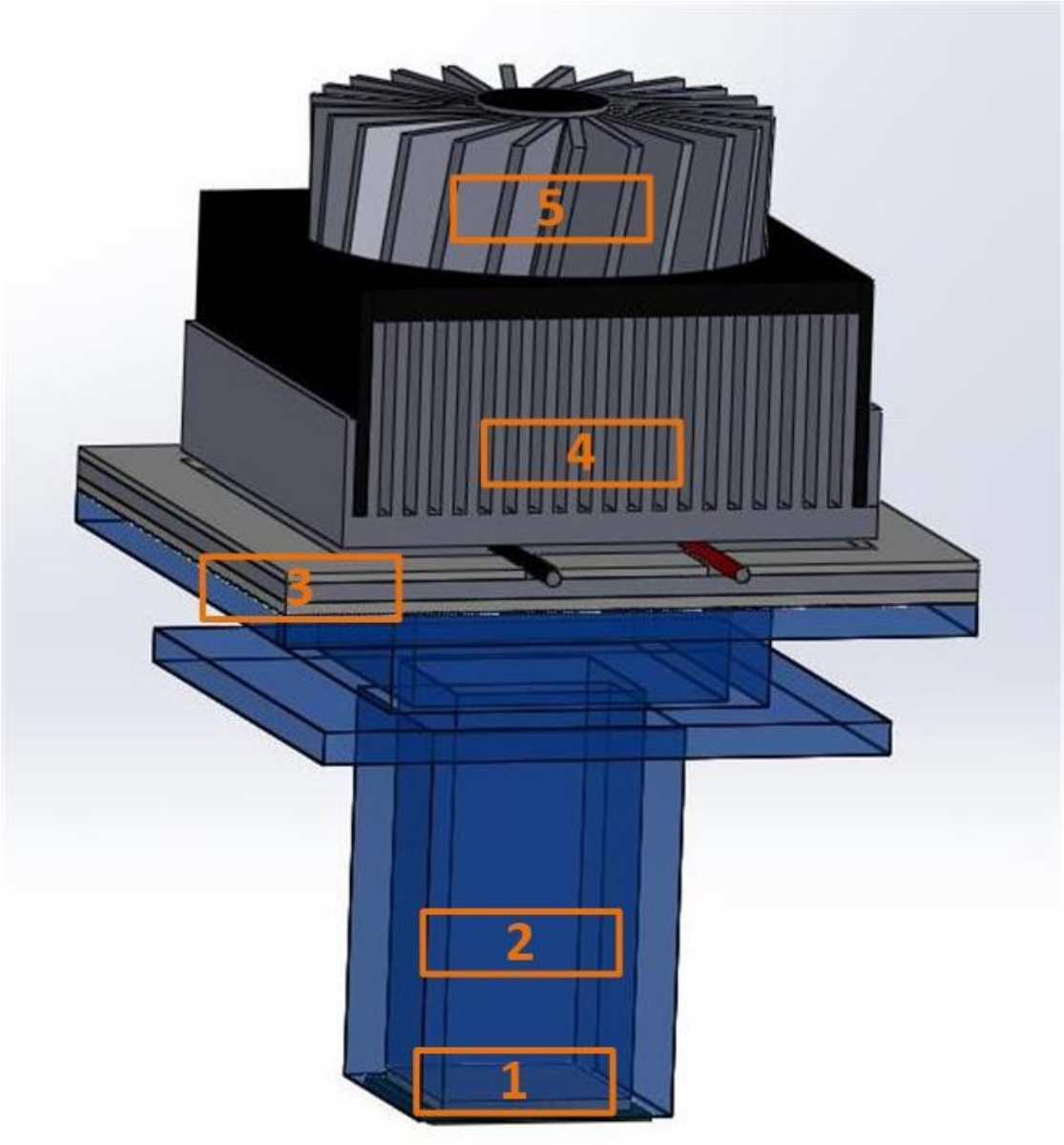

Figure 1.1 – Conceptual Design

1.2 Objectives

Following the context presented above, the objective of this work is to design a controlled condensation system using Peltier cells. This work is integrated in a project whose main objective is to study the feasibility of Direct Immersion Cooling and particularly pool boiling as a commercial cooling system. As aforementioned the system to be developed must fix the temperature of the surface responsible by the condensation of the fluid, accordingly to the power supplied to the Peltier cells. This adjustment is made taking into account the variations in the heat dissipation associated to different CPU loads.

The design of an efficient controller requires a good understanding of the working principles of the Peltier cells. So, a secondary objective is to characterize the Peltier cells under real working conditions, namely their internal properties and the dynamic response. This is expected to be useful to provide alternative methods and guiding values to characterize the internal properties of the cells in works focused on the application and not on the fundamental research, as these methodologies are still sparsely reported in the literature. Such characterization of the system is important for a closed-loop control and is vital to an open-loop operation, so it is an important task to accomplish.

Although one cannot aim at the development of a fully operational cooling system, as this is a complex task, which is out of the scope of a single Master Thesis, a preliminary configuration is proposed and tested in a real application test, which consists in the cooling of a personal computer.

1.3 Contents

The present thesis is composed of 7 chapters. Chapter 1 introduces the context and motivation for the present work and presents the objectives of this thesis. Chapter 2 provides a brief review of the literature in cooling techniques used in electronic cooling and of the work that has been performed focusing on Peltier cells. The latter includes fundamental studies on theoretical concepts, but also works concerning several applications of the Peltier cells. Chapter 3 deepens the basic heat transfer concepts which are required to understand the cooling techniques and some of the results which will be discussed later. Chapter 4 addresses the fundamental theoretical concepts governing the working principles of the Peltier cells, as well as benefits and drawbacks of using them for several purposes. Chapter 5 presents the experimental apparatus used and the experimental procedures followed as well the controller used. Chapter 6 discusses the results obtained by following the experimental procedures proposed. Finally, chapter 7 presents the conclusions that were taken from this work, as well as various suggestions for future work that can be performed to improve the designed system.

Chapter 2

State of the Art

This chapter presents a brief overview of the state-of-the-art on electronic cooling and on Peltier Cells, with and without control. In the latter case, one also shortly discuss which control systems were used.

2.1 Electronic Cooling Techniques

The need for new cooling techniques is driven by continuing increases in power dissipation of electronic parts and systems. In many instances standard techniques cannot achieve the required cooling performances due to physical limitations in heat transfer capabilities. These limitations are mostly related to the limited thermal conductivity of the fluids and of the materials used to cool the processors (air is usually used for forced convection and copper is the material made to dissipate the heat by conduction) [9]. Due to stringent cost and reliability constraints, air-cooling will remain an important thermal management approach for many electronic products in the foreseeable future [10]. Although considerable performance improvements have taken place in the last decades, it is generally accepted that traditional air-cooling techniques are about to reach their limit for cooling of high-power applications. For instance, Lasance et al. [9] state that with standard fans a maximum heat transfer coefficient of maybe $150\ W/(m^2K)$ can be reached with acceptable noise levels. However, several commercial brands in the computer cooling industry continuously release new designs. Air cooling is traditionally associated with the use of heat sinks, which are the most commonly-employed, cost-effective electronics thermal management hardware. Exception made to underwater or marine applications, heat removed from electronic systems is ultimately dissipated to the air [11]. Heat sinks function is mainly to extend the surface area of heat dissipating surfaces through the use of fins. Their design and analysis is one of the most extensive research areas in electronic cooling. Advances in heat sink cooling performance have been achieved through progress in manufacturing technology and to lesser extent, fan design, thereby resulting in more efficient heat removal [10]. However, these techniques are always limited by the temperature of the ambient air.

Cooling electronic chips does not only address the dissipation of the heat, but it also requires the junction temperature to be maintained within an acceptable range, typically 85-100ºC [12]. Conventional air cooled designs are no longer adequate to remove the actual heat fluxes, which can be much higher than the 150W and are not capable to keep the junction temperature within a safe range. Therefore, for a number of applications, air-cooling must be replaced or supplemented by other high performance compact cooling techniques [13]. There are several techniques which can be categorized as direct cooling. This context will be further explained in Chapter 3, but it is mainly related to the fact that the system to cool (e.g. the CPU) is in direct contact with the coolant fluid. Also, direct cooling is not a new concept. Already in the sixties, Bar-Cohen et al. [14] refer that direct application of fluids was used to cool macro electronics. However, this cooling strategy became more popular in the eighties after being used by big brands such as IBM. Nevertheless, direct liquid immersion often implied only the replacement of air with a liquid, which usually has higher convection coefficients, but advantages can be taken in terms of the convective coefficients, when phase change occurs. In this context Seok Ahn et al. [15] states that boiling is the most efficient heat transfer mechanism. They argue that boiling is an attractive option for tackling the thermal management

issues, particularly for cooling of microprocessors and high heat flux devices. There are several techniques that make use of materials phase change to cool down electronic components. Most of them use the boiling of a liquid to achieve higher heat fluxes. Some of these strategies include direct immersion cooling with liquid boiling, which is commonly known as pool boiling, micro-channels and spray or jet impingement. Direct immersion cooling is a well-established method for accommodating high heat fluxes backed by over thirty years of academic and industrial research [9]. Many researchers reported the enhancement of heat transfer by using newly materials or structures combined with pool boiling [15]. Boiling in micro-channel heat sinks is attractive for high-power performance electronics due to the high heat transfer rates that can be achieved. However, the physics of flow boiling in micro-channels, the flow patterns present and the effect of micro-channel size on the boiling regimes have not been investigated extensively, particularly with dielectric fluids [16]. Micro-channels have been studied by Silverio et al. [17], Argawal [18] and many others. However, the system miniaturization in diverse applications raises the need to better comprehend the scale effects induced on convective heat transfer inside micro-tubes. Several reviews related to mini-channel and micro-channel heat transfer, pressure drop, critical heat flux, flow instabilities and flow patterns are available in the literature [19] and all agree that there is no uniformity in the experimental data.

Bostanci et al. [20] performed experiments to investigate spray cooling on micro-structured surfaces. At $500\ W/cm^2$, the increases in the heat transfer coefficient for micro-structured with protrusions and indentations were 112% and 49% over smooth surface, respectively. Mudawar et al. [21] have shown that spray impingement cooling is one of the most efficient technologies for heat flux removal per unit of fluid flow. However, even with significant number of studies performed on spray cooling, relatively little is known about the exact mechanisms of energy transport or the peak heat flux in these systems. Thus, to date, engineers have not yet had the necessary tools to design robust, predictable spray systems for broader applications [22].

Regarding the application of Peltier cells to electronic cooling, they never were much used because of their Coefficient of Performance (C.O.P.) of about 1, which is rather low when compared to household refrigerators and air conditioners which goes from 2 to 4. Their cooling capability may also be limited over $5 - 10\ W/cm^2$. This makes thermoelectric cooling generally not competitive. Lasance et al [9] state that despite the low efficiency, the application of Peltier cells in different areas is increasing and include infrared detector cooling, charge coupled devices, microprocessors, blood analysers and portable picnic coolers. The main characteristics are still the accurate control of temperature and the possibility of cooling below ambient temperature. Additionally, the hardware simplicity is an advantage when compared to high pumping and expanding works required with refrigerators. The small size required for the pumps and turbines or valves in the context of cooling applications is also a complex task that has not been successfully achieved yet. According to Lasance et al [9] since the cooling density of a Peltier cooler is inversely proportional to its length, scaling to smaller size is desirable. The material structure produced by conventional crystal growth techniques to obtain bismuth telluride thermoelectric materials impose significant limitations on thermoelectric element dimensions due to poor manufacturing yields. So, this may also limit the minimum possible dimensions of the thermoelectric element. However, significant progress has been developed to

overcome this obstacle. Marlow industries reported that new-fine grain micro-alloyed bismuth telluride materials that do not suffer the element geometry limitation and can offer higher performance [23]. MicroPelt, a spin-off company from Fraunhofer and Infineon also sells promising thin films for near future claiming cooling of $160\ W/cm^2$.

Recently Cooler Master launched the V10 [24] which is a heat sink hybrid with fans and Peltier cell. This is composed of 10 heat pipes, 6 for the main body and 4 for the Peltier to maximise heat transfer. Dual PWM fan ensures high airflow over the heat sinks. The Peltier cell is activated once CPU reaches extremes temperatures.

2.2 Peltier Cells State of the Art

Regarding Peltier cells formulation and applications, Riffat et al. [25] provide an extensive review of present and potential applications of thermoelectric devices from applications of Peltier cells as coolers, as devices for power generation, thermal energy sensors, aeronautics and space applications. The formulation of the theoretical concepts governing the working principles of the Peltier cells is extensively described in the literature [26, 27, 28, 29]. Palacios et al. [30] provides an analytical procedure to obtain the internal parameters from performance curves of commercial thermoelectric modules. For a standard application it is not difficult to select the correct module looking at the performance values of an appropriate family of modules. Then, it is possible to estimate the final behaviour of cells in the application by using the performance curves (provided that the temperatures can be estimated correctly). However, for non-standard applications, such as those considered in the present work, the Peltier modules may work at atypical conditions, which are not considered in the performance curves. In this case, it is helpful to use an analytical model able to predict the behaviour of module. Alternatively, one must determine empirical approaches to characterize the cells working under those specific conditions. Although Palacios et al. [30] state that experimental measurements do not perfectly match the results estimated analytically, these measurements can be considered rather precise, taking into account the difficulties for attaining accurate experimental measurements in a standard laboratory. In this context, the present work will also discuss methodologies to characterize the Peltier cells internal properties, making use of experimental approaches.

Alternatively to the experimental characterization of the Peltier cells, few authors attempted to develop numerical models to predict the internal properties of cells. For instance, Pérez-Aparicio et al. [31] present a finite element simulation of a commercial thermoelectric cell, working as a heat pump. The specifically developed finite element is three-dimensional, non-linear in its formulation (using quadratic temperature-dependence on material properties) and fully coupled, including the Seebeck, the Peltier, the Thomson and the Joule effects. A thorough study of the distributions of voltage, temperatures and the corresponding fluxes is presented and the performance of cell is compared with that the data given by the manufacturer and with simplified analytical formulations, showing a good agreement. The concept is to define which variables need to be controlled in the design process of

Peltier cells to improve its performance. Pérez-Aparicio concluded such design variables are: length, electrical conductivity and Seebeck coefficients. Pérez-Aparicio states that these results agree with already known facts: a good thermoelectric module needs a high Seebeck coefficient to maximise the Peltier effect. Moreover, a high electrical conductivity is desired to reduce Joule effect and a low thermal conductivity results in a reduced heat transfer. This author also tested the influence of the temperature-dependence of the material properties in the Peltier cell performance and concluded that for the studied thermoelectric cell, the decreasing temperature-dependence of the electrical conductivity is more relevant for the Coefficient of Performance than the Seebeck coefficient and specially of thermal conductivity and of the consideration of reduced contact in the soldering connections. Similar study was performed by Yamashita [32] in which the author assumed that all of the thermoelectric properties are expressed by a quadratic function of temperature, which was confirmed experimentally. Cheng et al. [33] propose a three-dimensional theoretical model for predicting the transient behaviour of thermoelectric coolers. In his model, the thermoelectric cooler is divided in four major regions, namely, cold end (region 1), hot end (region 2) and the P-type and N-type thermoelectric elements (regions 3 and 4). The simulation model is adopted to perform a parametric study to investigate the effects of the parameters such as electrical current, cooling load per unit area, heat transfer coefficients on surfaces and geometrical parameters such as total area of heat sink and height of semiconductor elements. They concluded that the temperature of the hot end and the temperature difference between the hot and cold ends both increase with the applied current. They also found that the magnitude of the C.O.P. is rapidly decreased as the current is increased. Cheng et al. [33] also suggest that the convective heat transfer from the heat sink to ambient could be influential. The hot end temperature is remarkably reduced by increasing the convective heat transfer coefficient of the heat sink. The heat loss from the surfaces of the P-type and N-type elements causes a reduction in the C.O.P. However, the temperature difference is slightly influenced by variations in the heat transfer coefficient. Cheng et al. [33] also showed that the influence of an increase in element height is actually involved. Finally, the authors also found that the temperature difference between the two ends increases with the length. They also observed that both the temperature of the hot and cold side ends increase with cooling load and the value of C.O.P. linearly increases with the cooling load.

Huang et al. [34] studied the influence of the Thomson effect on the performance of a thermoelectric cooler. In this case, a one-dimensional thermal analysis for the performance of thermoelectric cooler was conducted under the influence of the Thomson effect, the Joule heating, the Fourier's heat conduction and the radiation and convection heat transfer. The temperature distribution and cooling power were analytically derived. For the cases in which the Thomson effect is important, (i.e. when the ratio of the Thomson heat to the conduction heat and the ratio of Joule's effect to the Thomson heat, play non-negligible roles), both temperatures distribution and the cooling power are affected by the Thomson effect. The fraction of both Fourier's conduction heat and Joule's heat that flow back to the cold side can be significantly reduced. Consequently, higher values of maximum temperature difference can be attained and the allowable heat load, providing that the thermoelectric cooler has P-type semiconductor material with the positive Thomson coefficient, is maxima.

Up to now, the reviewed studies are focused on the fundamental investigation of the internal

properties of the cells. Regarding the application of Peltier cells as a thermal control of various surfaces, it is worth mentioning the work of Deng et al. [35, 36] in which they propose a robust fault tolerant thermal control system of an aluminium plate with a Peltier Cell. This control system ensures that the control loop system remains insensitive to uncertain and random faults. Furthermore, it can tolerate some possible detrimental environment impacts.

Maruyama et al. [37] propose the development of a precise-temperature-controlled cooling apparatus, for medical application, using Peltier effect. In this study, a Peltier cryoprobe for dermis treatment and flexible cryoprobe for cryosurgery for deep region of human body were developed, based on the Peltier effect. The proposed apparatus has enough good performance to necrotize target diseased cells precisely. The flexible cryoprobe is composed of a resin tube flexible enough to treat the deeper parts of the human body with a catheter. A Peltier element is attached at the top of the probe for active heat transfer control of the cooling tip. Cooling experiments were conducted and the performance of the cryoprobe was evaluated. The authors report that the cryoproble could achieve temperatures as low as -43ºC at the tip. The motivation for this study is that the conventional cryoprobes generally have a high cooling ability, enough to freeze and destroy the disease part, but cannot control the cooling rate precisely, as it depends on refrigerative properties. Due to poor temperature control, the organ near the diseased part can get damaged. The results of this study were a cryoprobe which can control cooling and heating of a target accurately by utilizing the Peltier effect and boiling of liquid nitrogen. From animal experiments, it was confirmed that the cryoprobe has enough good cooling performance to freeze skin and destroy skin cells.

Another interesting work using Peltier cells is reported by Morimitsu and Katsura [38, 39]. These authors analysed an observer-based thermal control system of a Peltier device. The objective of this study is to use a Peltier cell, which is a suitable device to produce heat transfer, to induce thermal sensations, i.e., utilizing the device for haptics. Haptics is an academic field which deals with the transmission of touch sensation. In the present industry of communication engineering, audio and visual information are the most transmitted. However, humans can not only hear and see, but also smell, taste and feel tactile sensation. Haptics aims to present touch sensation which can become the third multimedia information to the operator. The idea behind transmitting thermal sensation is that temperature and heat flow are very important information for human actions. In this case, by touching a Peltier cell, the device would be able to read temperature and heat flow and this information can be transmitted across the network to other point and inversely reproduce the same sensation.

Recently, Oven industries released the 5R6-900 which is a new temperature controller [40]. 5R6-900 is a solid state MOSFET bidirectional compact ramp and soak benchtop temperature controller for Peltier cells with an internal power supply, full H bridge and is capable of load currents up to 10A User friendly PC programmable via the electrically isolated RS232 com port. The functions of this product are very similar to those proposed in the present thesis.

Chapter 3

Pool Boiling as a cooling technique

This chapter deepens the basic heat transfer concepts that are required to understand the cooling techniques. Particular emphasis is given to a cooling strategy using liquids phase change. Hence, section 3.1 introduces the heat transfer processes occurring at direct and indirect cooling techniques. Afterwards, the basic concepts on pool boiling are revised in section 3.2, which are vital to understand how the boiling of a liquid can be used as a cooling technique. Given that the present work addresses the development of a condensation system to reuse the vaporized liquid, basic condensation principles are described in section 3.3. Finally, the description of the possible configurations of cooling systems using liquids phase change is discussed in section 3.4, which also analyses advantages and disadvantages of several cooling configurations using phase change.

3.1 Indirect and Direct Contact cooling

Most modern day processors have some interface between the central processing unit (CPU) and its surrounding. This interface is usually called heat spreader and two of its most important functions are to physically protect the CPU and to increase the heat exchange area. Heat can be exchanged by three different physical mechanisms: conduction, convection and radiation. The heat transfer by conduction is associated to the diffusion of energy occurring by atomic and molecular activity, when a temperature gradient exists. Hence, during conductive heat transfer there is not a macroscopic motion of mass, but instead, the heat is transferred by diffusion from the region with highest temperature to that with lowest temperature. The convective heat transfer is the combined effect of diffusion with advection, being the latter related to the heat that is transferred by the motion of a quantity of mass. Finally, radiative heat transfer is related to the energy that is emitted by the matter, at a specific finite temperature.

By definition, the heat flux is the rate of heat that is transferred per unit area, being this area perpendicular to the direction of the flux. Thus, the heat flux $\dot{q}''$ (W/m^2) is proportional to the temperature gradient:

$$\dot{q}'' = -kA\frac{dT}{dx} \tag{3.1}$$

where k [W/(m.K)] is the thermal conductivity of the material (i.e. it is a property of the material, which can be in solid, liquid or vapor phase) and the signal minus is used to identify that the heat is transferred from the highest to the lowest temperatures. In steady state, the rate of heat $\dot{Q}$ that is transferred by conduction through a surface (e.g. the heat spreader) is given by:

$$\dot{Q} = -kA\frac{\Delta T}{L} \tag{3.2}$$

being A the area of the heat spreader and L its thickness. The heat spreader is in direct contact with the CPU, so the heat that is dissipated by the CPU is diffused to the heat spreader by conduction and only afterwards is removed from the heat spreader. Hence, most computer cooling systems cool the heat spreader, so that the categorization of the cooling techniques in direct or indirect cooling depends if the heat spreader is in direct or indirect contact with the cooling system.

Indirect cooling systems use an additional thermal interface which cools the heat spreader by conduction. However this thermal interface also needs to be cooled, resorting to forced air convection or systems that use some kind of fluid. Whichever the system used, the thermal interface is cooled by convection by the fluid (gas or liquid). In direct cooling this additional thermal interface does not exist, so the cooling fluid is directly in contact with the heat spreader. The rate of heat that is removed from the surface (of the heat spreader or of the thermal interface) by the fluid is given by the Newton's cooling law:

$$\dot{Q} = hA(T_s - T_{fl}) \tag{3.3}$$

where h $[W/(m^2.K)]$ is the convective heat transfer coefficient (which, contrarily to the thermal conductivity, is not a property of the material), A is the surface area, T_s is the surface temperature of the heat spreader or of the thermal interface and T_{fl} is the temperature of the fluid.

Indirect and direct cooling can be schematically represented as depicted in Figure 3.1 and Figure 3.2, respectively. Following these figures it is relevant to introduce the concept of thermal resistance. This term implicates an analogy between heat exchange and the flowing of electrical current. Reminding eq. (3.2) and considering that the temperature difference ΔT is analogous to the current and that the heat transfer rate is the analogous of the electrical tension, the thermal resistance by conduction is defined as:

$$R_{cond} = \frac{\Delta T}{\dot{Q}} = \frac{L}{kA} \tag{3.4}$$

Similarly, a convective heat transfer resistance can be defined as:

$$R_{conv} = \frac{T_s - T_{fl}}{\dot{Q}} = \frac{1}{hA} \tag{3.5}$$

There is a third type of thermal resistance that plays an important role in heat exchange. This is referred to as Contact Resistance and it is due to roughness on the surface that creates cavities, most of the time filled with air. The usual solution to decrease the contact resistance consists in applying on these cavities a fluid with higher thermal conductivity than that of the material used.

The concept of thermal resistance is relevant because it allows analysing the problem of heat transfer as an analogy to an electrical circuit. As matter of fact, thermal resistances can be associated in parallel or series just as electrical resistances. The association of thermal resistances in series equals to the sum of their resistances while the association of thermal resistances in parallel equals the sum of the inverse of their value

$$R_{T_{series}} = R_1 + R_2 \tag{3.6}$$

$$\frac{1}{R_{T_{parallel}}} = \frac{1}{R_1} + \frac{1}{R_2} \tag{3.7}$$

As shown in Figure 3.1, the use of indirect cooling systems introduces an additional thermal conduction resistance between the heat spreader and the thermal interface. This is pertinent when considering the heat transfer equation for the entire system (eq. 3.7). The heat exchange depends on the global thermal resistance and on the temperature difference between the CPU and ambient temperature. The ambient temperature is actually a limiting value for most of the current cooling systems. This is obvious when the cooling fluid is air. When other fluids are used (e.g. liquids), the heat that they remove from the heat spreader or from the thermal interface is usually exchanged to the ambient, for instance using a radiator.

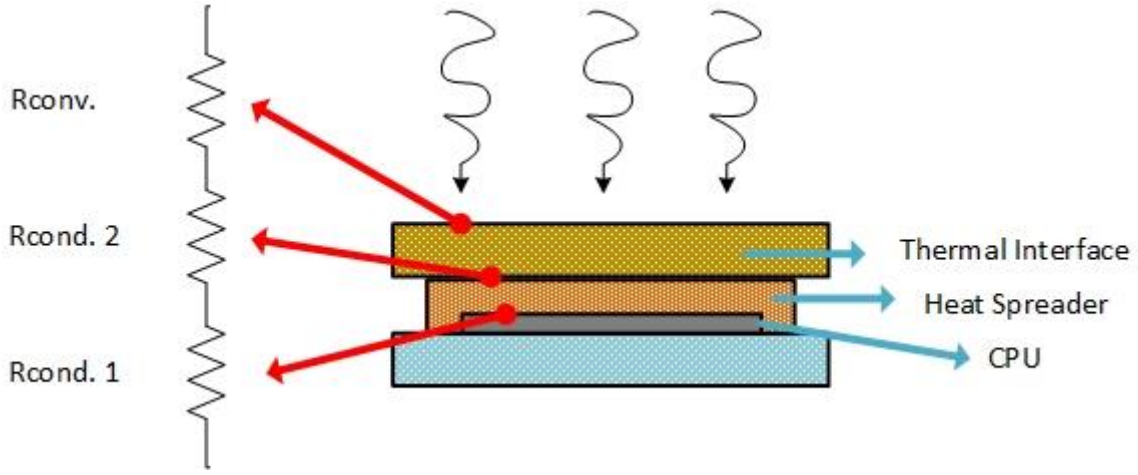

Figure 3.1 – Indirect Contact

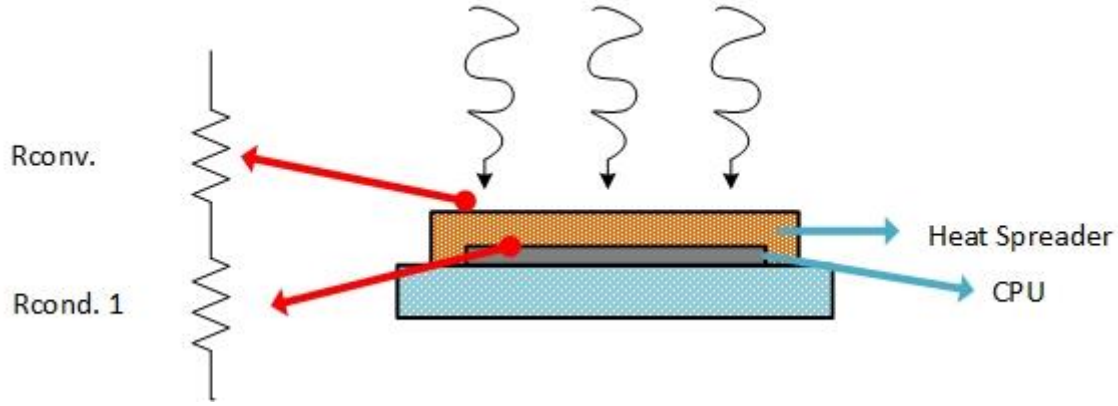

Figure 3.2 – Direct Contact

$$Q = \frac{1}{R_{T_{Global}}}\Delta T = \frac{1}{R_{T_{Global}}}(T_{CPU} - T_{amb}) \tag{3.8}$$

In computer cooling, the goal is to reduce the CPU temperature which is achieved by reducing the global thermal resistance.

$$T_{CPU} = QR_{T_{Global}} + T_{amb} \tag{3.9}$$

As seen in Figure 3.1, the global thermal resistance of an indirect cooling system corresponds to the sum of each resistance resulting in ($R_{T_{Global}} = R_{T_{Cond.1}} + R_{T_{Cond.2}} + R_{T_{Conv.}}$), while in direct cooling systems (Figure 3.2) the absence of the thermal interface results in a lower global thermal resistance ($R_{T_{Global}} = R_{T_{Cond.1}} + R_{T_{Conv.}}$). From this simple analysis one can conclude that direct cooling systems have higher potential to achieve lower CPU temperatures because of the lower global thermal resistance.

Back to Figure 3.1 and Figure 3.2, it can be seen that the thermal convection resistance is present independently of the technique used to cool down the system. When cooling a system by convection, this can be either forced, in which the fluid motion is driven by external forces, or natural, in which the motion is induced by density differences caused by temperature differences of the fluid.

Besides the presence of a larger or lower thermal resistance, the “better” or “worse” performance of the cooling systems is strongly related to the heat transfer coefficient, given the important role of convection in the cooling process. Actually, the noticeable higher performance of systems that use water instead of air (e.g. Watercooling) is due to the fact that the values of h for liquids such as water are significantly larger than those of gases. The heat transfer coefficient also depends on the velocity of the fluid so that *h* of forced convection systems is larger than that obtained in free convection systems. Representative values of the convective heat transfer coefficient are given in Table 3.1. The much higher value of *h* presented for phase change processes (boiling or condensation) in comparison to the values obtained for free or forced convection will be explained in the following section, but in line with the discussion presented so far, such high value foresees the great potential of using phase change processes to cool the processors.

Table 3.1 - Convective Heat Transfer Coefficient for several processes

Process	$\boldsymbol{h}$ $(\boldsymbol{W/m^2K})$
Free convection gas	2-25
Free convection liquid	50-1000
Forced convection gas	25-250
Forced convection liquid	100-20,000
Boiling or Condensation	2500-100,000

3.2 Boiling Curve and regimes and Condensation

Vaporization of a substance is the phase transition from liquid to gas phase. There are two types of vaporization: evaporation and boiling. Boiling generally refers to the process that occurs along solid surfaces submerged in the liquid and is characterized by the creation of vapour bubbles while evaporation usually occurs at liquid/vapour interface.

Boiling typically starts when the heated surface temperature is above the liquid saturation temperature (the boiling point) by $\Delta T_{superheat} = T_{surface} - T_{saturation}$ large enough to promote the creation and departure of vapour bubbles from the heated surface.

For a surface experiencing boiling heat transfer, the variation of heat flux results in a characteristic temperature response at the surface, reflecting a progression through particular regimes of ebullient heat transfer. In 1934, Shiro Nukiyama [41] was the first to define the different boiling regimes resulting in the Nukiyama curve which relates the heat flux and $\Delta T_{superheat}$ between the

surface temperature and liquid saturation temperature.

Nukiyama conducted experiments with a horizontal nichrome wire (melting point: 1500K) at atmospheric pressure, immersed in saturated water. The heat flux was determined by the measurement of the electrical current I and potential drop V. The wire temperature was measured from the change of the electrical resistance due to temperature variation.

Nukiyama noticed that as he increased the power given to the wire, bubbles started to form at $\Delta T_{superheat}$ of roughly $5ºC$. He noticed the power supplied to the wire could be increased greatly without a large increase in temperature until point C, which he defined as where the critical heat flux occurred. As he continued to increase the power supplied, he observed a sudden decrease in temperature and the wire reached the melting point (point E).

While repeating the experiment with a platinum wire, Nukiyama was able to obtain the curve remarked by red arrows in Figure 3.3. As it can be observed, Nukiyama obtained a hysteresis phenomenon due to the fact that the curve obtained is different whether one gradually increases or decreasing the heat flux. This hysteresis was due to the Power Control mechanisms used by Nukiyama. Therefore, increasing the heat flux, the resulting curve is defined through the points A-B-P-C-E, while decreasing the heat flux results in the curve defined through points E-D-A.

Nukiyama believed that a method to control $\Delta T_{superheat}$, instead of power controlled method, would yield a better curve. Later in 1937, Drew and Muller [42] performed the experiment using a steam pipe and obtained a curve similar to the black one reported in Figure 3.3.

Assuming a temperature controlled system, the following pool boiling regimes can be identified:

Natural Convection

The underlying physical mechanism of region 1 of the boiling curve demonstrated in Figure 3.3 is natural convection. While $\Delta T_{superheat}$ is lower than that observed in point A, the fluid motion is mainly governed by natural convection effects. i.e., the fluid near to the heated surface is heated, becomes less dense and rises due to buoyancy. The surrounding, cooler fluid then moves to replace it being in turn heated and forming a convective current. This process transfers the heat energy from the heated surface from the bottom to the top of the pool. The process is characterized by single-phase natural convection from the hot surface to the saturation fluid without formation of bubbles on the surface.

Nucleate Boiling

Above a certain $\Delta T_{superheat}$ (point A), vapour bubbles appear on the heated surface. This is referred as the onset of nucleate boiling. The bubbles form on scratches or cavities on the surface that contain pre-existing vapour nuclei. In liquids with low surface tension, the onset of nucleation may be delayed. For these fluids, a reduction in the surface temperature occurs while the heat flux remains constant due to a sudden inception of a large number of cavities. This difference in the wall temperature before and after boiling incipience is called “incipience overshoot”.

After this, a dramatic increase in the boiling curve is observed which corresponds to Region II in Figure 3.3. In the partial nucleate boiling regime, isolated bubbles are released from randomly active sites on the wire surface. This release of the bubbles from the surface induces a considerable motion near the surface, resulting in a direct heat transfer from the surface to liquid leading to a substantially increase in h and $\dot{q}''$.

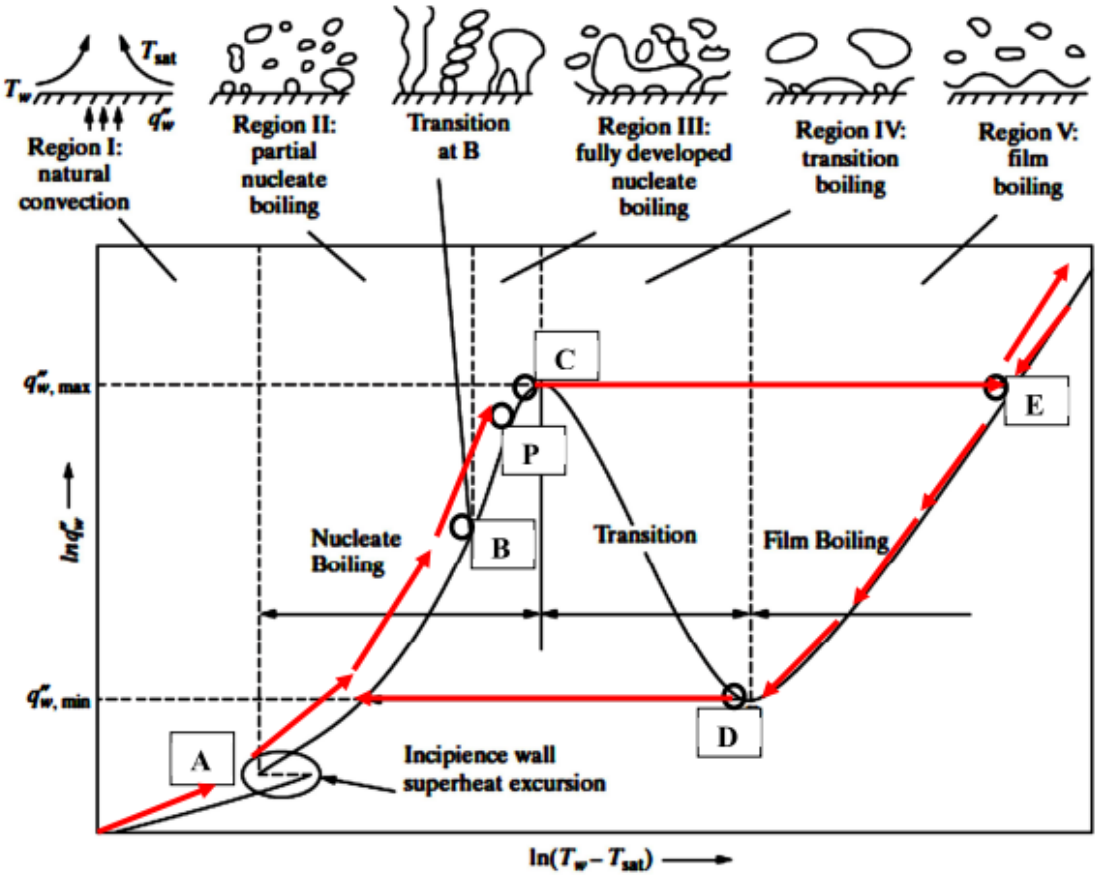

Figure 3.3 - Drew and Muller Experiment (Black) and Nukiyama Curve (Red arrows)

The transition from isolated bubbles to fully developed nucleate boiling (region III) occurs when bubbles at a given site begin to emerge in a vertical direction. In this phase, the bubbles are released in the form of jets and due to the densely formation of bubbles, they interfere between each other causing a decrease of the heat transfer coefficient. Point P of Figure 3.3 corresponds to an inflection in the boiling curve in which the slope of heat transfer coefficient reaches its maximum value. After this point, even though $\dot{q}''$ continues to increase there is a decrease in the slope of the boiling curve. $\dot{q}''$ continues to increase until point C which is called critical heat flux region and is the upper limit of the nucleate boiling region, at which the heat transfer is maximum. For cooling purposes, the critical heat flux is the limiting value to work. As one passes this region, the heat flux decreases dramatically, so that the system to cool can be easily damaged by overheating (the so called system burnout).

Transition Boiling

The region IV called transition boiling is the phase resulting from the mix of features between nucleate boiling and film boiling. Bubble formation is now so fast that a blanket of vapour forms on the surface. The fraction of film boiling over nucleate boiling increases with the increase of $\Delta T_{superheat}$, but any given location on the surface can oscillate between one or the other. However, the conductivity of vapour is lower than a liquid and thus *h* decreases with the increase of $\Delta T_{superheat}$.

Film Boiling

Region V is called Film Boiling which is represented by curve ED. At point D, referred as Leidefrost Point, the heat flux shows a minimum q''_{min} and the fraction of vapour blanket is unitary. In this phase, heat exchange from the surface occurs by conduction and radiation through the vapour. In 1756, Johann Leidenfrost [43] observed that a liquid in near contact with a mass significantly hotter than the liquid's boiling point produces an insulating vapour layer keeping that liquid from boiling rapidly. As the surface temperature is increased, radiation through the vapour film becomes more significant and the *h* increases with $\Delta T_{superheat}$.

During boiling, an additional heat transfer quantity is removed by the liquid over the surface, which is related to the energy that is required to provide for the phase change. This amount of energy is proportional to $\dot{m} h_{fg}$ where $\dot{m}$ is the mass flow of liquid that turns into vapour and h_{fg} is the latent heat of vaporization. This amount of energy can be quite high, particularly in certain fluids like water and it is the main reason for the high value of *h*, earlier depicted in Table 3.1 for boiling processes. Additionally, while the pressure is kept constant, the temperature of a liquid during phase change is kept constant, thus allowing good control on the temperature of a cooling process. In this context, several cooling configurations have been explored within the last years, which try to take advantage of the latent heat. These configurations, which were summarized in the State of the Art, are now presented in more detail in section 3.4.

3.3 Condensation

Given that the system developed here is actually acting on the condensation of the vapour that is generated during pool boiling, it is relevant to introduce the condensation theory that is important to understand the design of the final setup, as well as the discussion of the results presented at the end of the work. When vapour temperature is reduced below its saturation value, the vapor condenses. In engineering applications, the vapor is condensed when it comes into contact with a cold surface. The steam condensers for power plants are typical examples of the application of condensing steam [44]. If the liquid wets the surface, condensation occurs in the form of a smooth film, which slips down the surface because of the action of gravity. By having liquid film over the surface a thermal resistance to heat flow is created. This resistance is called filmwise condensation.

So, numerous experimental and theoretical investigations have been done to determine the heat-transfer coefficient of film condensation over surfaces. The first fundamental analysis that allowed determining of the heat transfer coefficient that exists in filmwise condensation of pure vapors on a flat plate and a circular tube was done by Nusselt in 1916. Over the years, improvements have been made to Nusselt's theory of film condensation. However, with the exception to the condensation of liquid metals, Nusselt's original theory has been experimentally and is still widely used. The following paragraphs briefly describe Nusselt's theory of film condensation of pure vapors on a vertical plate.

Considering the condensation of a vapour on a vertical plate, as represented in Figure 3.4, where x is the axial coordinate, measured from top to bottom along the plate, and y is the coordinate normal to the condensing surface. The condensate thickness is represented by $\delta \equiv \delta(x)$. This condensation problem was first analyzed by Nusselt under the following assumptions:

1. The plate is maintained at a uniform temperature T_w that is less than the saturation temperature T_v of the vapour.
2. The vapour is stationary or has low velocity, and so it exerts no drag on the motion of the condensate.
3. The flow from top to bottom of condensate under the action of gravity is laminar.
4. The flow velocity associated with the condensate film is low; as a result, the flow acceleration in the condensate layer is negligible.
5. Fluid properties are constant.
6. Heat transfer across the condensate layer is by pure conduction, hence the liquid temperature distribution is linear.

The velocity distribution $u(y)$ at any location x across the condensate layer can be determined from a force balance on a volume element, which is shown by the shaded area in Figure 3.4. Equating the shear force upward to the buoyancy force acting downward, this force balance renders to:

$$\mu_l \frac{d\mu}{dy} = (\rho_l - \rho_v)(\delta - y) g \, dx \tag{3.10}$$

or

$$\frac{d\mu}{dy} = \frac{g(\rho_l - \rho_v)}{\mu_l}(\delta - y) \tag{3.11}$$

where $\delta \equiv \delta(x)$ is the thickness of the condensate layer at the position x, μ is the dynamic viscosity and the subscripts l and v refer to the liquid and vapor phases, respectively. In this case one can assume zero shear stress at the liquid-vapor interface, because the vapour is considered almost stationary by assumption 2. At the wall surface, the liquid velocity is zero:

$$u = 0 \text{ at } y = 0 \tag{3.12}$$

The integration of equation 3.11 subject to the boundary condition equation 3.12 gives the velocity distribution in the condensate layer:

$$u(y) = \frac{g(\rho_l - \rho_v)}{\mu_l}(\delta y - \tfrac{1}{2} y^2) \tag{3.13}$$

The mass flow rate of the condensate $m(x)$ through any axial position x per unit width of the plate is given by

$$m(x) = \int_0^{\delta} \rho_l u \, dy \tag{3.14}$$

Introducing u from equation 3.13 into equation 3.14 and performing the integration yields:

$$m(x) = \frac{g\rho_l(\rho_l - \rho_v)\delta^3}{3\mu_l} \tag{3.15}$$

and differentiation with respect to δ gives:

$$dm = \frac{g\rho_l(\rho_l - \rho_v)\delta^2}{\mu_l} d\delta \tag{3.16}$$

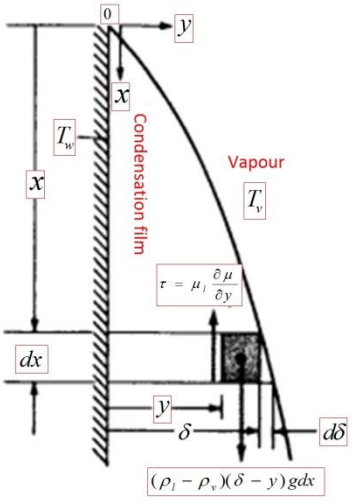

Figure 3.4 – Nomenclature for filmwise condensation on a vertical plane surface [44]

Here dm represents the rate of condensation over the distance dx per unit width of the plate, since the condensate thickness by $d\delta$ over the differential length dx.

The rate of heat released dQ associated with the rate of condensation dm is

$$dQ = h_{fg} dm \tag{3.17}$$

where h_{fg} is the latent heat of condensation. The amount of heat released dQ over the area $dx \cdot 1$ must be transferred across the condensate layer thickness δ by conduction, according to assumption 6. Therefore,

$$dQ = k_l \frac{T_v - T_w}{\delta} dx \cdot 1 \tag{3.18}$$

where k_l is the thermal conductivity of liquid and T_v and T_w are the vapour saturation and wall surfaces, respectively. From equations 3.16 and 3.18 into equation 3.17, one can obtain the following differential equation for the thickness of the condensate layer:

$$\frac{d\delta}{dx} = \frac{\mu_l k_l (T_v - T_w)}{g\rho_l(\rho_l - \rho_v)h_{fg}} \frac{1}{\delta^3} \tag{3.19}$$

The integration of equation 3.19 with the condition $\delta = 0$ and $x = 0$ yields the thickness of the condensate layer as a function of the position x along the plate:

$$\delta(x) = \left[\frac{4\mu_l k_l (T_v - T_w)x}{g(\rho_l - \rho_v)\rho_l h_{fg}}\right]^{1/4} \tag{3.20}$$

Since the relation for the thickness of the condensate layer was already established, the local heat transfer coefficient h_x for condensation is determined from the definition

$$h_x = \frac{k_l}{\delta(x)} \tag{3.21}$$

Introducing $\delta(x)$ from equation 3.20 into equation 3.21, one obtains:

$$h_x = \left[\frac{g(\rho_l - \rho_v)h_{fg}k_l^3}{4\mu_l(T_v - T_w)x}\right]^{1/4} \tag{3.22}$$

and the local Nusselt number Nu_x is expressed as

$$Nu_x = \frac{h_x x}{k_l} = \left[\frac{g(\rho_l - \rho_v)h_{fg}k_l^3}{4\mu_l(T_v - T_w)x}\right]^{1/4} \tag{3.23}$$

One may notice from equations (3.20-22) that the local heat transfer coefficient h_x varies with the distance as $x^{-1/4}$. Then the average heat transfer coefficient h_m over the length $0 \leq x \leq \mathrm{L}$ of the plate is:

$$h_m = \frac{1}{L}\int_0^L h_x\, dx = \frac{4}{3}h_x\Big|_{x=L} \tag{3.24}$$

Or, introducing equations (3.20-22) into equations (3.20-24), one obtains:

$$h_m = 0.943\left[\frac{g\rho_l(\rho_l - \rho_v)h_{fg}k_l^3}{\mu_l(T_v - T_w)L}\right]^{1/4} \qquad W/(m^2 \cdot {}^{\circ}C) \tag{3.25}$$

The physical properties in equations (3.20-22) and (3.20-3.25), including h_{fg}, should be evaluated at the film temperature

$$T_f = \frac{1}{2}(T_w + T_v) \tag{3.26}$$

The additional energy needed to cool the condensate film below saturation temperature is accommodated approximately by evaluating h_{fg} at the film temperature instead of the saturation temperature.

A comparison of the average heat transfer coefficient for vertical surfaces given by equations (3.20-25) with that found by experiments shown that the measured heat transfer coefficient is about 20% higher than theory would suggest. Therefore, McAdams recommends that Nusselt's equation for h_m on a vertical surface is multiplied by a factor of 1.2; hence equations (3.20-25) should be replaced by

$$h_m = 1.13\left[\frac{g\rho_l(\rho_l - \rho_v)h_{fg}k_l^3}{\mu_l(T_v - T_w)L}\right]^{1/4} \tag{3.27}$$

3.4 Cooling configurations using phase change

Several techniques make use of materials phase change to cool down electronic components. Most of them use the boiling of a liquid to achieve higher heat fluxes. Some of these strategies include pool boiling [45, 46, 47, 14, 12, 15, 48], micro-channels [17, 19, 49, 16, 18], jet or spray impingement [20, 8, 13, 22, 50, 51], as revised in Chapter 2. Each of these techniques has different advantages and drawbacks, which will be briefly reviewed in this sub-section.

Pool boiling, is a direct immersion liquid cooling technique, since there are no physical walls separating the heated surface from the liquid coolant. This form of cooling offers the opportunity to remove heat directly from the heated surface, in this case, the CPU with no intervening thermal conduction resistance, other than that between the CPU and the heat spreader surface in contact with the liquid. With pool boiling one can achieve a high heat transfer coefficient which reduces the temperature of the heated surface above the liquid coolant temperature. The selection of a liquid for Pool boiling cannot be made solely on the basis of heat transfer characteristics alone. Chemical compatibility of the coolant with the heated surface, in this case the CPU which is an electronic component and other materials exposed to the liquid must be a primary consideration.

The term ‘micro’ is applied to hydraulic tubes having diameters of ten to several hundred micrometers. The main advantage of micro-channels is to increase the surface area so that heat dissipation is easier. The reviewed literature shows that the small flow rate within micro-channels produces laminar flow resulting in a heat transfer coefficient inversely proportional to the hydraulic diameter. This means that the smaller the channel, the higher the heat transfer coefficient. Unfortunately, it is widely reported that the pressure drop increases with the inverse of the second power of the channel width, keeping the mass flow constant and this limits in practice the miniaturization. Mudawar [21] reviewed high-heat-flux thermal management schemes, including ultra-high-heat-fluxes in the range of $1000 - 100{,}000\ W/cm^2$.

In recent years spray cooling has received increasing attention as a means of supporting higher heat flux in electronic cooling applications. Spray cooling consists on impinging a spray, produced by a nozzle, into a heat surface. By using multiple nozzles liquid breaks up into fine droplets that impinge individually on the heated wall. Cooling of the surface is achieved through a combination of thermal conduction through the liquid in contact with the surface and evaporation at the liquid-vapour interface. Spray cooling has gained a foothold in the military sector providing for improved thermal management, dense system packaging, and reduced weight.

Pool boiling is not the technique which offers the highest heat transfer coefficients, but it was chosen as its the simple hardware requirements and the almost absence of pumping auxiliary components provide great advantages over other much more complex configurations. At this stage it is worth mentioning that not all the liquids can be used for cooling. For instance, although it has high values of thermal properties and particularly high values of the latent heat of vaporization, liquids like water are dangerous to use, even in indirect cooling techniques, due to the risk of leakage. Hence, the working fluids must be dielectric. Additionally, it is recommended that the saturation temperature of the

working fluid at ambient pressure (the temperature at which phase change begins) is as close as possible to the working temperature of the system to cool.

Chapter 4

Peltier Cells

Given that the achievement of the objectives of the present work requires deep understanding on the Peltier cells working principles and main characteristics, this chapter addresses the fundamental theoretical concepts governing the working principles of the Peltier cells, as well as benefits and drawbacks of using them for several purposes (including cooling systems). Section 4.1 provides a brief historical introduction to the Peltier cells. Section 4.2 will discuss some of benefits and drawbacks of using the Peltier cells in various relevant applications. Section 4.3 explains the thermoelectric effect in more detail and section 4.4 introduces the formulation that describes its behaviour. Finally, Section 4.5 explains the main characteristics and procedures that must be considered to select the appropriate Peltier cell for the required application.

4.1 Introduction

Peltier thermoelectric cells (TEC) are solid-state devices that create an electrical voltage from a temperature gradient (Seebeck effect) or convert an electrical voltage into a temperature gradient (Peltier effect).

Baltic German physicist Thomas Johann Seebeck, in 1821, was the first to find that in a loop made of two dissimilar conductors, with junctions at different temperatures would deflect a compass magnet [52]. Seebeck initially thought that this temperature gradient caused an induced magnetism and this was related to Earth's magnetic field [53]. Quickly he realized that an electromotive force (emf) and consequently, by Ampère's Law, an electric current is generated due to the temperature difference. This is known as the Seebeck effect and it is widely used to measure temperature with great sensitivity and accuracy in thermocouples.

Later in 1834, French physicist Jean Charles Athanase Peltier discovered that when an electrical current is made to flow between two dissimilar conductors, one junction is cooled and the other is heated, thus creating a temperature gradient. In 1838, Heinrich Lenz showed that depending on the direction of the current flowing, heat could be removed from a junction to turn water into ice, or reversely could be added to the junction to melt ice [53].

Twenty years later (1854), British physicist William Thomson (Lord Kelvin) issued a comprehensive explanation of the Seebeck and Peltier effects and described their interrelationship [53]. The Seebeck and Peltier coefficients are related, being the Peltier coefficient simply equal to the Seebeck coefficient multiplied by the absolute temperature. This thermodynamic derivation led Thomson to predict a third thermoelectric effect, now known as Thomson effect, which occurs when heat is absorbed or produced while an electric current passes through a circuit composed of a single material that has a temperature difference along its length. If a copper wire carrying a steady electric current is subjected to external heating at a short section while the rest remains cooled, heat is absorbed from the copper as the conventional current approaches the hot point and heat is transferred to the copper just beyond the hot point.

4.2 Peltier cells in various applications: advantages and drawbacks

Peltier cells provide numerous solutions to many applications and in several cases they are the only reliable solution [54]. Working on a thermoelectric basis, Peltier cells are widely used as heat pumps or coolers. They are often applied as thermal energy sensors, in aeronautics and space, in small-scale refrigeration [25].

While one cannot select a cooling method to be the best, given the numerous variables that

must be considered in heat transfer problems, Peltier cells have several characteristics that make them a very interesting solution to approach [30]. Some advantages of using Peltier cells are:

- No moving parts: so maintenance is required less frequently.
- Small size and weight: they are much smaller than comparable mechanical systems and come in a wide variety of sizes and forms to comply with strict requirements [31].
- Ability to cool below ambient temperature: unlike air cooling, Peltier cells have the ability to cool the temperature below the ambient value.
- Ability to either heat or cool with the same module: as demonstrated by Lenz, to exchange between heating or cooling, one just has to reverse the polarity of the applied current.
- Precise temperature control: with an appropriate control system, Peltier cells are able to control the temperature with an accuracy of +/- 0.1ºC [55].
- High reliability: due to the solid-state construction with mean time between failures (MTBF) exceeding 100,000 hours [55].
- Quiet operation: unlike air cooling they produce no noise.
- Operation in any orientation: they can operate in any direction and in zero gravity environments.
- Spot cooling (e.g. for electronic circuits): Peltier cells allow cooling a specific region of the circuit, thus not wasting energy cooling other components.
- Ability to generate electric power: when temperature gradient is applied, it is possible to generate current.
- Environmentally friendly: conventional refrigeration systems often use chlorofluorocarbons that can be harmful to the environment. Peltier cells do not use or generate gases of any kind.

However, there also have some disadvantages:

- Able to dissipate limited amounts of heat flux.
- Condensation is another potential dangerous problem, occurring if components are cooled too much below the ambient temperature
- Not as efficient, in terms of the Coefficient of Performance (C.O.P), as vapour-compression systems (The C.O.P is further defined in section 4.5).

4.3 Thermoelectric Effect

The thermoelectric effect is much larger at metal-semiconductor junction than in a junction between two metals. In the world of thermoelectric technology, semiconductors (usually Bismuth-Telluride) are the material of choice for producing the Peltier effect. These semiconductors are used because designers can easily optimize the pumping of heat by controlling the type of charge carrier employed within the conductor. A Peltier cell in its simplest form can be composed of a single n-type

pellet [56] which is connected to an electrically-conductive wire on each end (Figure 4.1).

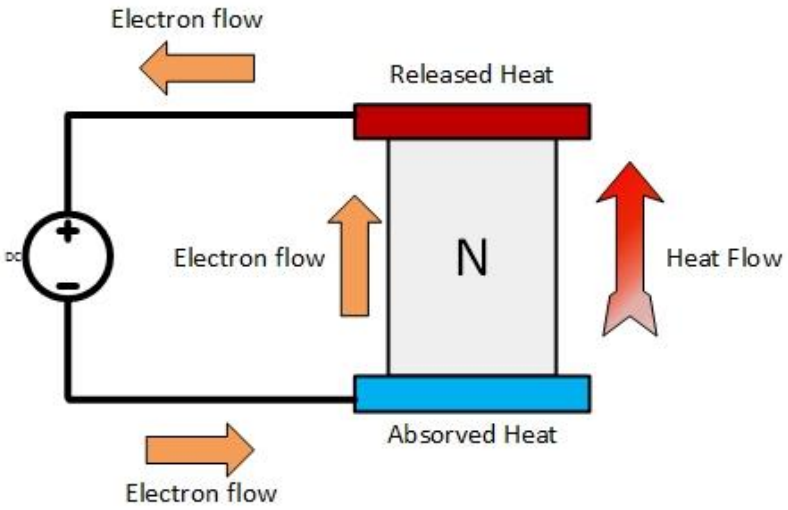

Figure 4.1 – Single N-type pellet

As shown in Figure 4.1, the heat will be pumped in the direction of the charge flow. Actually the heat is transferred by the carrier charges. In this N-type semiconductor the electrons will be the charge carriers within the molecular structure. When a DC voltage source is applied, the electrons will be repelled by the negative pole of the source and attracted to the positive pole as shown in the figure. With the electrons flowing through the n-type semiconductor from bottom to top, the heat is absorbed in the bottom and actively pumped to the top junction. P-type pellets (Figure 4.2) are also widely used in thermoelectric industry.

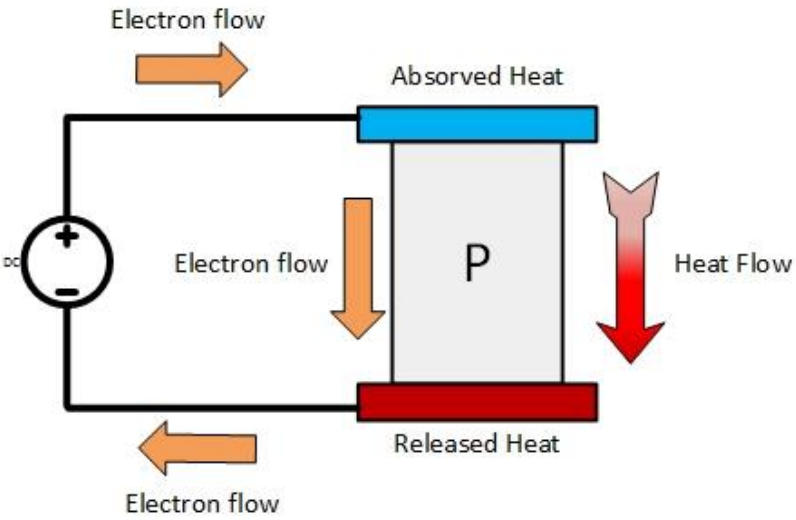

Figure 4.2 – Single P-type pellet

P-type pellets are manufactured so that the charge carriers in the semiconductors are positive (known as “holes”). These are places where the electrons can easily fit when a voltage is applied, thus enhancing the electrical conductivity of the material. Positive charge carriers are repelled by the

positive pole of the voltage source and attracted to the negative pole, so that “hole” current flows in an opposite direction to that of the electron flow and so the heat is moved from top to bottom.

This contrast in heat pumping between N-type and P-type pellets is very important in the design of Peltier cells. Although it is possible to make a simple thermoelectric cooler with a single semiconductor pellet, we are unable to pump a considerable amount of heat through it. Hence, Peltier cells are not made solely by one N-type or one P-type pellets, but instead it is composed of several N-type and P-type pellets. In order to pump larger amount of heat, the most intuitive though is to connect the pellets in parallel, both electrically and thermally, as shown in Figure 4.3.

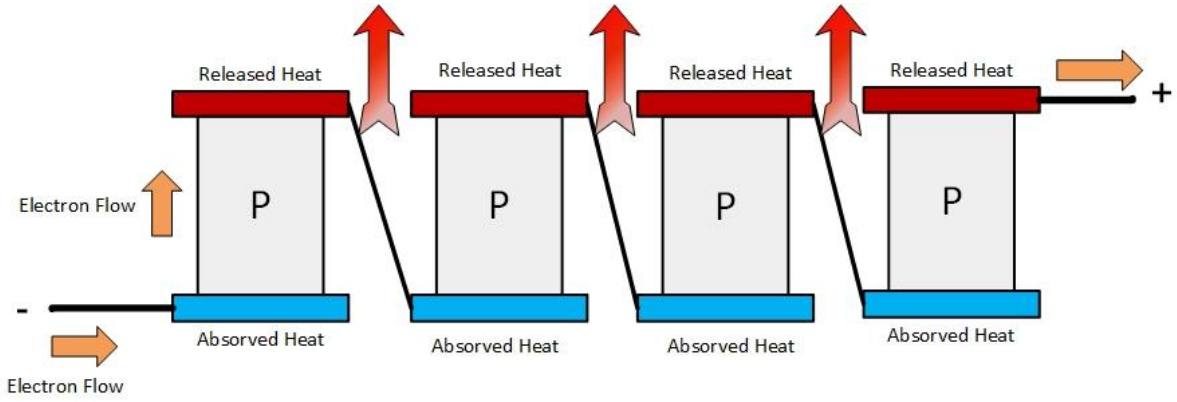

Figure 4.3 – Multiple P-type pellets connected in parallel

However, this is a very unpractical approach since the typical thermoelectric semiconductor pellet is rated for only a very small voltage while it can draw a considerable amount of current. For example, a single pellet in an ordinary thermoelectric cell may draw five amps or more with only 60mV applied; if wired in parallel in a typical 254-pellet configuration, the device would draw over 1270A with the application of only 60mV. As easily seen, this is an unpractical approach. So, the only realistic solution is to make the electrical connection of the pellets in series, while keep them thermally in parallel. Here the idea could be to connect them in a zigzag fashion from pellet to pellet to achieve a series circuit. In theory this is a good idea, however, in reality the interconnections between the pellets introduce thermal shorting that significantly compromises the performance of the device.

Fortunately, there is one final approach that serves the intended purpose which is to arrange n and p-type pellets in a couple and forming a junction between them with a platted copper tab. With this configuration it is possible to pump all the heat in the same direction.

As shown in Figure 4.4, with the bottom of the p-type pellet connected to the positive pole of the voltage source we are able to reverse the direction of the charge carriers and with this we are able to pump all the heat in the same direction. In this configuration the electrons in the n-type pellet are repelled by the negative pole of the source and flow into the copper plate. When they reach the p-type material they simply flow through the holes and into the positive pole of the source. The “holes” from the p-type pellet are repelled by the positive pole and drawn into the negative pole of the supply. This way, the heat and the charge carriers are both flowing into the same direction through the pellets (bottom to top). Using this configuration it is possible to arrange multiple pellets with this configuration

and pump a considerable amount of heat. Furthermore, with the electrical wiring in series this configuration is suitable for DC power supplies. Thus the most common thermoelectric devices nowadays, connecting 254 alternating n and p-type pellets, can run from 12 to 16VDC supply and draw 4 to 5A, rather than 1270A at 60mV, for example (Figure 4.5).

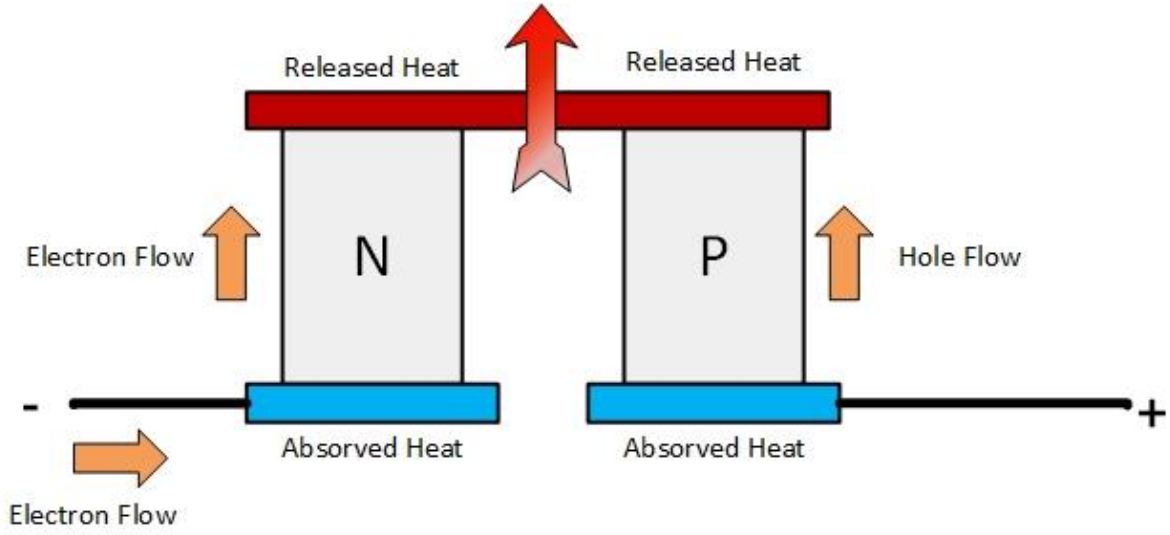

Figure 4.4 – Single N-P-type pellet

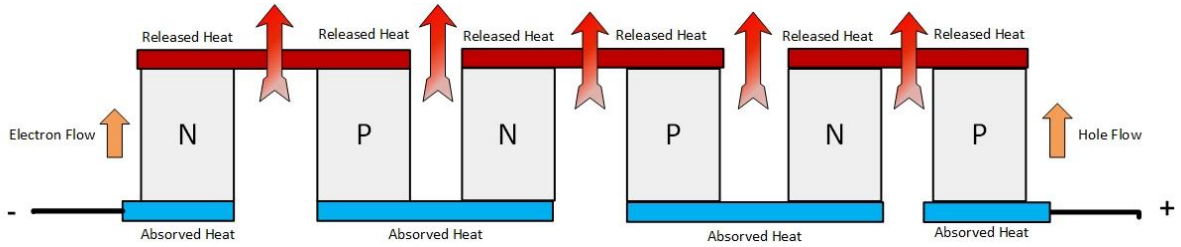

Figure 4.5 – Multiple N-P-type pellets

When manufacturing devices with multiple pellet arrays, one must have the means to mechanically hold everything together. The industry standard solution is to use thin ceramic substrates mounted on both sides of the conductive tabs (Figure 4.6). Besides providing protection against mechanical external forces, the ceramic substrates also act as the thermal interface between the Peltier cell and its surrounding. These have become the industry standard because they represent the best compromise between mechanical strength, electrical resistivity, thermal conductivity and cost.

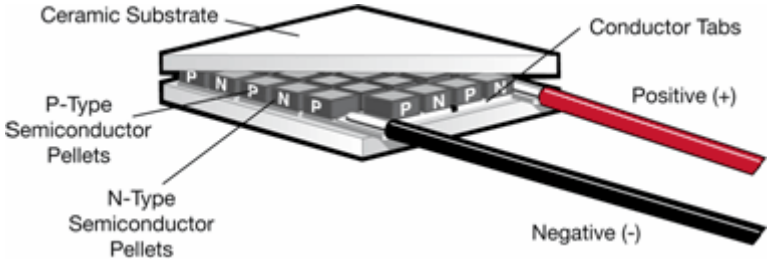

Figure 4.6 – Typical Configuration of a Peltier device [56]

4.4 Thermoelectric Cooling

With the configuration shown in Figure 4.5, the thermoelectric power of these devices is large enough to be of practical interest for electronic cooling, particularly where the absence of moving parts and the strong restriction to use small size components are issues of vital importance.

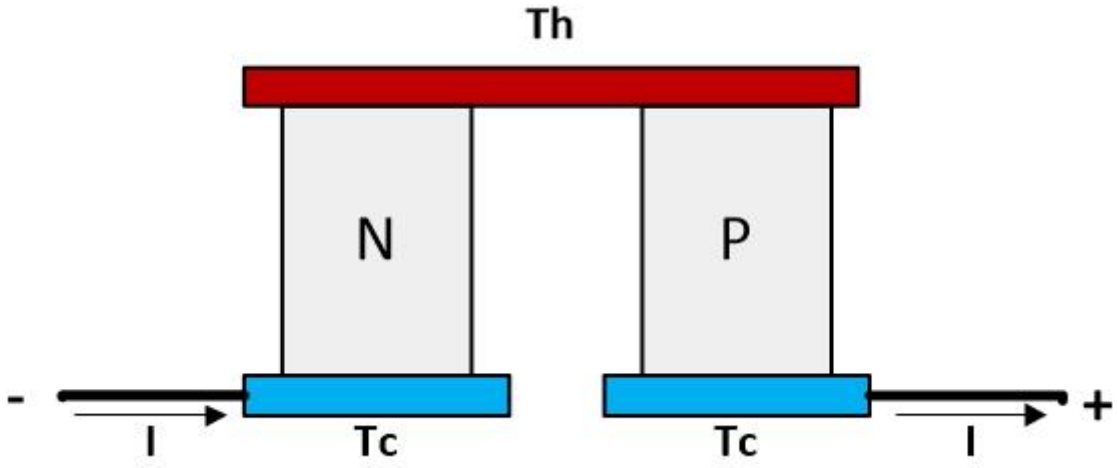

Figure 4.7 – Current Flowing through N-P junction

The current I in Figure 4.7 pumps heat from bottom (cold) junction to the top (hot) junction, cooling it by ΔT below the temperature of the hot junction ($\Delta T = T_h - T_c$). The cooling effect of Peltier cells is reduced by Joule effect and thermal conductance of the material used. The heat removed at the cold junction is expressed as [26, 55, 30, 31, 27]:

$$\dot{Q}_c = 2N[s\ I\ T_c - \frac{1}{2}I^2\frac{\rho}{G} - kG\Delta T] \quad (4.1)$$

or

$$\dot{Q}_c = 2N[PI - \frac{1}{2}I^2\frac{\rho}{G} - kG\Delta T] \quad (4.2)$$

where, $\dot{Q}_c$ is the heat removed from the cold junction,

s is the Seebeck Coefficient,

ρ is the electrical conductivity of the semiconductor,

k is the thermal conductivity,

N is number of pairs of thermoelectric elements

G is area/length of thermoelectric cell,

P is the Peltier Coefficient ($P = S\ T_c$).

The factor $\frac{1}{2}$ of Joule effect comes from the equation of heat-transport. The equation 4.1 is easily explained by Figure 4.8. Also there is the thermal conductance where heat naturally moves to colder regions when there is a temperature gradient. For simplicity, one can define [27]:

$$S_m = 2Ns \tag{4.3}$$

$$R_m = 2N\frac{\rho}{G} \tag{4.4}$$

$$K_m = 2N\frac{k}{G} \tag{4.5}$$

where s, ρ and k are physical properties of the thermoelectric materials and S_m, R_m and K_m are physical characteristics of Peltier cell as devices, i.e., the latter depend on the geometry, dimensions and the arrangement of the pairs of thermoelectric elements. With equations 4.3, 4.4 and 4.5, equations 4.1 and 4.2 can be rewritten as

$$\dot{Q}_c = S_m\, I\, T_c - \frac{1}{2}I^2R_m - K_m\Delta T \tag{4.6}$$

and

$$\dot{Q}_c = P_m\, I - \frac{1}{2}I^2R_m - K_m\Delta T \tag{4.7}$$

Similar equations can be used for the heat power released at the hot side junction, where the Joule effect adds heat to the equation:

$$\dot{Q}_h = S_m I\, T_h + \frac{1}{2}I^2R_m - K_m\Delta T \tag{4.8}$$

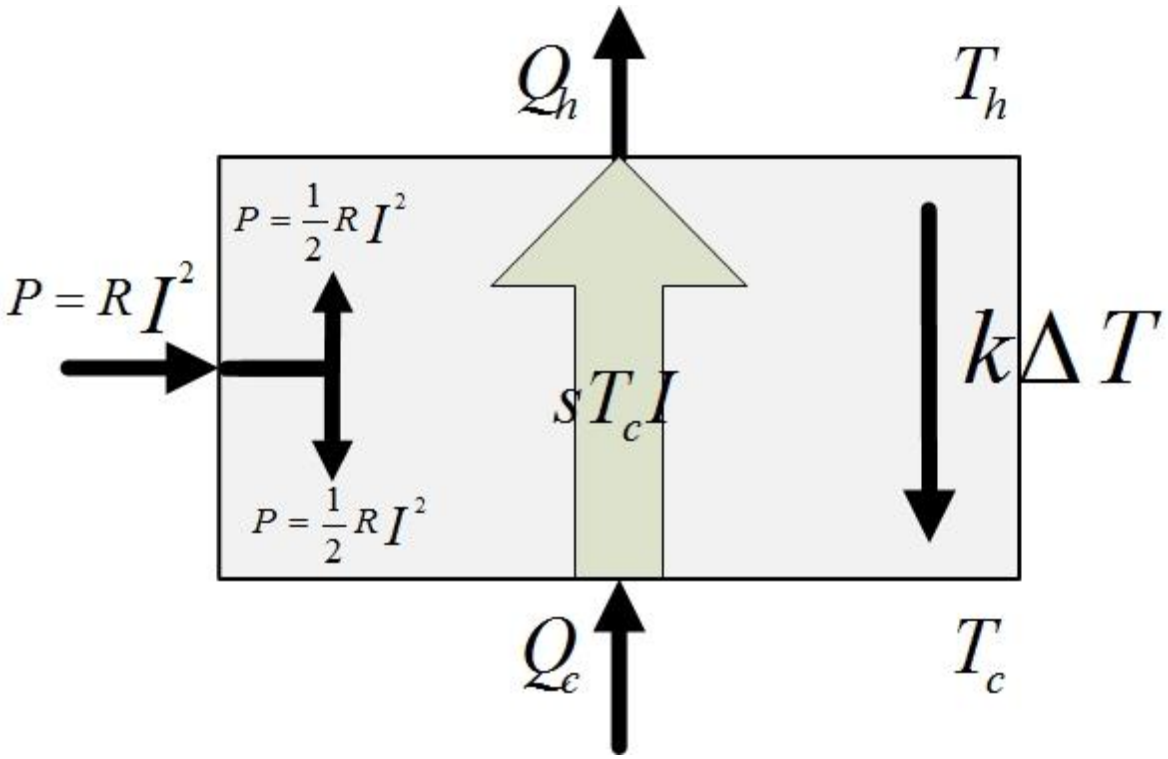

Figure 4.8 – Heat flow through a Peltier cell

The Joule effect is simply the result of the electrical power supplied to the system which is the product of the current and voltage. These magnitudes are not related by a constant resistor value like in other electronic circuits, since for a given current, the required voltage depends on the temperature

of the system, given that ρ depends on the temperature.

$$P = VI \tag{4.9}$$

So the power balance equation will be given by:

$$P = \dot{Q}_h - \dot{Q}_c \tag{4.10}$$

$$VI = S_m I\, T_h + \frac{1}{2} I^2 R_m - K_m \Delta T - S_m I\, T_c + \frac{1}{2} I^2 R + K_m \Delta T \tag{4.11}$$

$$VI = R_m I^2 + S_m (T_h - T_c) I \tag{4.12}$$

Therefore the simplified equation for the voltage across the Peltier cells is:

$$V = R_m I + S_m \Delta T \tag{4.13}$$

This equation is very important when estimating R_m and S_m from the performance curves of Peltier cells manufacturers. Usually, a certain ΔT is obtained for a given voltage and current, for different values of $\dot{Q}_c$. Equation 4.13 contains just two parameters that can be easily estimated knowing the V, I and ΔT. After obtaining R_m and S_m, other physical properties (s, ρ and k) can be derived directly.

In datasheet curves, only two extreme situations are represented, $\Delta T = 0$ and $\dot{Q}_c = 0$, since all others are in between. These situations are presented as the maximum achievable ΔT occurs when no heat is being transported. Reversely, the maximum amount of heat ($\dot{Q}_c$) is absorbed at $\Delta T = 0$, i.e., $T_h = T_c$. Therefore assuming $\Delta T = 0$, equation 4.13 becomes $V = R_m\, I$:

$$R_m = \frac{V}{I} \tag{4.14}$$

Knowing the maximum amount of heat pumped Q_c, which usually is one of the key parameters given by the manufacturers, it is possible to apply to equation 4.6

$$\dot{Q}_c = S_m\, I\, T_c - \frac{1}{2} R_m I^2 \tag{4.15}$$

And obtain the value S_m from

$$S_m = \frac{\dot{Q}_c - \frac{1}{2} R_m I^2}{I\, T_c} \tag{4.16}$$

Finally, the last characteristic of the module is parameter K_m, related to thermal conductivity. In this case, assuming $\dot{Q}_c = 0$, equation 4.6 becomes

$$K_m = \frac{S_m\, I\, T_c - \frac{1}{2} R_m I^2}{\Delta T} \tag{4.17}$$

4.5 Selection of the Peltier cells: Relevant characteristics and procedures

There are several characteristics that one must take into account when selecting the appropriate Peltier cell to use. The key parameters usually given in a datasheet are $\dot{Q}_{c_{max}}$, ΔT_{max}, V_{max} and I_{max}. The most relevant is the amount of heat ($\dot{Q}_{c_{max}}$) the Peltier cell can remove. One must ensure that $\dot{Q}_{c_{max}}$ is higher than the maximum amount of heat $\dot{Q}_c$ generated by the system to be cooled. The next step is to determine the current (I) required to remove $\dot{Q}_c$ and to generate the desired ΔT. By knowing the power consumed $P = VI$ to remove $\dot{Q}_c$ one can estimate the Coefficient of Performance (C.O.P.)

$$C.O.P. = \frac{\dot{Q}_c}{P} \tag{4.18}$$

It is not unusual to have a C.O.P. lower than one, i.e., consuming more power than the power removed. Peltier cells are inefficient in comparison to other cooling solutions, like vapour-compression systems. Their advantage is the precise control of temperature and being almost independent of the ambient temperature. However, with careful design of the system one can easily rise the C.O.P to values higher than 1.5. This can be achieved, for example, by using a Peltier device with a $\dot{Q}_{c_{max}}$ much higher than $\dot{Q}_c$. Assume two different Peltier devices, number one with $\dot{Q}_{c_{max}} = 80W$ and number 2 with $\dot{Q}_{c_{max}} = 300W$. If they should remove a $\dot{Q}_c = 60W$, the device number two will probably have a higher C.O.P. than number one. This happens because number one is much closer to its maximum potential than number two. While it is true that as one increases the current supplied to the Peltier device so increases the amount of power that the Peltier device is able to remove, after a certain current, the additional power gained is outweighed by the additional heating (Joule effect) generated by the device itself. Given that device number one is much closer to its potential, its Joule effect will be larger than that of number two.

Another way to increase the C.O.P. is to change the number of Peltier cells one is going to use. For example, assume a Peltier device that can remove 60W with 5A and 30W with 2.2A. For 30W the current drawn is not 2.5A because the amount of heat removed by the cell in nonlinear with the power given, i.e., they are more inefficient as they reach their potential. If one chooses to use to use 2 Peltier cells of the same model in thermodynamic parallel we are able to remove 60W with 2.2A each (4.4A total instead of 5A). This allows removing the same amount of heat with lower power given to the cells, which results in lower Joule effect and consequently in a higher C.O.P..

Chapter 5

Experimental Apparatus, Procedures and PID Controller

This chapter starts by presenting in section 5.1 the conceptual design of the system, its main components and requirements. To achieve a practical system it is important to understand and characterize the Peltier cells. In this context, an additional setup had to be developed for accomplishing with this characterization and with the design of the control system, which is presented in section 5.2. This setup is already a good approximation of the final system. Finally, a preliminary configuration of the final setup for the use of the cooling system in a personal computer is proposed in section 5.3.

The characterization tests of the Peltier cells, PID controller gains and final setup were performed following well established experimental procedures, which are described in section 5.4.

5.1 Conceptual Design

The conceptual design of the system is represented in Figure 5.1, which is mainly composed by a CPU, a pool, a Peltier cell, a dissipator and a fan. Furthermore, it is vital a control system.

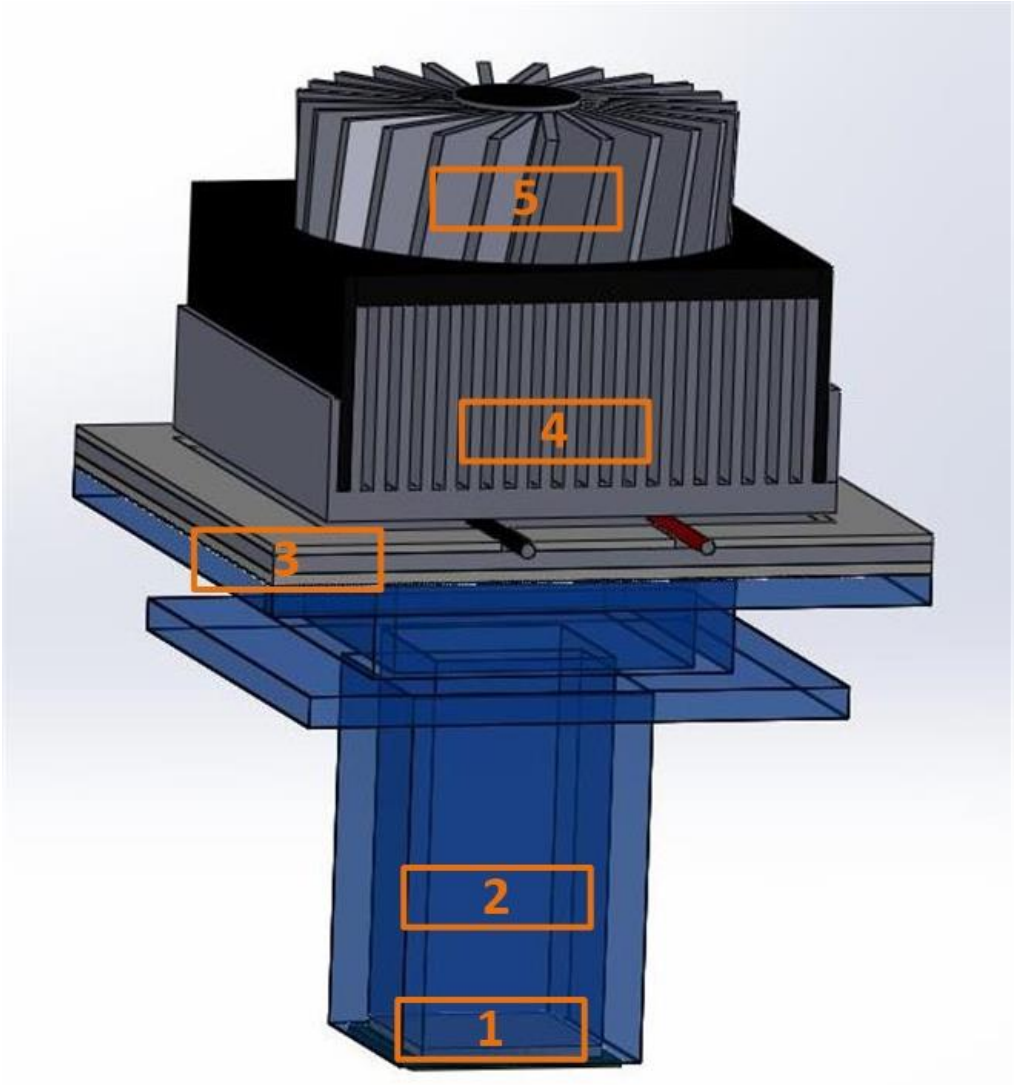

Figure 5.1 – Conceptual design. The numbers identify each of the aforementioned essential components of the system, 1 - CPU, 2 - Pool, 3 – Peltier cell, 4 – Dissipator, 5 - Fan.

Each component of the system was chosen carefully to satisfy the various requirements that the system must meet. The following paragraphs will explain the reasoning for the selection of each component and its requirements.

5.1.1 Central Processing Unit (CPU)

The purpose of the larger project in which this work is inserted is to develop a cooling system

for the latest generation of personal computers. However, a Pentium 4 2.4B GHz was chosen for the first tests since there was already a prototype of the pool designed for this processor. Also, the thermal management problems observed in the Pentium 4 processors [57] are well known, so this processor can already be a test to the cooling system developed here.

5.1.2 Pool

In the initial prototype, the pool was designed taking into account thermodynamical requirements. The purpose of the initial design was to be the simplest possible, and to demonstrate the feasibility of the cooling system. The pool was made of acrylic due to its thermal isolating properties. Some thermodynamical requirements were satisfied, although without an extensive study of the dimensions required. Given that the CPU is surrounded by other components, the minimum height of the pool was restricted to 60mm. The size of the condensation surfaces was chosen to ensure that all the fluid mass at the most demanding cooling conditions was condensed for a given ΔT imposed by the Peltier cells.

5.1.3 Peltier Cell

Several characteristics must be taken into account when choosing a Peltier cell. As previously explained in section 4.5, the most relevant is the maximum amount of heat that can be removed by the device ($\dot{Q}_{c_{max}}$). One must ensure that the maximum possible heat generated ($\dot{Q}_c$) by the system is lower than $\dot{Q}_{c_{max}}$. Two other relevant characteristics are: the energy consumed by the device and the internal heat generated by its functioning (Joule effect). When choosing a Peltier cell, one must take into account how to supply the energy required for the device to remove a defined amount of heat. There are several ways to supply the energy required by the device: pulse-width modulation (PWM), with voltage source or with current source. Peltier cells work on current but usually have significant enough resistance so that voltage control is possible. Running the Peltier cell with pulses is a bad choice, particularly in cooling applications: while cooling increases with increasing current, efficiency is reduced as the current increases. The cooling effect is proportional to the current, but the Joule effect is proportional to the square of the current (RI^2). Above a determined current, the Joule effect outweighs the additional cooling power obtained by the higher current. Therefore, to PWM a Peltier device between 0 and the maximum cooling current is not desired. By PWM a Peltier device one would be alternating between off and a state of the Peltier cell which is extremely inefficient because at the maximum cooling current the Joule effect clearly outweighs the heat removed. Finally, if thermally cycling occurs as a part of the control process, the mechanical wear will strongly reduce the lifespan of the device. Since Peltier devices work on current, a current control approach is preferred to a voltage control. Section 5.2.5 will provide an additional reason why it was chosen to control the Peltier device by imposing current.

The Joule effect is relevant when choosing a Peltier device because, if the device chosen has a $\dot{Q}_{c_{max}}$ very close to the heat being removed, the device will be running close to its maximum

potential and Joule effect will increase significantly, resulting in a very poor C.O.P. (as defined in Section 4.5, eq. 4.18) and creating several difficulties to dissipate the total heat of the system (as the amount of heat to be removed to cool the device is added to a significant amount of heat that is dissipated in the cell by Joule effect). This is a very important factor to be taken into account since, if the characteristics and working conditions of the cells are not carefully chosen, the Joule effect may imply the use of much powerful additional systems to cool the cells, which would overcome the advantage of using the Peltier cells, thus jeopardizing the implementation of the current cooling configuration.

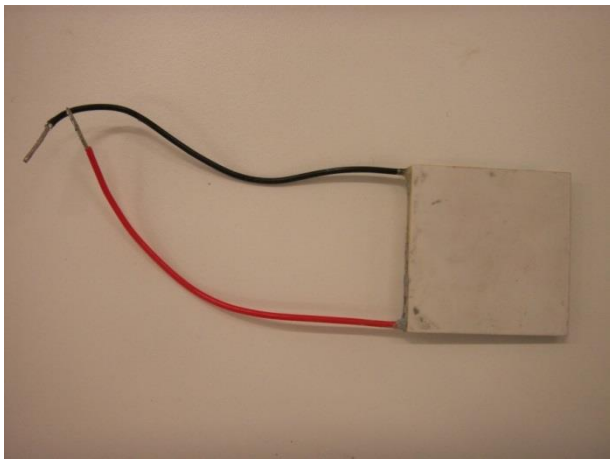

Figure 5.2 – Multicomp MCPF-127-14-11-E

The Peltier device used in the following setups is the MCPF-127-14-11-E, depicted in Figure 5.2, manufactured by Multicomp. Its most relevant characteristics are presented in Table 5.1. However, this Peltier cell was our second choice. The first choice was the TEC1-26316 manufactured by Hebei which has $\dot{Q}_{c_{max}} = 300W$ and $\Delta T_{max} = 66ºC$. This was first selected taking in mind the Thermal Design Power (TDP) of the latest generation personal computer which is higher than 150W. This would give a greater flexibility and a better C.O.P. as explained in section 4.5. After some preliminary tests, one concluded that a very efficient cooling of the Peltier cell was required to remove the significant additional amount of thermal energy which was generated by Joule effect. Another problem raised in the use of the TEC1-26316 cells was the high current drawn ($I_{max} = 16A$), which is higher than most power supplies available could output. Instead, the MCPF-127-14-11-E was used because its $\dot{Q}_{c_{max}} = 79W$ is higher than the TDP of the CPU we intend to test (59W), which could still assure flexibility. Its maximum current was 8.5A which is a much more reasonable and safe value to work with, particularly when compared to the 16A required by the TEC1-26316.

As explained in section 4.5, the use of two Peltier devices instead of one allows reducing the Joule effect of the system and hence improving the C.O.P. One of the requirements of the condensation system is to generate a ΔT around 8-10ºC on the top of the pool so that condensation of HFE-7000 is ensured. This ΔT is a typical reference value so that condensation occurs. According to preliminary results from the characterization of the Peltier cells, while removing 30W with a current of 6A, the T_c of the Peltier device was at 30ºC. Hence, to remove the 59W of the Pentium 4, two Peltier

cells would be needed. Only by using two Peltier cells one could remove the 59W released by the CPU and create a temperature difference large enough so that condensation could occur.

Table 5.1 - Multicomp MCPF-127-14-11-E Characteristics

Manufacturer Reference	MCPF-127-14-11-E
Power Rating	79W
Internal Resistance	1.59Ω
Current Max at ΔT_{max}	8.5A
Voltage Max at ΔT_{max}	15.7V
ΔT_{max}	70ºC
External Length / Height	40mm
Solder Melting Point	232ºC

5.1.4 Zalman CNPS7500-AlCu LED Fan

The fan used was the CNPS7500-AlCu LED, depicted in Figure 5.3, manufactured by Zalman. The purpose of the fan is simply to dissipate the additional amount of heat which is generated by Joule effect in the Peltier cell. This fan was chosen because of its good performance/price ratio. The base material is composed by pure copper and pure aluminium. Its dimensions are 121mm (Length) x 121mm (Width) x 67mm (Height) with a weight of 500g. The dissipation area (fins area) is $3500cm^2$. The fan operates at 2,550rpm (34,5dBA) if connected directly to the power supply without the use of Fan Speed Controller FAN MATE2.

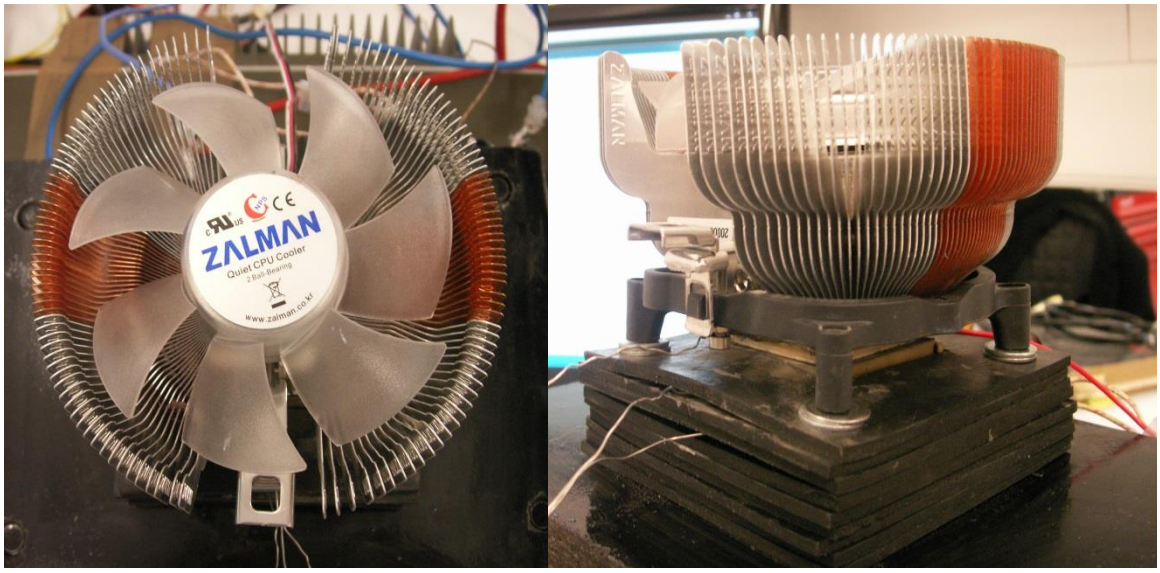

Figure 5.3 – Zalman CNPS7500-AlCu LED

5.2 Peltier cell characterization setup

The design of a controlled condensation system, using Peltier cells requires an accurate characterization of the cells, which is fundamental to obtain several characteristic parameters, such as the internal resistance R_m, the Seebeck coefficient S_m and Thermal Conductance K_m. The dynamic response of the cell in time is also important, as further discussed in the results in sub-section 6.1.1. These properties must be known a priori, so these tests cannot be performed in the final setup.

Confirming the characteristics of the selected cells under real operating conditions is also a crucial step, as the data provided in the datasheet are often obtained at testing conditions quite different from ours. Actually, the temperature, which is a key parameter, is significantly different since in datasheets, the performance curves are usually given for a fixed temperature (T_h) of the hot surface, which is very difficult to obtain in a real application.

In this context, an additional setup was developed. This setup is a simplified version of the conceptual design, in which the CPU was replaced by a resistance regulated by a potentiometer. This was done so that one could impose a well-defined heat power. Also, the pool was omitted from this setup, since the main purpose is to characterize the Peltier device itself and not its performance under the configuration for which the cells are used for liquid condensation. All tests were performed with a single Peltier device cooled by one fan.

The setup used is represented in Figure 5.4, in which the main components are identified by numbers. As aforementioned, the CPU was replaced in this setup by a resistance of 823Ω (1 in Figure 5.4) regulated by a potentiometer (2 in Figure 5.4). The potentiometer was connected directly to the power grid, so alternating current was flowing through the resistance. In this way, one could determine at any given time the $\dot{Q}_c$ removed by the Peltier cell, which equals the power imposed to the resistance. This resistance is thermally isolated with natural rubber. The calibration of the potentiometer was made by measuring the voltage and current flowing at the entrance of the resistance with the use of two different multimeters. The multimeter Range RE-68, identified by the number 3, measured the alternating current and the multimeter Xindar DB600.031, identified by the number 4, measured the alternating voltage. Figure 5.5 shows the potentiometer used. The multimeter RE-68 has an accuracy of +-0.5% for DCV, +-0.8% for ACV, +-1.2% for DCA and +-1.2% for ACA.

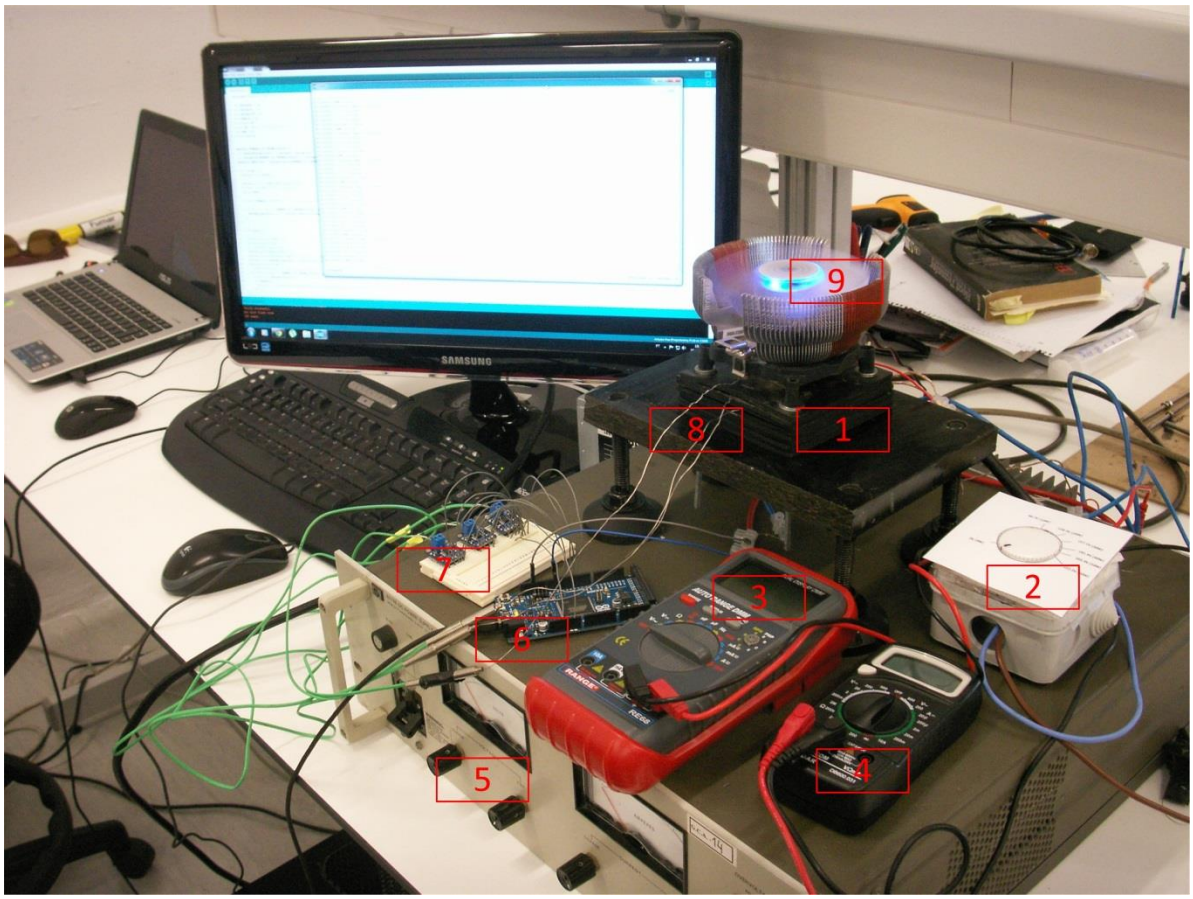

Figure 5.4 – Setup developed to characterize the Peltier cells

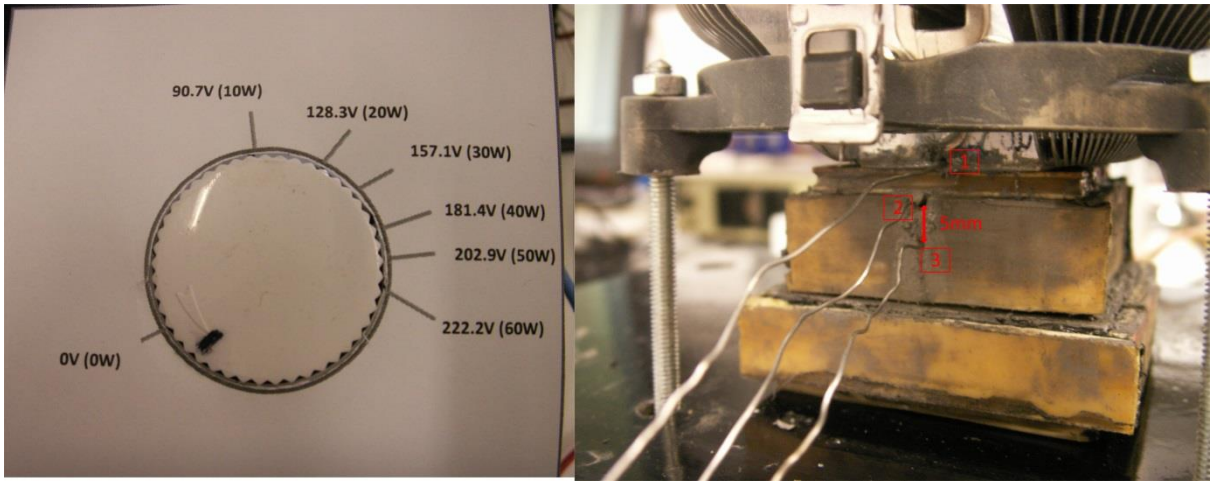

Figure 5.5 – Potentiometer and Thermocouples placement in the resistance

This resistance is inserted in a stainless steel block over which the Peltier cell is placed, being in contact with the cold surface of the Peltier cell. The hot surface of the cell is in contact with the fan. The entire block is isolated with rubber to assure that the heat flux is mainly directed upwards and to minimize the heat losses to the environment. Three type K thermocouples are inserted to acquire the temperature of the steel surface, the temperature of the cold surface (number 2 in Figure 5.5) and the temperature of the hot surface (number 1 in Figure 5.5) of the Peltier cell. The thermocouples are positioned at 1mm below and above the cold and hot surfaces of the Peltier cell, respectively. The

third thermocouple (number 3 in Figure 5.5) is placed 5mm below the one measuring the cold surface. The third thermocouple was placed to evaluate the heat flux imposed by the resistance. Due to the accuracy of the assembly thermocouple+acquisition system this method would have generated considerable mistakes in the final results. Hence, the thermocouple was used only for monitoring purposes. Nevertheless, during the test it has been considered an heat loss through the isolation of the system of about 10% of the power imposed.

The characteristics of the Peltier cells that were used here are presented Table 5.1. To have a controlled condensation system, one must be able to remotely control the amount of current given to the cells, by the power supply. Following this, several options were taken into consideration, namely:

- Power supply controlled by a PC through a GPIB interface
- Power supply remotely controllable by a voltage/resistance reference
- Modified Computer Power supply
- Transformer design

The easiest solution to implement was the power supply with GPIB interface. However, these power supplies are usually expensive in comparison to the other solutions and there was not any power supply available with the adequate characteristics, which met the target maximum current of 8.5A.

The second option consisted in using an analog power supply remotely controllable by a voltage/resistance reference. This option was easy to implement, since there was a power supply available which met the requirements. However, one would have to choose a suitable device that would generate the voltage/resistance reference.

Given that the purpose of the project in which the present thesis is included is to create a commercial product, these two options were not commercially viable. Another option considered was to modify a computer power supply to draw the current output required. However, we do not want to generate a fixed value, so considerable study of the current computer power supplies was needed and additional electrical circuitry was required, whose complexity was out of the scope of the present work. The final option considered was to develop from scratch a transformer specific for this Peltier device. This would be the ideal solution and the most appealing from the commercial perspective. However, after considerable counseling we concluded that it was not viable, as its development was also significantly complex and time consuming, being, once again out of the main objectives of the present work.

After considering the benefits and drawbacks of each solution, in addition to the fact that by that time it was not yet demonstrated that the cooling system proposed was thermodynamically viable to be worth a considerable effort developing a specific power supply, it was decided to use an analog power supply remotely controllable by a voltage/resistance reference. This was the ideal solution fulfilling all the requirements. In addition, from all the solutions which were possible to implement within the time window of this project, this is also the most appealing from the commercial perspective.

The power supply available was the Hewlett Packard 6274B DC Power Supply (5 in Figure 5.4). Details of front and back panels, showing the connections to use for our specific application are given in Figure 5.6. The output of this power supply is 0-60V at 0-15A. It can be either operated in constant voltage or constant current. Optional operating modes are: remote voltage sensing, remote programming, auto-parallel operation, auto-series operation and auto-tracking operation. The operating mode suitable for this work is the remote programming. In remote programming, the output voltage or current can be remotely controlled by connecting an external resistor or applying an external voltage to rear panel terminals. The programming coefficients for each of these solutions are presented in Table 5.2. Considering that, as mentioned earlier, the Peltier devices should preferably be used in constant current and that the coefficient for constant voltage output with a voltage input was unitary, which would require another power supply to control, only two of the four options were viable. The option chosen was constant current output controlled by a voltage input (marked at bold in Table 5.2) because the values of input were more reasonable and easier to provide. The electronic device chosen to generate the programmed voltage input was the microcontroller Arduino Due [58].

Table 5.2 - Remote programming coefficients

Constant Voltage Output, Resistance Input	200Ω/V
Constant Voltage Output, Voltage Input	1V/V
Constant Current Output, Resistance Input	67Ω/A
Constant Current Output, Voltage Input	**33.3mV/A**

Figure 5.6 – Hewlett Packard 6274B DC Power Supply and Rear-Panel connections

Several reasons were taken into consideration when choosing the use of an Arduino Due (Figure 5.8):

- it allows creating a voltage reference up to 3.3V by PWM or through the use of the incorporated 12 bits Digital-Analog Converter,
- It also allows incorporating the PID controller made in software used to control the Peltier device, which will be explained in section 5.3.
- Readings from the thermocouples used to acquire the temperature of both surfaces of

the Peltier device could easily be integrated with the Arduino.

- Furthermore, since the minimum interval between readings used was 1s, the Clock Speed of 84MHz allowed implementing thousands of instructions between each reading. The 512KB of flash memory for code were more than enough. Also, there is much documentation about numerous applications using Arduino as microcontroller making it easier to use.

The main characteristics of the Arduino Due are presented in Table 5.3 [58].The Arduino Due contains a 12bit Digital-Analog Converter (DAC) which allows creating a voltage reference. Later, one realized that the DAC only allow creating an analog voltage between 1/6 (0.55V) and 5/6 (2.75V) of the input voltage (3.3V) of the Arduino Due, surpassing the limit of the HP 6274B which was 500mV ($\frac{33mV}{A} * 15A = 495mV$). Hence, PWM was the method chosen to generate the voltage reference needed to remotely control the HP 6275B between 0-500mV. Having a 12bit PWM output instead of the 8bit PWM output of Arduino Uno, allows a better accuracy when generating a voltage reference.

Table 5.3 – Main characteristics of Arduino Due

Microcontroller	AT91SAM3X8E
Operating voltage	3.3V
Input Voltage (recommended)	7-12V
Digital I/O Pins	54 (of which 12 provide PWM Output)
Analog Input Pins	12
Analog Output Pins	2 (DAC)
Total DC Output current in all I/O lines	130mA
DC Current for 3.3V and 5V Pin	800mA
Flash Memory	512 KB all available for user applications
SRAM	96 KB (two banks: 64 KB and 32 KB)
Clock Speed	84 MHz

Finally, the Arduino is responsible for reading the temperature and accordingly act for implementing a PID controller and generates a voltage reference that will result in a higher/lower current to the Peltier cells. This way, the condensation system is independent of the system to be

cooled. In this work, the application chosen was the cooling system of a personal computer, but the cooling system with the Peltier cells, and the PID controller, is designed to be easily adjusted to other applications.

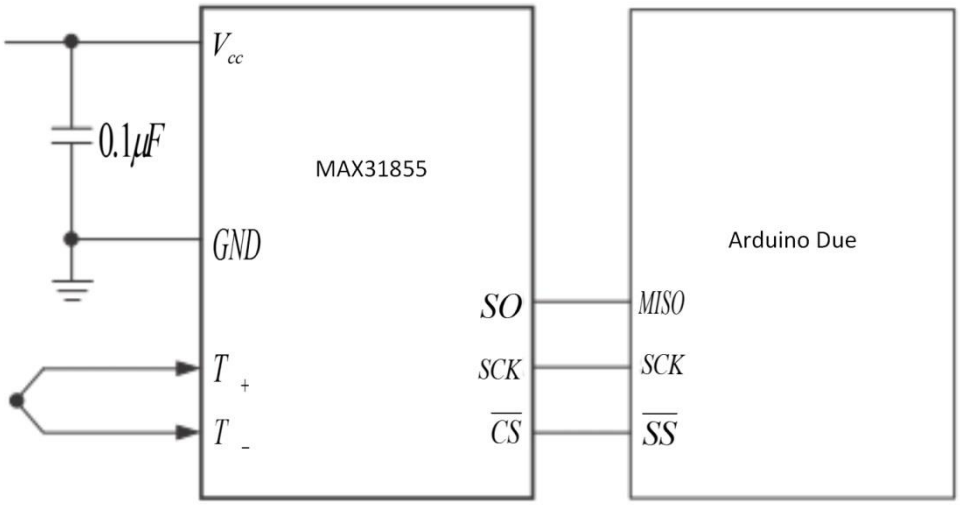

Figure 5.7 - Schematic of connections between MAX31855 and the Arduino Due

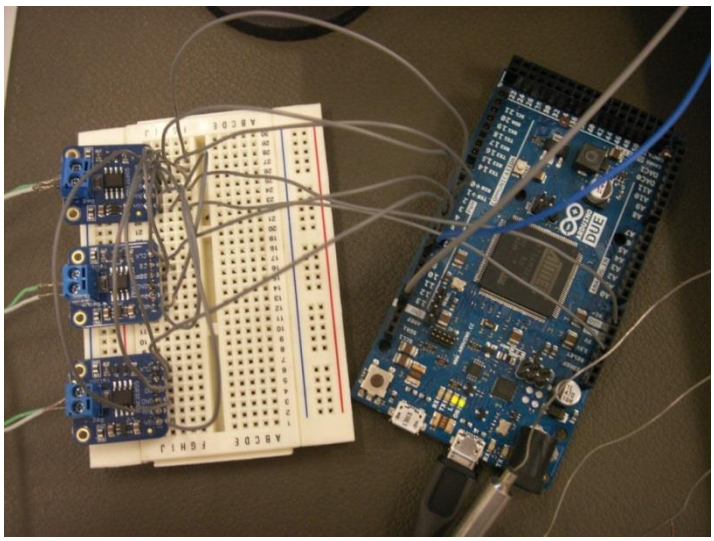

Figure 5.8 – Arduino Due

Maxim MAX31855 was used for the integration of the thermocouples readings with Arduino. Three of these circuits are mounted on the breadboard, as shown in Figure 5.8. The Maxim Integrated MAX31855 is a sophisticated thermocouple-to-digital converter with a built-in 14-bit analog-to-digital converter (ADC). The device also contains cold-junction compensation sensing and correction, a digital controller, an SPI- compatible (Serial Peripheral Interface) interface, and associated control logic. The device is designed to work in together with an external microcontroller in thermostatic, process-control, or monitoring applications.

This converter has a resolution of 0.25ºC, allows reading values as high as 1800ºC and as low

as -270ºC, and exhibits thermocouple accuracy of +-2ºC for temperature ranging from -200ºC to 700ºC for K-type thermocouples. Several specifications are presented in Table 5.4. The schematic of connections between the IC MAX31855 and the Arduino Due is presented in Figure 5.7 In this setup, three integrated circuits were used, to get the reading of the three thermocouples. As referenced in the product datasheet, if multiple MAX31855 are used, all pins can be shared in the microcontroller except $\overline{CS}$.

Table 5.4 - MAX31855 Specifications

Supply Voltage Range	-0.3V to 4.0V
Operating Temperature Range	-40ºC to 125ºC
Junction Temperature	150ºC
Thermocouple Gain and Offset Error	+-2ºC
Thermocouple Temperature Data Resolution	0.25ºC
Internal Cold-Junction Temperature Error	+-2ºC
Cold-Junction Temperature Data Resolution	0.0625
Temperature Conversion Time	70ms

5.3 Final Setup

To test the feasibility of the condensation system implemented, a preliminary cooling setup was developed, which was in a personal computer (PC), as depicted in Figure 5.9. In this setup, the CPU device (number 1) used is a Pentium 4 operating at 2.40GHz. As mentioned earlier, since the cooling system is independent of the CPU used, this can be replaced by a more powerful one in the future, with minor modifications. The geometry of the pool was redesigned for the implementation of two Peltier cells in order to optimise the condensation process. A complete overall picture of this setup is shown in Figure 5.9. The number 2 is the redesigned pool to optimize the condensation system. Number 3 are the fans used. The Peltier cells cannot be seen in the figure because they are positioned between the pool and the fans. Device number 4 is the Arduino Due, device number 5 the breadboard with the three MAX31855 and finally device number 6 is the power supply HP 6274B.

The CPU used in this setup is the Intel Pentium 4 2.4B GHz, with 512KB of L2 Cache and 533MHz Front-Side Bus Speed. Its lithography is 130nm, and the maximum thermal design power is 59.8W. The package size is 35mm x 35mm and the socket supported is the PPGA478.

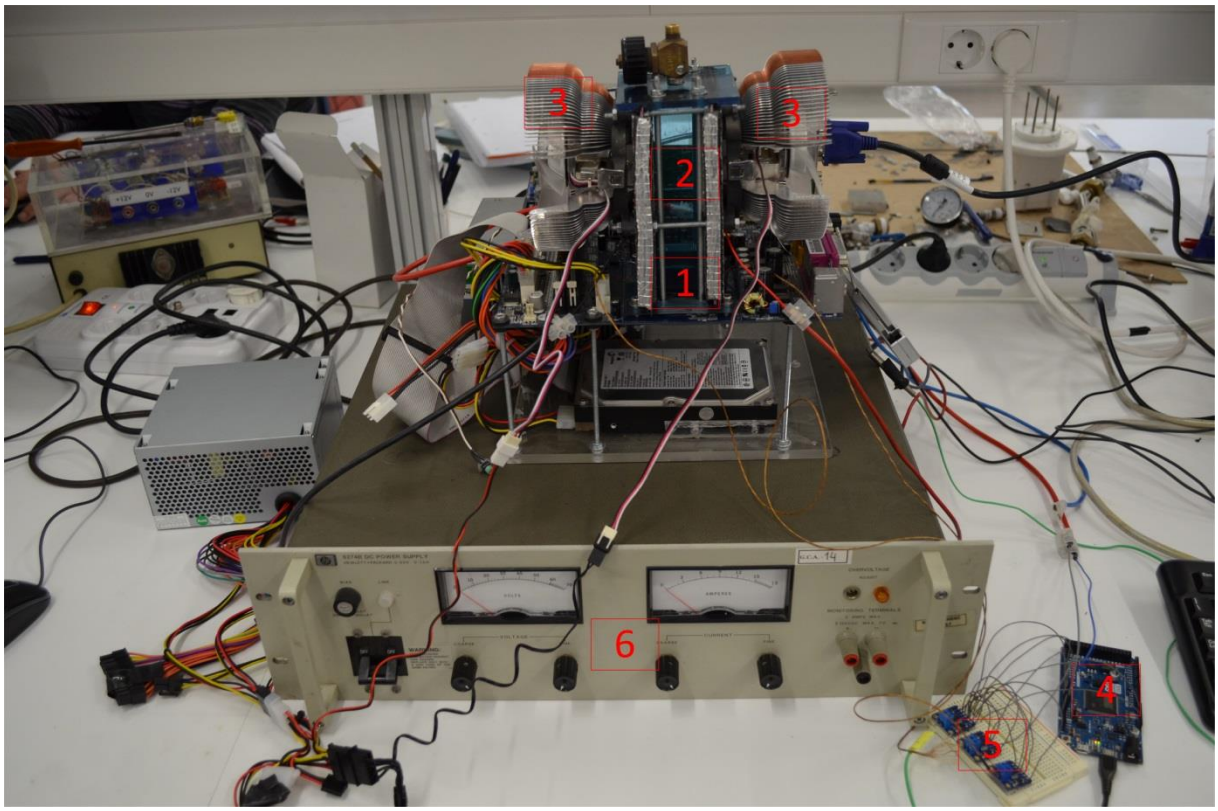

Figure 5.9 – Final Setup

In Figure 5.10 is presented the schematic of the final setup. In this schematic there are two distinct sub-systems: cooling system and controlling system. The cooling system is composed by the CPU that is immersed in a pool of HFE-7000. The bottom of vertical walls of the pool are isolated from the fluid by a layer of rubber while the upper part is composed of aluminum which internally is used to condense the vapour and externally is in contact with the Peltier cells. The Peltier cells are cooled by the fans and have a thermocouple measuring the temperature of the external side of the aluminum wall.

The controlling system is composed by the power supply HP6274B which supplies the current to the Peltier cells that are connected in electrical series. The power supply is controlled by the Arduino Due through a voltage reference. The Arduino Due obtains the temperature readings of the thermocouple through the use of IC MAX31855.

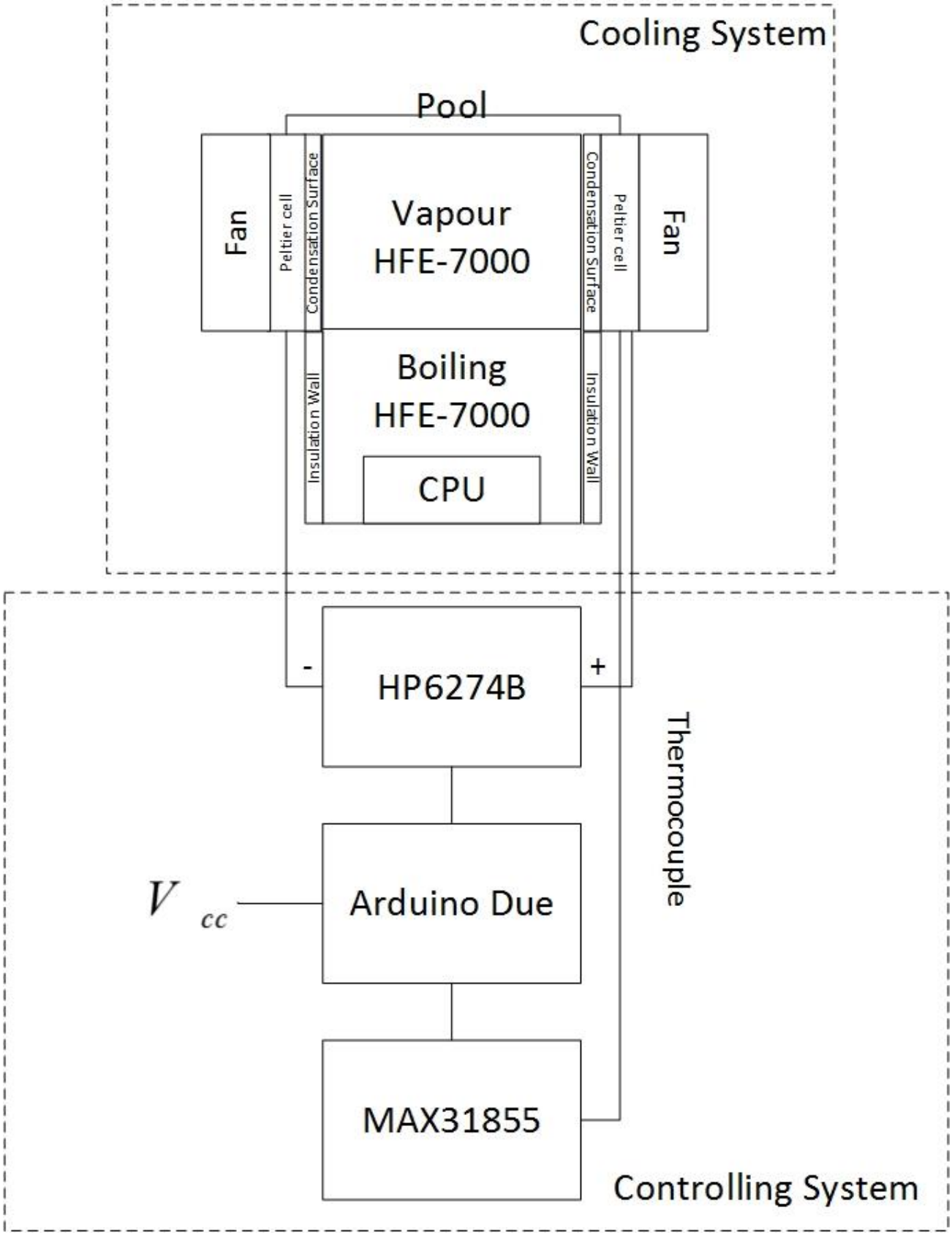

Figure 5.10 - Schematic of the final setup

5.3.1 Final Pool

To maximize the condensation area and to take the most out of the Peltier cells performance without taking them to extreme working conditions, the pool configuration chosen to test the final set-up considered the use of 2 Peltier cells mounted vertically on each side wall of the pool.

The dimensioning, fabrication and assembly of the pool have been perfomed taking into account thermodynamic and geometrical constraints related with the particular application. Extreme attention had to be paid in how to fix the assembly pool/fans/peltier cells and how to proper positioning it on top of the CPU taking into account the presence of the others components of the motherboard. In Figure 5.11 and Figure 5.12 depict the global view and the typical dimensions of the assembly pool/fans/peltier cells.

The dielectric liquid (HFE 7000) contained inside the pool is directly in contact with the CPU and starts to boil as soon as the computer starts to work. Then it condenses mostly on the vertical aluminum walls that are constantly cooled by mean of the Peltier cells. The fans are then used to cool the Peltier cells during the application. The aluminum walls are in contact in the internal side with the condensing vapour for an area of 40x115 mm^2. To avoid external environmental influence, the aluminum walls are insulated all around the Peltier cells. Figure 5.13 highlightst a detail of the coupling Fan/Peltier/Insulation/aluminum wall.

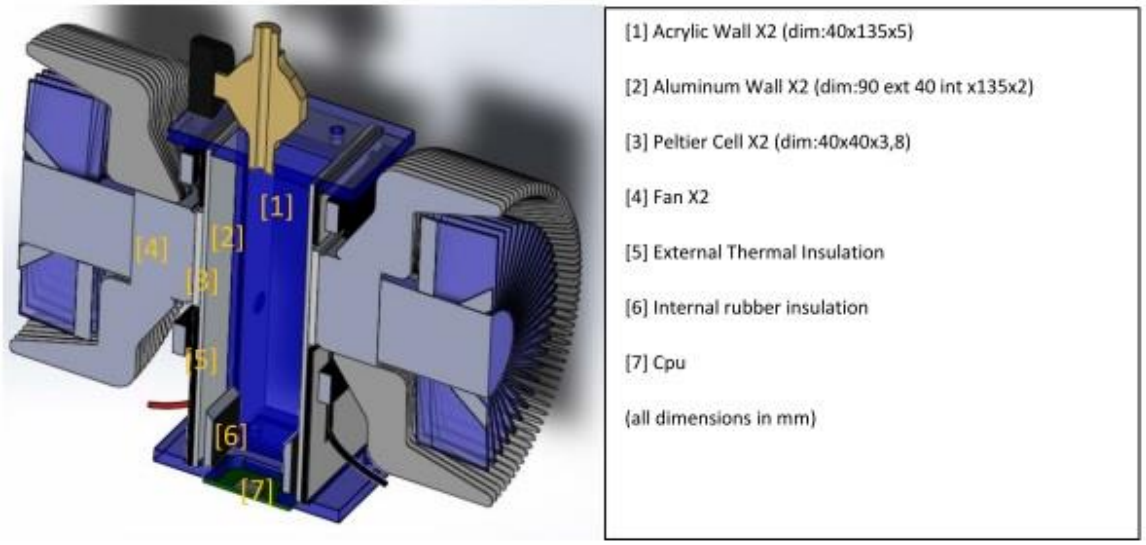

Figure 5.11 – Dimensions of the final pool

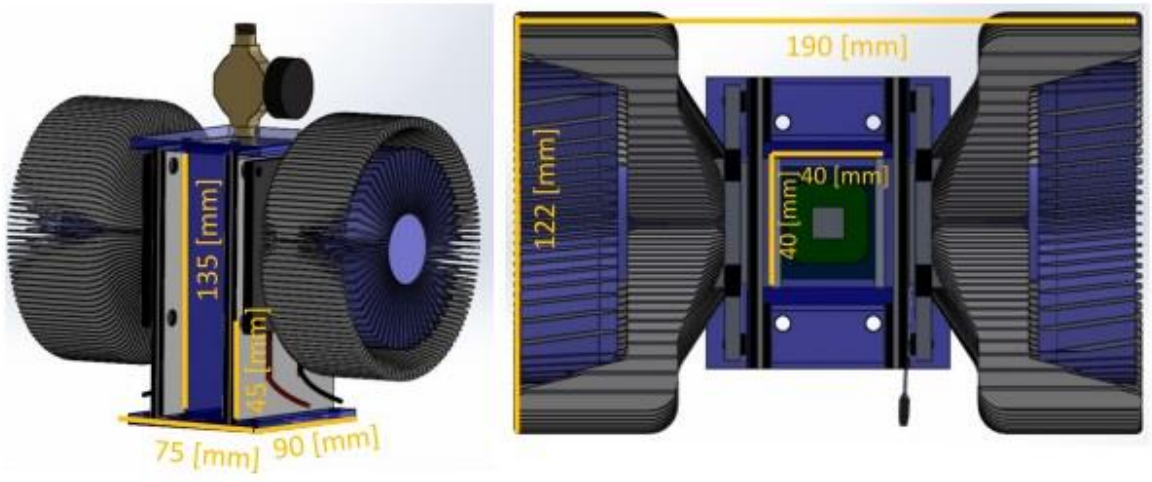

Figure 5.12 – Dimensions of the final pool

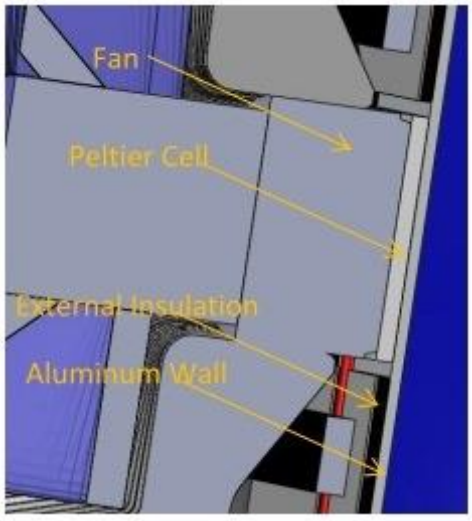

Figure 5.13 - Detail of the Coupling Fan/Peltier/Insulation/Aluminum wall

The amount of fluid that could be contained in the pool has been evaluated taking into account the fact that to condensate is required a specific cooled area. In this case only the aluminum slabs cooled by the cells have been considered as active condensation area. Considering the theory of film condensation on a vertical wall, as previously explained in section 3.4, the following procedure was addressed to evaluate the liquid level.

1- The heat power to be removed is:

$$\dot{Q}_{cpu}[W] = 59$$

2- Previous preliminary experiments have revealed that the two Peltier cells could remove 30 W of heat power, while keeping the wall temperature $T_{wall} = 26 - 28\ ℃$. Thus since for HFE-7000 the $T_{sat} = 34\ ℃$, one can have a $T_{sat} - T_{wall} = 8 - 6\ ℃$ to condense the vapour generated.

3- Considering film condensation on vertical walls, one can determine the value of average heat transfer coefficient h_m according to the Nusselt equation (equation 3.27) taking into account the thermo physical properties of the fluid at $T=(T_{sat} - T_{wall})/2$.

$$h_m \left[\frac{W}{m^2 K}\right] = 1.13 \left[\frac{g\rho_l(\rho_l - \rho_v)h_{fg}k_l^3}{\mu_l(T_{sat} - T_{wall})L_{cond}}\right]^{\frac{1}{4}}$$

4- In this formulation, the parameter L_{cond} is the vertical length of the condensing area. Therefore, imposing the heat to be removed and the $T_{sat} - T_{wall}$ available one can find the required Area to condense as:

$$A[m^2] = \frac{Q_{cpu}}{h_m(T_{sat} - T_{wall})}$$

and L_{cond} as:

$$L_{cond}[m] = \frac{A}{S}$$

in which S is the horizontal dimension of the aluminum wall (40 mm)

5- Finally the level of liquid (L_{liquid}) that can be contained in the pool resulted as:

$$L_{liquid}[mm] = L_{tot} - L_{cond}$$

in which L_{tot} is the total vertical extension of the aluminum wall. By the evaluation here proposed, the final level of liquid chosen was 20mm.

5.3.2 Working fluid - HFE-7000

HFE-7000 was the fluid chosen to perform pool boiling, since it fulfils all the requirements identified in Chapter 3 (section 3.4), namely it is a dielectric fluid, which boils at 34ºC. Hence, its boiling point at ambient pressure assures that phase change of this liquid will occur for the typical working temperatures of the processor, thus ensuring the processor will keep working at a stable temperature. Furthermore, for the range of working temperatures considered here, the system will operate in region III of the boiling curve between point B and C (Figure 3.3 in Chapter 3). The drawback of this fluid, which is common to most of the refrigerants is its low thermal properties and particularly the low value of the latent heat of vaporation. The most relevant thermophysical properties of HFE 7000 are depicted in Table 5.5, together with the properties of water, to provide a term of comparison.

Table 5.5 - Thermophysical properties of the liquids used in the present study, taken at saturation, at $1.013x10^5$Pa.

Property	Water	HFE7000
Saturation Temperature - T_{sat} (°C)	100	34
Liquid density - ρ_l (kg/m^3)	957.8	1374.7
Vapor density - ρ_v (kg/m^3)	0.5956	4.01
Liquid dynamic viscosity - μ_l (mN m/s^2)	0.279	0.3437
Heat capacity - c_{pl} (J/kgK)	4217	1352.5
Thermal conductivity - k_l (W/mK)	0.68	0.07
Latent heat of vaporization - h_{fg} (kJ/kg)	2257	142
Liquid surface tension - σ_{lv} (N/m)x10^3	58	12.4

Nevertheless, the low saturation temperature is an advantage that must be well managed to overcome the aforementioned disadvantages. Hence, efficient control of the condensation system allowing efficient recovery of the vaporized liquid is a key issue.

5.4 PID Controller

The Proportional integral derivative (PID) controller was chosen to be implemented because without knowledge of the complete underlying process, the PID controller is a feedback controller mechanism that allow to achieve the target values on the controlled device. Therefore, PID is a control loop feedback mechanism that tries to minimize the error in outputs by adjusting the process control inputs [59]. The PID controller algorithm involves three separate terms: the proportional, the integral and the derivative denoted P, I and D, respectively. The proportional term corresponds to the present error, the integrative term corresponds to accumulation of past errors and the derivative the prediction of errors. Defining u(t) has the controller output, the equation that describes the PID controller is:

$$u(t) = K_p e(t) + K_i \int_0^t e(\tau)\, d\tau + K_d \frac{d}{dt} e(t) \quad (5.1)$$

in which K_p is the proportional term,

K_i is the integrative term,

K_d is the derivative term,

e is the error,

t is the instantaneous time,

τ is the variable of integration, that can take values between 0 and t.

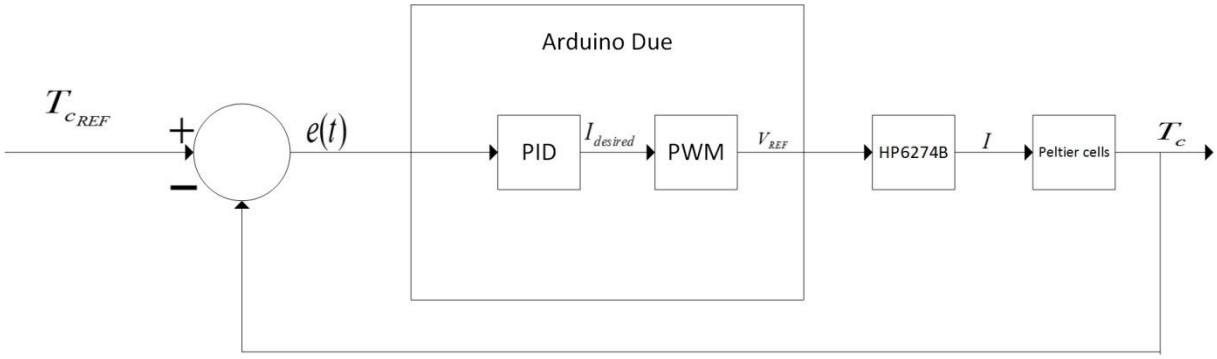

Figure 5.14 - PID controller

In Figure 5.14 is presented the block diagram of our controller. By setting a reference temperature $T_{c_{REF}}$, the error is the difference between the measured value T_c and the reference. This error is multiplied by K_p which results in the proportional term of the output. In this work a discrete approach was adopted and thus the average sum of the previous and present error, multiplied by K_i results in the integrative term. The derivative term is obtained from the difference between the previous and present error multiplied by K_d. The weight of each term in the output depends of the value given to K_p, K_i and K_d. If a high value is given to K_p the proportional term of the controller will be more influential than K_i and K_d and vice-versa. In our case, the PID controller outputs a current desired $I_{desired}$ which in turn is transformed into a voltage reference V_{REF} that is the input of the remotely controllable power supply HP6274B. According to the programming coefficient, the HP6274B will transform this voltage reference into the current I that is supplied to the Peltier cells. With this new current, the Peltier cell will change the temperature of the cold surface T_c which will in turn be measured by the thermocouple and provide the feedback to the controller.

A pseudo-code of the algorithm used is presented:

```
define kp, ki, kd;
define reference;
current = 0.0;
error = 0.0;
previous error =0.0;

loop(){
      tc = acquire temperature;

      error = tc - reference;
      integral = (error + previous error)/2;
      derivative = (error – previous error)/2;
```

```
        previous error = error;

        current=current + (kp*error) + (ki*integral) + (kd+derivative);

        if( current < current min) current = current min;
        if( current > current max) current = current max;

        pwm (current);

        delay (5 seconds);
}
```

Since it is not possible to define exactly the equations that model our system and therefore establish the equation which describes the Peltier cell and how their physical characteristics are changing for all the tested situations, the gains of the PID controller were experimentally obtained.

5.5 Experimental Procedures

This section describes the experimental procedures used to accomplish the characterization of the Peltier cell, the analysis of the each term of the PID controller and the evaluation of the entire condensation system in the final cooling setup.

5.5.1 Characterization of Peltier Cells

As aforementioned, characterization of the Peltier cells is relevant, as little information about the full range of performance of a Peltier device is given in the datasheet. Usually, the parameters provided in the datasheet are: the maximum voltage and current that can be supplied to the cell, the internal resistance of the cell and the maximum temperature difference (ΔT_{max}) and power removed ($\dot{Q}_{c_{max}}$) achievable. Furthermore, the datasheet also gives the performance curve that relates the power removed ($\dot{Q}_c$) by the Peltier device and the temperature difference between the two surfaces of the Peltier cell for several fixed values of current supplied to the device. However, this curve is only true for a fixed value of T_h, which is provided. For this reason, it is relevant to characterize the Peltier device for other values of T_h since it is very difficult of maintain a fixed value of T_h in a cooling application and this value can largely depend on the ambient temperature. Also, no information is given about the dynamic response of the Peltier device and the variation of internal resistance with temperature.

5.5.1.1 Dynamic Response

For the characterization of the dynamic response of the Peltier device, the following procedure is considered:

1. Fix a current supplied to the Peltier device.
2. Choose a known heat power created by the resistance

3. Allow the Peltier device to reach a stationary state

4. Repeat step 2 and 3 with an increased heat flux while the potentiometer has not reached its maximum value, or the temperatures are reasonable so that no damage may occur to the setup.

In this procedure, the cold surface of the Peltier cell is in contact with the resistance. The Arduino is reading the temperatures measurements every 5 seconds in both the hot and cold surface of the Peltier cell and controlling the current supplied by the HP 6274B to the Peltier cells. This interval was chosen because as any significant change in the system was observed justifying the use of a smaller time interval of time. The temperature measurements are made by K type thermocouples. However, these temperature measurements are converted to a digital signal by the MAX31855, which has accuracy of +-2ºC and a resolution of 0.25ºC, to be read by the Arduino. The heat power created by the resistance, described in section 5.2, is the product of the voltage and current measured at its entrance by two different multimeters.

Following this procedure, starting from the ambient temperature, the Arduino is turned on and is controlling the power supply to give a certain value of current to the Peltier cell (e.g. 1A). In this moment, the potentiometer regulating the heat power created by the resistance is off, i.e., creating 0W. Both the hot and cold surfaces of the Peltier cells will adjust their values until stationary state is achieved for this situation (1A/0W). It is assumed that the Peltier cell is in a stationary state when the Arduino is reading for 30 consecutive times (which is equivalent to 150 seconds) the same temperature measurements from the thermocouples. However, even though the stationary state was reached before 20 minutes, for comparative analysis the system was running for 20 minutes for a given combination of current-heat power. After 20 minutes, the heat power created by the resistance was increased to 11.4W and afterwards, the Peltier cell started to change from the stationary state achieved with the combination of 1A/0W to a stationary state achieved with the combination 1A/11.4W. After the 20 minutes where the Peltier cell transitioned between states, the heat power was changed again, this time for 22.13W and then for 30.8W, 40.67W, 47.73W and finally for 61.7W, which is the maximum heat power the resistance could output.

From this test the result achieved is a certain difference ΔT_c in the temperature of the cold surface of the Peltier cell, for an imposed heat power created by the resistance. This procedure was repeated for several fixed values of current equally spread within the range of working conditions of the Peltier cell (1A, 2A, 3A, 4A, 5A, 6A, 7A, 8A, and finally 8.5A) which is 0-8.5A.

5.5.1.2 Internal Resistance $\boldsymbol{R_m}$

For the characterization of the internal resistance of the Peltier cell used, the following procedure was addressed: for a fixed current supplied to the Peltier device, the heat power created by the resistance is varied along the time. This results in a temperature difference on both surfaces of the Peltier cell. These temperature measurements are made following exactly the same procedure used to characterize the dynamic response, as described in the previous sub-section. For each 5ºC difference

in the cold surface of the Peltier cell, the voltage and current flowing at the entrance of the Peltier cell were measured with different multimeters for the voltage and current with the precision mentioned in section 5.2. In this way, one is able to obtain the relation between the cold surface of the Peltier cell and voltage across the Peltier cell as well as the relation between the temperature difference between both surfaces of the Peltier cell and the voltage across the Peltier cell. It is worth noting that the current is always fixed and thus it is the voltage that changes due to the variation of the internal resistance. As in the dynamic response, the Arduino was responsible for obtaining measurements every 5 seconds and controlling the current that the power supply was giving to the Peltier cell. Also, the cold surface of the Peltier cell is in contact with the resistance.

Hence, starting from ambient temperature, assume, for instance, a current of 1A is applied to the Peltier cell and 0W are imposed by the resistance regulated by the potentiometer. The cold surface of the Peltier cell starts to cool. For every 5ºC difference in the cold surface, the voltage across the Peltier cell is measured with a multimeter. When the cold surface has reached its minimum value, a heat power is imposed. The value of heat power imposed is not relevant for this procedure as long as it is high enough so that the temperature of the cold surface rises. For every 5ºC difference, the voltage across the cell is measured. The procedure is continuously performed until the temperature of the cold surface is lower than 80ºC. Afterwards, the procedure is stopped, to avoid any damage to the system and to assure that one reached the highest heat power outputted by the resistance (61.7W). This procedure was repeated for several fixed values of current equally spread the Peltier cell range (1A, 2A, 3A, 4A, 5A, 6A, 7A, 8A) which is 0-8.5A. This way, it is also possible to obtain the relation between the current supplied and the internal resistance.

5.5.1.3 Seebeck Coefficient S_m

Regarding the characterization of the Seebeck coefficient, minor modifications were made to the setup. Here, one followed the procedure described in the literature [26]. Hence, the Peltier cell was inverted, so now it is the hot surface of the Peltier cell that is in contact with the resistance instead of the cold surface, which is in contact with the fan. Furthermore, in this setup no current is supplied to the Peltier cell. Starting from ambient temperature, a heat power is imposed by the resistance regulated with the potentiometer. This results in an increase of the temperature of the hot surface of the Peltier cells and consequently creates a temperature difference between both surfaces of the Peltier cell. From this temperature difference, a voltage is created at the entrance of the Peltier cell due to the Seebeck coefficient. The Seebeck coefficient is the division of the voltage at the entrance of the Peltier cell and the temperature difference between its both surfaces. The heat power imposed by the resistance is not relevant as long as the temperature of the hot surface of the Peltier cell increases. This procedure is followed while the temperature of the hot surface is lower than 100ºC to assure that the system is not damaged. As in the previous procedures, the voltage across the Peltier cell was measured by the multimeter Range RE-68 and the temperature measurements were acquired with the Arduino.

5.5.1.4 Thermal Conductance K_m

The thermal conductance was characterized using the same setup considered in the characterization of the Seebeck coefficient and this procedure is also described in the literature [26]. So, the Peltier cell is also inverted and it is the hot surface of the Peltier cell that is in contact with the resistance instead of the cold surface, which is in contact with the fan. Furthermore, in this setup no current is supplied to the Peltier cell. Starting from ambient temperature, a heat power is imposed by the resistance regulated with the potentiometer. The power imposed is well known since the potentiometer has been calibrated before. This results in an increase of the temperature of the hot surface of the Peltier cells and consequently generates a temperature difference between both surfaces of the cell. The thermal conductance Km is the division of the heat power imposed by the resistance and the temperature difference between both surfaces of the Peltier cell. This procedure is followed while the temperature of the hot surface is lower than 100ºC, also to assure that the system is not damaged. The voltage across the Peltier cell was measured by the multimeter Range RE-68 and the temperature measurements were acquired with the Arduino.

5.5.2 Proportional Integral Derivative (PID) Controller

In the present work the adopted approach consists on testing several solutions for each of the three terms and manually tune the different gains for each term as required. The procedure used consisted of imposing a known heat power created by the resistance and a temperature reference and observe how rapidly the system responded to variations of heat power imposed and how the temperature measured oscillated around the reference. For each difference between the temperature read and the reference temperature temperature, the Arduino controls the current supplied to the Peltier cell so that the error is minimized. In this case, starting from ambient temperature, a heat power of 25W was imposed and temperature readings were acquired each 5 seconds by the Arduino with the same accuracy as in the previous procedures. After 250 seconds, the heat power was changed to 5W and at 500 seconds has changed once again to 25W, to observe how well the controller responded to the variations in the heat power variations. The time of 250 seconds was chosen for each heat power imposed because it was observed that is was more than enough time for the adequately tuned controller to respond to the variation and follow the reference. The only requirement for the system was that the overshoot, when variations in the heat power occurred was not higher than 1.5ºC. Exception is made to the initial overshooting, that could not be higher than 2.5ºC.

5.5.3 Final Setup

Since the transient response of the CPU is different from that of the resistance regulated by a potentiometer, the PID controller gains may need to be manually adjusted for this final setup. In this context, several values were tested to infer on the best combination of each gain. In this procedure, since a well-defined heat power could not be imposed, the CPU working load was used instead, to induce the thermal variations to the system. The procedure followed consisted of starting from 0% of

the CPU load and measure the temperature readings for 250 seconds. After this the CPU load was changed to 100%, which is the worst case scenario. At 500 seconds the CPU load was reduced to 25% and at 750 seconds the CPU load was increased to 75%. The temperature measurements were conducted by the Arduino every 5 seconds. The CPU loads were imposed by using a code download from [60].

To study the feasibility of the system, a final test was conducted for 72 hours under 100% of the CPU load, which is the worst case scenario for the condensation system. In this test, the Arduino was measuring the temperature of each Peltier cell and the temperature of the fan, every 5 seconds and it was controlling the current supplied to the Peltier cells accordingly. In this test, one of the most important variable results to quantify is the difference in volume of the fluid after the 72 hours, as it provides an indirect measure of the efficiency of the condensation system: low variations in the volume of fluid in the pool indicates that the vaporized liquid was successfully condensed.

Chapter 6

Results

This chapter presents the results obtained following the experimental procedures previously described. The characterization of the Peltier cells used here is discussed in section 6.1. The performance of the implemented PID controller is analysed in section 6.2. Here, the response of the system is evaluated in by tuning the gains of the controller. At the end of this chapter, in section 6.3, the performance of the final setup proposed in this work, controlled by the implemented PID controller is shown and analysed.

6.1 Characterization of the Peltier cells

In order to develop a feasible cooling system, one must characterize the Peltier cells. Besides being important, as already explained in Chapter 5, to characterize the properties of the cells under real working conditions, as they can differ significantly from those presented in the datasheet, the characterization of the cells is important to design the control system, particularly using an open-loop controller. Although a close loop (PID controller) was chosen to assure better accuracy and reliability of the system, these properties can be useful for future modifications of the control system.

Finally, there are several studies in the literature concerning the characterization of the Peltier cells, but it is recognized in many of them, that a reliable method for this characterization is very difficult to establish. Hence, despite the efforts made, quantification of the properties such as the Seebeck coefficient S_m and the Thermal conductance K_m are sparsely reported in practical studies, like the one proposed here and are difficult to obtain from the literature. In this context, this characterization is expected to provide useful information on how such properties can be quantified in practical studies. By doing this, one can validate the experimental procedures described in section 5.4.1.

6.1.1 Dynamic Response

Following the experimental procedure described in section 5.5.1.1 several results were obtained for each of the fixed currents, as discussed in the next paragraphs. The results depicted in this sub-section mainly allow analyzing the difference between the initial and final temperatures of the cold surface of the Peltier cell ΔT_C, for a combination of current/heat power imposed by the resistance $\dot{Q}_{imp}$ within the range (1-8.5A / 0-61.7W). In this procedure several considerations must be taken into account. For each fixed current, the procedure starts from the ambient temperature with a $\dot{Q}_{imp} = 0W$. However, when the $\dot{Q}_{imp}$ is increased, the ΔT_C obtained is cumulative and not in comparison against the ambient temperature but against the previous state, as shown in Figure 6.1. In this figure one can see that for 1A of current the Peltier cell reduces the temperature of the cold surface T_c if the $\dot{Q}_{imp} = 0W$. In this case the experiment starts with an initial temperature of $T_{c_i} = 17.25ºC$ and an equilibrium is reached after 1200 seconds, when the final temperature of the cold surface is $T_{c_f} = 5.75ºC$, hence the $\Delta T_c = 11.5ºC$ as shown in Figure 6.2. After $\dot{Q}_{imp}$ is increased to 11.4W T_c starts to increase, thus the initial temperature of this new $\dot{Q}_{imp}$ is the final temperature of the previous state, hence $T_{c_i} = 5.75ºC$ and the final temperature of the cold surface is $T_{c_f} = 35.75ºC$ resulting in a $\Delta T_c = 30ºC$.

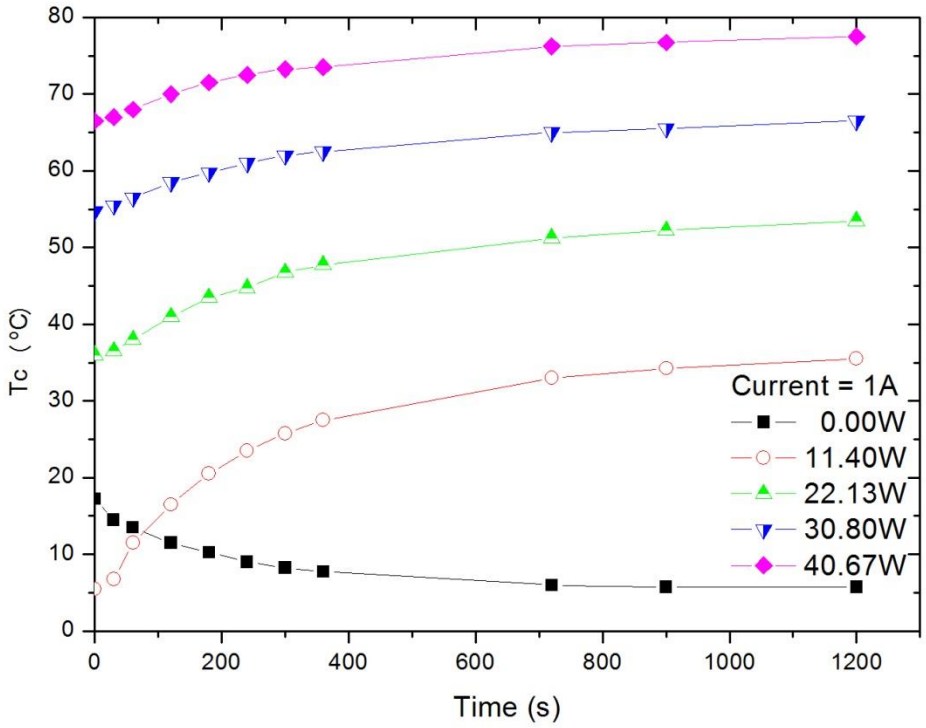

Figure 6.1 - Absolute temperature of the cold surface for 1A of current

Figure 6.3 depicts the difference temperature ΔT between the hot surface and cold surface of the Peltier cell. In this figure it is clear that when $\dot{Q}_{imp} = 11.4W$, after 190 seconds ΔT is negative. This means that the Peltier cell is unable to remove $\dot{Q}_{imp} = 11.4W$ imposed. From equation 4.6 in chapter 4, one can see that the power removed $\dot{Q}_c$ by the Peltier cell equals the sum pf three terms: the heat power removed by the Peltier effect (first term), the Joule effect in the cell (2nd term) and finally the conductive heat transport (third term).

$$\dot{Q}_c = S_m \, I \, T_c - \frac{1}{2} I^2 R_m - K_m \Delta T$$

This means that if $\dot{Q}_{imp}$ is higher than the $\dot{Q}_c$ that the Peltier cell is able to remove, for a given current, the ΔT between both surfaces of the cell is negative. Hence the difference between $\dot{Q}_{imp}$ and $\dot{Q}_c$ is $\dot{Q}_{cond}$, i.e., the power removed by conduction to the fan. Figure 6.4 shows that for $\dot{Q}_{imp} = 11.4W$ the temperature of the hot surface is $T_h = 23ºC$. From Figure 6.1 one can take $T_c = 35.75ºC$, so $\Delta T = -12.75ºC$ in Figure 6.3. This difference is more noticeable for higher $\dot{Q}_{imp}$, e.g. $\dot{Q}_{imp} = 40{,}67W$

where $T_h = 29.5ºC$ and $T_c = 78ºC$. These high negative values for ΔT are due to the low thermal conductance of the Peltier cell, which in this case acts as an insulator. This is not desired in a cooling application because it means that the Peltier cell is not allowing the power to be removed, so, consequently, the heated surface is not cooled.

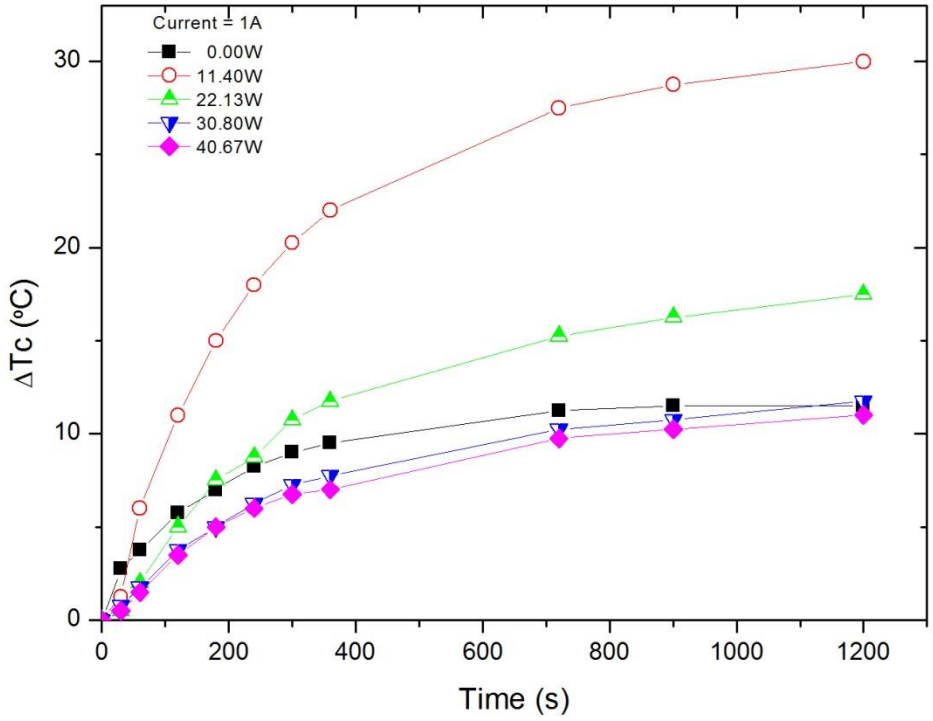

Figure 6.2 - Dynamic response for 1A of current

Following this argument for $\dot{Q}_{imp} = 0W$, an higher ΔT_C is better, because it means that starting from ambient temperature the Peltier cell is able to reduce T_c more. But when $\dot{Q}_{imp}$ is increased, ΔT_C is in comparison to the final value of temperature of the previous state and not the ambient temperature. Hence, in this case a higher value of ΔT_C actually means that T_c is increasing, which now is the opposite of the desired effect. So, for each current and no imposed heat flux, i.e. $\dot{Q}_{imp} = 0W$, the highest values of ΔT_C correspond to a better performance of the system. However, when $\dot{Q}_{imp} \neq 0$, the opposite trend occurs, i.e. the best performance corresponds to lower values of ΔT_C. Here, ΔT_C is taken as the relevant parameter because the cold surface (with temperature T_c) is the one in contact with the wall to be cooled.

Figure 6.2 shows this temporal variation when the current is set to 1A and $\dot{Q}_{imp}$ is varied from 0W to 40.67W. Overall the figure shows that the curves follow the same trend: after a steep response of system, in which T_c varies significantly until t=400s, the temperature of the cold surface then slowly increases until t=600s and finally attains a plateau value from t=600 to t=1200s. Taking for instance the curve for $\dot{Q}_{imp} = 0W$, the $\Delta T_c = 11{,}5\ ºC$ after 1200s, which means that the initial temperature for the cold surface was $T_{c_i} = 17{,}25\ ºC$ and the final temperature (i.e. after the 1200s) is $T_{c_f} = 5{,}75\ ºC$ as can be seen in Figure 6.3. In this case since $\dot{Q}_{imp} = 0W$, all the current supplied is used to cool T_c. From this temperature, $\dot{Q}_{imp}$ is increased to 11.4W, starting to increase T_c. In this case, a $\Delta T_c = 30ºC$ was achieved resulting in the final temperature of the cold surface $T_{c_f} = 35{,}75\ ºC$ after 1200s. This means that if the comparison was made in relation to the ambient temperature, the ΔT_c would be 18.5ºC instead of the 30ºC that is obtained because the temperature difference is cumulative. After this, $\dot{Q}_{imp}$ is increased to 22.13W and T_c continues to increase. After reaching a new stationary state, $\dot{Q}_{imp}$ is increased again to 30.8W and afterwards to 40.67W.

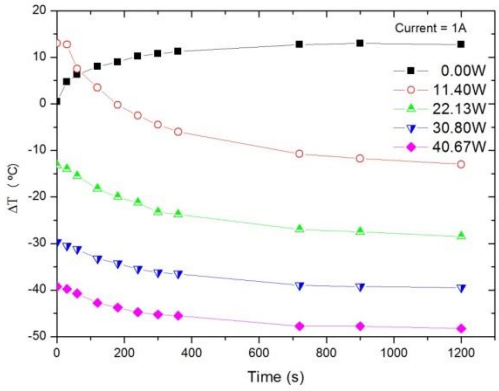

Figure 6.3 – Temperature difference between both surfaces of the Pelier cell for 1A of current

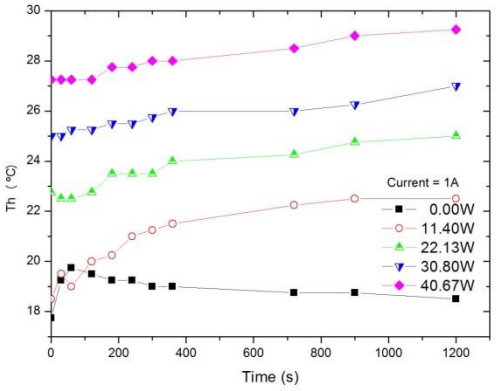

Figure 6.4 – Absolute temperature of the hot surface for 1A of current

This is true for all the cases test, so one may argue that the Peltier cell+fan takes roughly 400s to reach 2/3 of the final ΔT achieved in stationary state, even when large variation in $\dot{Q}_{imp}$ occurs.

While for other currents it was possible to further increase $\dot{Q}_{imp}$, with 1A of current T_c was higher than 80ºC for $\dot{Q}_{imp} > 40.67W$. Therefore, this was the limiting value, to assure that the system would not be damaged by overheat.

Figure 6.5 presents the results of the dynamic response of the Peltier cell for 2A of current.

The same procedure was followed as with 1A of current. However, with this current it is possible to reach a higher $\dot{Q}_{imp}$ due to lower T_c when imposing higher $\dot{Q}_{imp}$. While comparing Figure 6.5 with Figure 6.2, one can observe that for 2A the ΔT_c achieved for $\dot{Q}_{imp} = 0W$ is higher than the one achieved at 1A, i.e., the Peltier cell is able to cool more with a higher current. While it may not be clear, for every $\dot{Q}_{imp} \neq 0W$, the ΔT_c achieved are lower. This is relevant because it means that as we increase $\dot{Q}_{imp}$, T_c increases less with a higher current supplied to the cell which is exactly what is expected in a cooling application, i.e., T_C to be the lowest possible. Again in Figure 6.5, we can observe that when large variation in $\dot{Q}_{imp}$ occurs, the Peltier cell takes roughly 400s to reach 2/3 of the final ΔT_c achieved in stationary state.

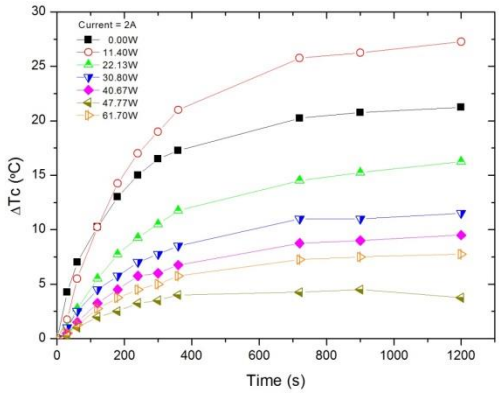

Figure 6.5 - Dynamic response for 2A of current

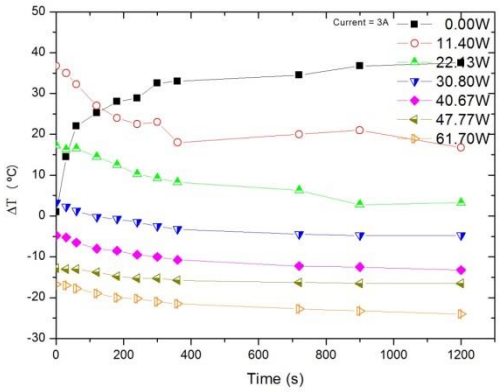

Figure 6.6 - Temperature difference between both surfaces of the Pelier cell for 3A of current

The dynamic response for 3A of current can be observed in Figure 6.7. In this figure there is noticeable difference in comparison to the previous results. The highest ΔT_c obtained was with $\dot{Q}_{imp} = 0W$instead of with 11.40W. This happens because with 3A of current the Peltier cell can remove $\dot{Q}_c > 11.4W$, hence ΔT_c does not increase so much as in the previous cases. Actually, from Figure 6.6 it can be observed that $\dot{Q}_{c_{max}}$ with 3A of current is close to 30.8W because it is at this $\dot{Q}_{imp}$ that ΔT becomes negative as explained in Chapter 4. Thus, when $\dot{Q}_{c_{max}}$ is surpassed, the behaviour of the system is very similar. In this case, the extra heat power $\dot{Q}_{cond}$ the Peltier cell is unable to remove is actually moved by conduction to the fan. One can wonder why the ΔT_c obtained for $\dot{Q}_{imp} = 47.77W$ is lower than with 61.70W. This happens because the increase from 40.67W to 47.77W is of 7.10W and from 47.77W to 61.70W is of 13.93W, hence the ΔT_c is also lower.

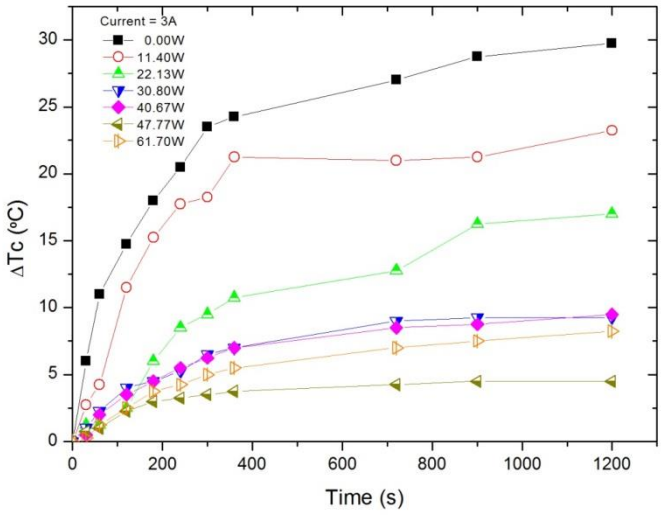

Figure 6.7 - Dynamic response for 3A of current

Figure 6.8 and Figure 6.9 present the dynamic response of the Peltier cell for 4A and 5A of current, respectively. For $\dot{Q}_{imp} = 0W$, a $\Delta T_c = 32.25ºC$ is achieved for 4A, while for 5A, a $\Delta T_c = 35ºC$ is achieved. These results confirm the trends discussed in the previous paragraph, i.e., the higher the current, the higher ΔT_c is achieved, which corresponds to a lower value of T_c.

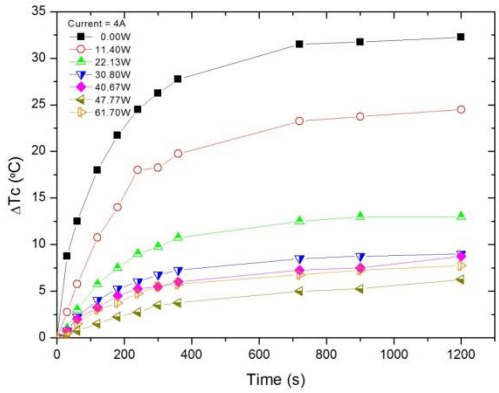

Figure 6.8 - Dynamic response for 4A of current

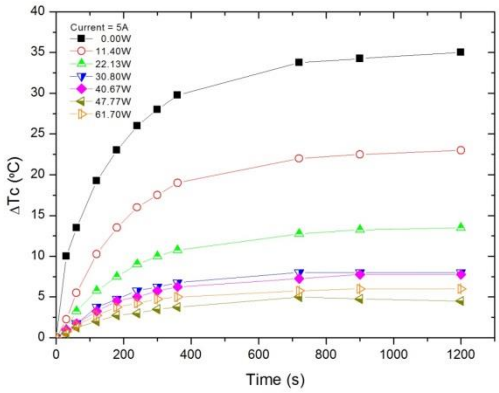

Figure 6.9 - Dynamic response for 5A of current

Figure 6.10 and Figure 6.11 depict the dynamic response for 6A and 7A of current, respectively. In comparison with Figure 6.9, these figures show that for $\dot{Q}_{imp} = 0W$ the ΔT_c achieved is lower. This is due to Joule effect of the Peltier cell. With these currents, the Joule effect is 82W and 115W for 6A and 7A, respectively. According to the datasheet, the optimal current if 0.7 of Imax, which corresponds to 5.95A. After this point, the additional cooling power obtained by increased current does not compensate the additional Joule effect created by an increased current. From this analysis, it can

be concluded that one should operate between 3A-6A, which is in agreement with the recommendations of the manufacturer. Actually, as can be observed in Figure 6.12 and Figure 6.13, for 8A and 8.5A the cooling efficiency decreases considerably. This is due to a limitation of the fan. In theory, if the fan was able to remove all the heat dissipated by the Peltier cell, the ΔT_c achieved for $\dot{Q}_{imp} = 0W$ should have been higher for 8.5A. The problem is that the temperature of hot surface of the cell T_h rises so quickly due to the Joule effect, as observed in Figure 6.14, that T_c cannot reach lower temperatures in comparison with 5A of current. However, the highest ΔT achieved is with 8A of current as can be seen in Figure 6.15. This means that the Peltier cell behaves at it is supposed, the problem is that the fan is unable to remove the Joule effect created by the Peltier cell and T_h increases. If a high performance radiator was used and could maintain the T_h at lower values, T_c would be in fact lower. However, by using such a radiator one would be defeating the purpose of this work.

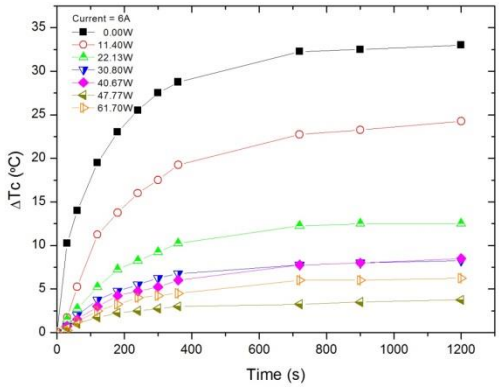

Figure 6.10 - Dynamic response for 6A of current

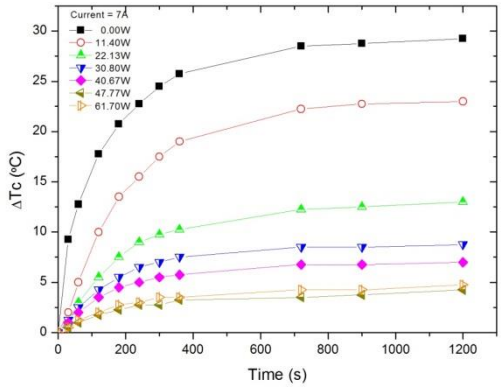

Figure 6.11 - Dynamic response for 7A of current

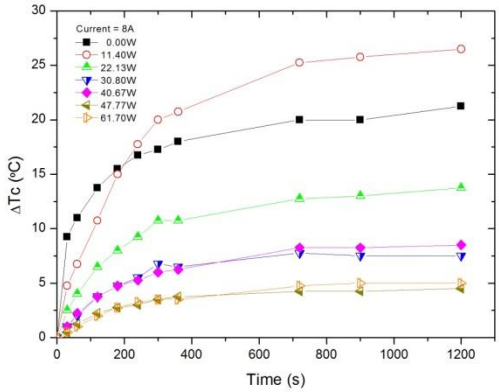

Figure 6.12 - Dynamic response for 8A of current

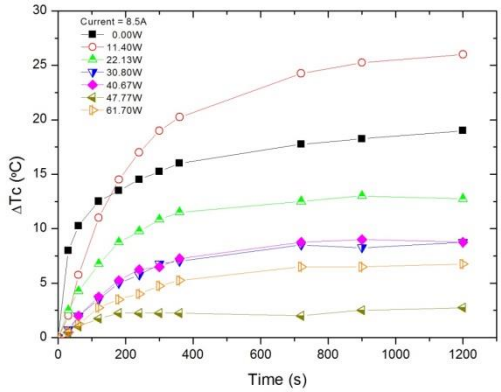

Figure 6.13 - Dynamic response for 8.5A of current

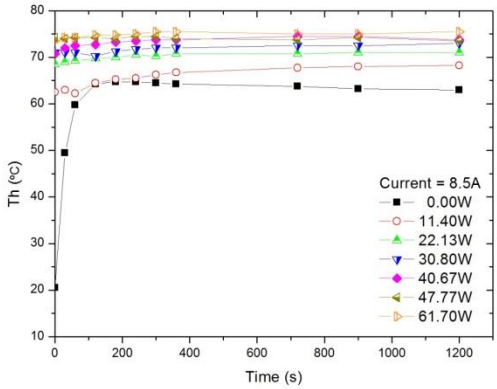

Figure 6.14 - Absolute temperature of the hot surface for 8.5A of current

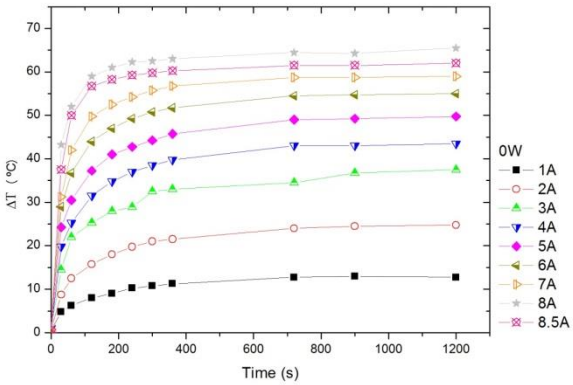

Figure 6.15 - ΔT for $\dot{Q}_{imp} = 0W$, for each of the currents tested

To finalize, one may observe that the Peltier device takes roughly 400s to reach 2/3 of the final ΔT_c achieved in stationary state, even when large variation $\dot{Q}_{imp}$ occurs. This trend is observed for all the currents tested. It also can be concluded that the highest ΔT was achieved with the highest current possible, which is in agreement with the information taken from the datasheet. However, the lowest T_c was obtained with 5A. One may argue that the best range to operate this sytem composed of Peltier cell+Fan is between 3-6A, since for currents lower than 3A, the Peltier cell does not have enough cooling power. For currents higher than 6A, the Joule effect outweighs the additional cooling power.

6.1.2 Internal Resistance R_m

Following the experimental procedure described in section 5.5.1.2 several interesting results were obtained for the characterization of the internal resistance of the Peltier cell variation in relation to ΔT. Figure 6.16 shows how the internal resistance of the Peltier cell changes with variation of the temperature difference between both surfaces of the Peltier cell for multiple currents. The values obtained were calculated using equation 4.13 in order to R_m which results in:

$$R_m = \frac{V - S_m \Delta T}{I}$$

From this figure one can argue that the internal resistance decreases with the increase of the temperature difference between both surfaces of the Peltier cell. However this effect is much more noticeable for lower currents. Also it can be deduced that as the power drawn by the Peltier device is increased, the internal resistance increases and tends to vary less variation at higher currents. Damodara das et al [61] state that the electrical resistivity of bismuth telluride fins exponentially decreases with increasing temperature and is mildly temperature-dependent thermoelectric power, the

latter's magnitude increasing with increasing temperature, which is qualitatively in agreement with the results presented here.

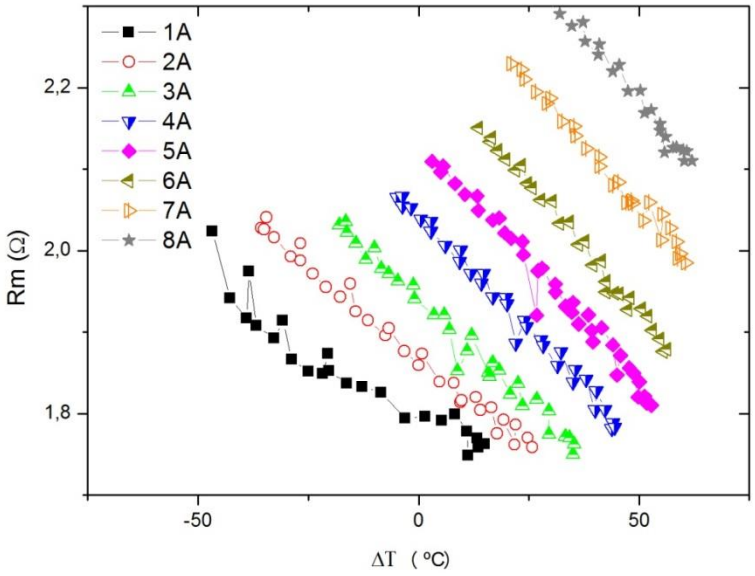

Figure 6.16 – R_m vs ΔT

6.1.3 Seebeck Coefficient S_m

The procedure described in section 5.5.1.3, was followed to obtain the Seebeck effect. Figure 6.17 depicts the relation obtained between the Seebeck coefficient S_m and the temperature difference ΔT between the two surfaces of the Peltier cell. It is important to emphasize that this is not the Seebeck coefficient of the material, but the Seebeck coefficient of the Peltier cell as a device, taking into account its dimensions. The results were obtained by using the expression [26]:

$$S_m = \frac{V}{\Delta T} \tag{6.1}$$

It can be noticed that the Seebeck coefficient is roughly constant in relation to the temperature difference between the two surfaces of the Peltier cell. The average of values obtained is 0.044793 and maximum deviation is 4.3% in relation to the average. The difference observed is so small that the deviations shown can surely be attributed to the accuracy of the multimeter used and of the temperature readings with the Arduino. The value of Seebeck coefficient obtained is within the range of values reported in the literature, for studies performed under similar condiitons. Zhang et al. [62] calculated the parameters for several Peltier cells, including one with characteristics similar to those of the cell used in this work and obtained a Seebeck coefficient of 0.048, which is quite consistent with the value determined here.

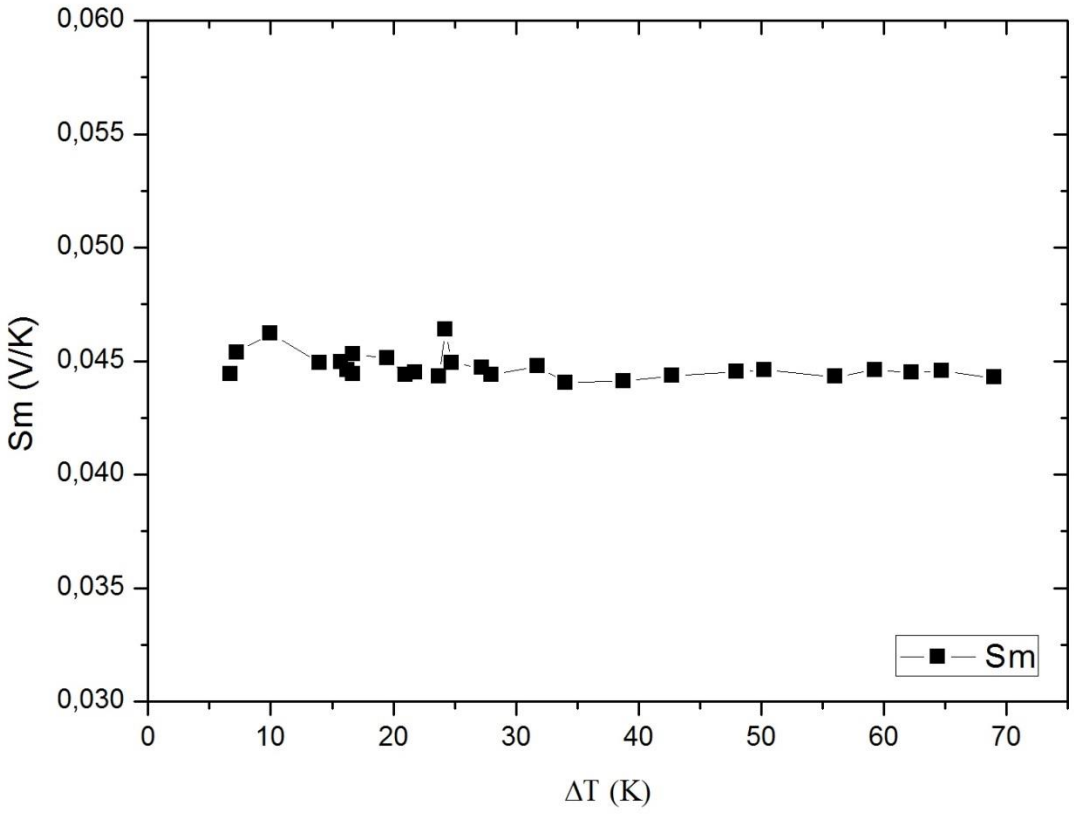

Figure 6.17 – Relation between Seebeck Coefficient and ΔT between both surfaces of the Peltier cell

6.1.4 Thermal Conductance K_m

Figure 6.18 shows the relation obtained between the Thermal conductance K_m and the temperature difference ΔT between the two surfaces of the Peltier cell. These values were taken according to the procedure described in section 5.4.1.3. The following expression was used [26]:

$$K_m = \frac{\dot{Q}_c}{\Delta T} \tag{6.2}$$

Once again, it is worth mentioning that this is not the thermal conductivity of the material, but the thermal conductance of the Peltier cell as a device, taking into account its dimensions. It can be noticed that the thermal conductance linearly increases with the temperature difference between the two surfaces. This trend is also in agreement with that reported by Dirmyer et al. [63]. The values obtained are also within the expected range for the thermal conductance considering the characteristics of the Peltier cell [62].

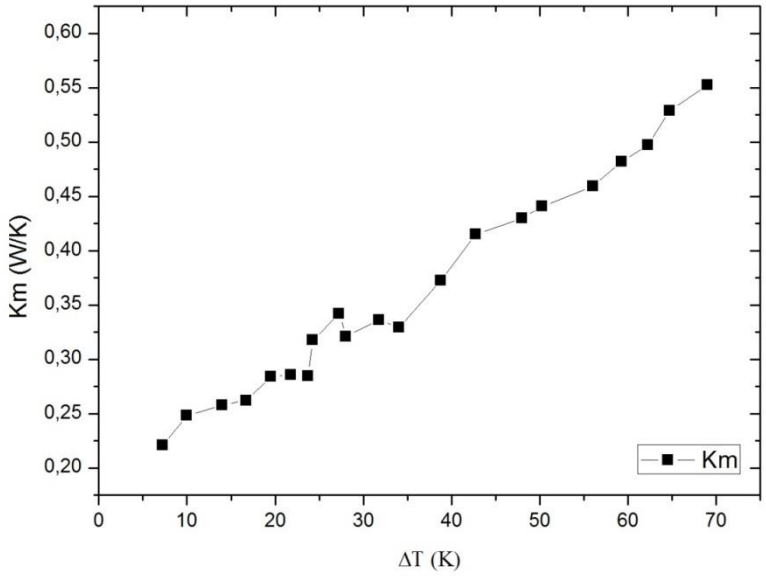

Figure 6.18 - Relation between Thermal Conductance and ΔT between both surfaces of the Peltier cell

6.2 PID Controller

The characterization of the cells previously discussed is important to design the control system, particularly using an open-loop controller. Although a close-loop (PID controller) was chosen to assure better accuracy and reliability of the system, these properties can be useful for future modifications of the control system.

Given that an analytical model of the system could not be derived, several values for each gain of the PID controller were tested within an appropriate range and the response of the system was evaluated. The final values of the gains Kp, Ki and Kd were therefore determined from this experimental approach.

The reference used in all tests is $T_c = 28ºC$. The requirements set for a good behaviour of the condensation system is that the temperature measured would not go more than 1.5ºC above the reference for more than 10 minutes. In all the results reported in this sub-section, the initial heat power imposed is 25W which is changed after 250 seconds to 5W and back again to 25W after 500 seconds as can be seen in each figure.

6.2.1 Kp

The following values were considered for the proportional term of the PID controller: Kp=5.0, Kp=1.0 and Kp=0.2. The integrative term used is Ki=0.01 and the derivative term used is Kd=1.0.

Figure 6.19, Figure 6.20 and Figure 6.21 show the results obtained for the proportional term Kp=5.0, Kp=0.2 and Kp=1.0, respectively. As can be seen in Figure 6.19 with Kp=5.0, whenever there is a slight variation in the heat power imposed, the overshoot of the controller is very high. When the heat power is changed at 250 seconds and 500 seconds the controller settling time is also very high. At 600 seconds one bad reading led to an increase in the current supplied which in turn led to a rise in the Joule effect and the controller could not follow the reference anymore. This behaviour leads to argue that a gain of 5.0 turns the controller unstable. Figure 6.20 shows the result obtained with Kp=0.2, Ki=0.01 and Kd=1.0. In this figure, it is possible to see a much more stable result and this much more noticeable when there were variations in the imposed heat power. However, when these variations occur, the overshoot is roughly 2.0ºC which is higher than the requirements. Hence, in this case one may argue that the gain is not high enough to compensate the variations imposed. A final value was tested for the proportional term which wielded the best result and was within the requirements previously set. Figure 6.21 shows the behaviour of the controller with the proportional term set for Kp=1.0. For this gain, while there is an initial overshoot of 1.25ºC, the controller is much more stable than in the previous cases. After the heat power was increased at 250 seconds, there was an overshoot of 1.25ºC which was promptly corrected by the controller. At 500 seconds one can detect an overshoot of 0.75ºC with a rapid settling time of the controller. Figure 6.22 shows the comparison between the previous cases presented. While Kp=5.0 has a lower initial overshoot, it is clear that Kp=1.0 yields the best response to fluctuations in the system and a better stability.

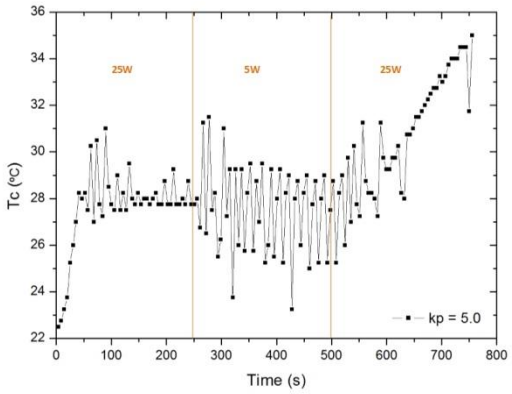

Figure 6.19 – Kp=5.0; Ki=0.01; Kd=1.0 for $T_{C_{ref}} = 28ºC$

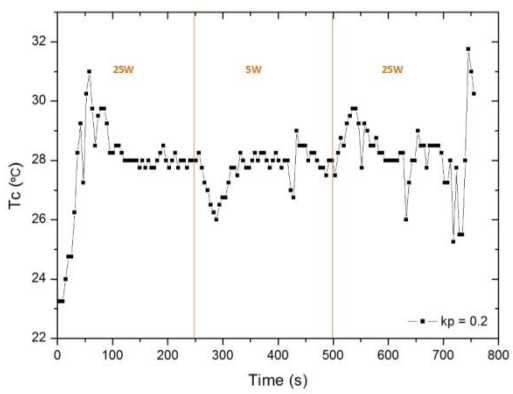

Figure 6.20 - Kp=0.2; Ki=0.01; Kd=1.0 for $T_{C_{ref}} = 28ºC$

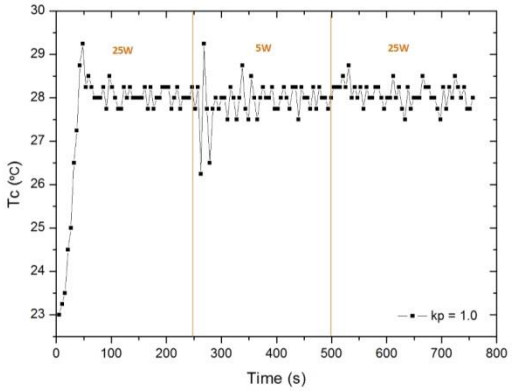

Figure 6.21 - Kp=1.0; Ki=0.01; Kd=1.0 for $T_{C_{ref}} = 28ºC$

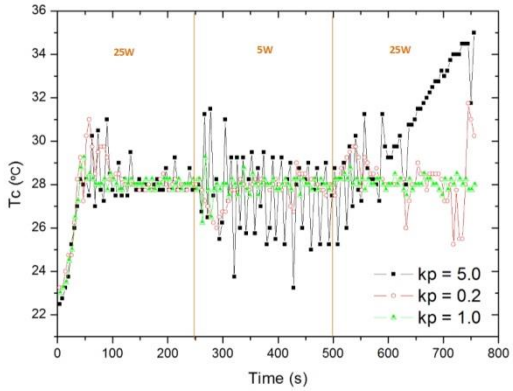

Figure 6.22 – Comparison of the proportional terms

6.2.2 Ki

The integrative term of the PID controller was tested with Ki=0.05, Ki=0.01 and Ki=0.002. The proportional term used is Kp=1.0 and the derivative term used is Kd=1.0. Figure 6.23 shows the controller with Ki=0.05. While for several intervals of time the controller follows the reference, the initial overshoot and settling time is high. Figure 6.24 shows the controller with the integrative term of Ki=0.002. In this case, the initial overshoot is still high but when the heat power is changed the overshoot is 0.75ºC which is very good taking in account that the accuracy of the MAX31855 is 0.25ºC. In this case the controller oscillations are lower, the stability is better than before and the settling time is also better. Figure 6.25 shows the controller response with Ki=0.01. In this case, the initial overshoot is lower than the previous case but there were some oscillations after 250 seconds and the steady-state error was higher than with Ki=0.002. Figure 6.26 summarises the comparison between the values used for the integrative term and is Ki=0.002 which yields the best results. Although the initial overshoot is higher than with Ki=0.01, the controller has more stability and is less prone to oscillations. In this case, since the initial overshoot is acceptable (1.75ºC) in comparison with the required which was 1.5ºC, Ki=0.002 was the value selected for the integrative term. The reasoning behind is that since the system supposed to be working for several days, it is preferable to have more stability in long time periods than a lower initial overshoot.

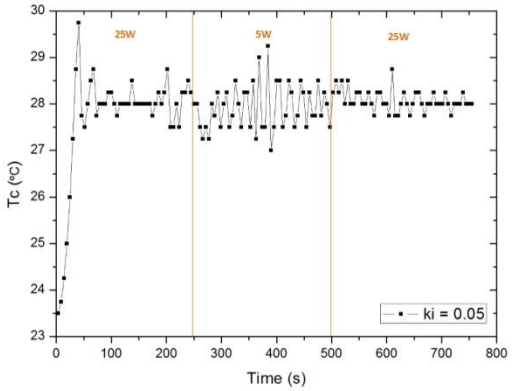

Figure 6.23 - Ki=0.05; Kp=1.0; Kd=1.0 for $T_{C_{ref}} = 28ºC$

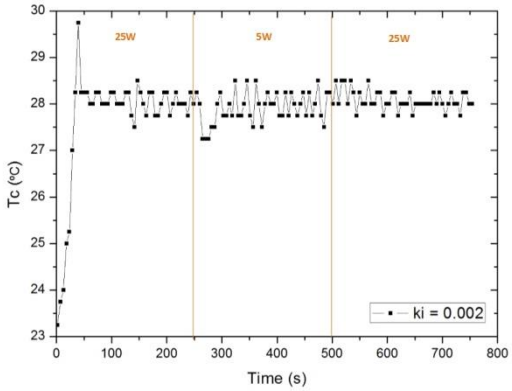

Figure 6.24 - Ki=0.002; Kp=1.0; Kd=1.0 for $T_{C_{ref}} = 28ºC$

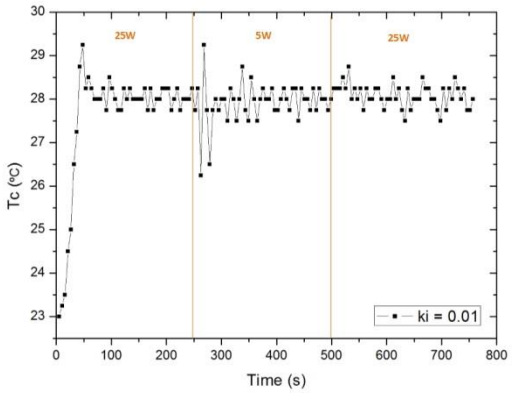

Figure 6.25 - Ki=0.01; Kp=1.0; Kd=1.0 for $T_{C_{ref}} = 28ºC$

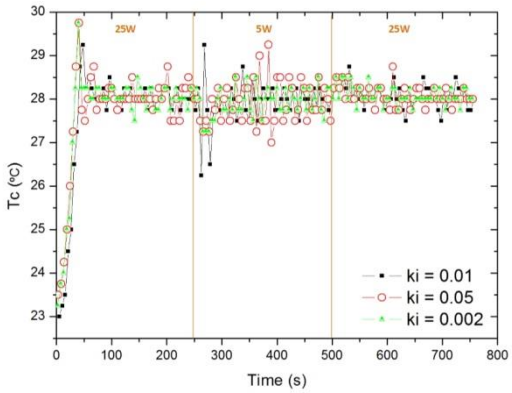

Figure 6.26 - Comparison of the integrative terms

6.2.3 Kd

The derivative term of the PID controller was tested with Kd=5.0, Kd=0.2 and Kd=1.0. The proportional term used is Kp=1.0 and the integrative term used is Ki=0.01. Figure 6.27 presents the controller with the derivative term of Kd=5.0. As can be seen, a high derivative term leads to very high oscillations. Whenever there is a slight oscillation in the temperature, for example when the temperature starts to drop, the derivative term compensates by starting to reduce the current supplied to the Peltier cell. If the derivative term is very high, this will result in a much reduced current and the Peltier cell temperature will start to rise and vice-versa. This will lead to much oscillation around the reference, as observed in Figure 6.27. In Figure 6.28, the derivative term Kd=0.2 is very small which will lead to a larger initial overshoot and slow response to the derivative error. Figure 6.29 presents the controller with Kd=1.0. In this case, the initial overshoot is lower than with Kd=0.2 and the oscillations around the reference are not as noticeable as with Kd=5.0. This value for the derivative term wields the best result. Figure 6.30 shows the previous results side by side, to emphasize the best

performance obtained with Kd=1.0.

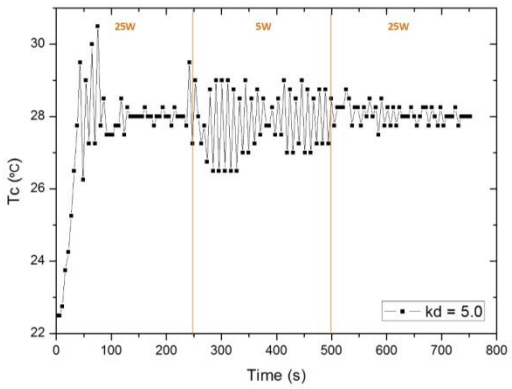

Figure 6.27 - Kd=5.0; Kp=1.0; Ki=0.01 for $T_{C_{ref}} = 28ºC$

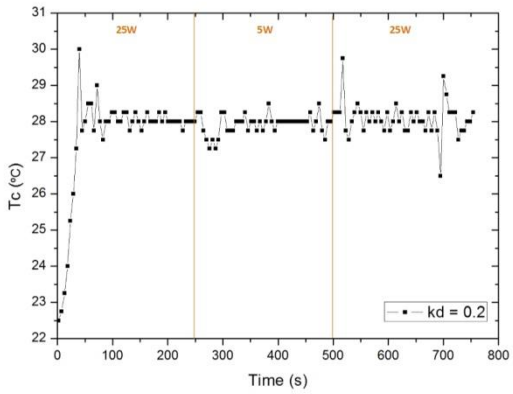

Figure 6.28 - Kd=0.2; Kp=1.0; Ki=0.01 for $T_{C_{ref}} = 28ºC$

Based on the analysis discussed in the previous paragraphs, the gains selected which lead to the best performance of the system are Kp=1.0, Ki=0.02 and Kd=1.0. The final results when setting the controller with these gains are depicted in Figure 6.24. As aforementioned, there is an initial overshoot of 1.75ºC that last for roughly 10 seconds, which is acceptable. In the long run, the highest overshoot obtained is 0.75ºC which is very good considering that the accuracy of the temperature readings obtained from the Arduino are 0.25ºC.

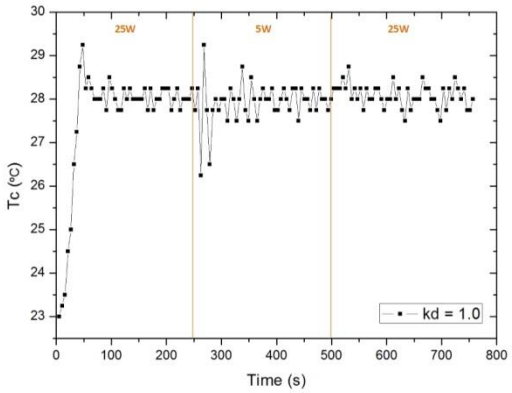

Figure 6.29 - Kd=1.0; Kp=1.0; Ki=0.01 for $T_{C_{ref}} = 28ºC$

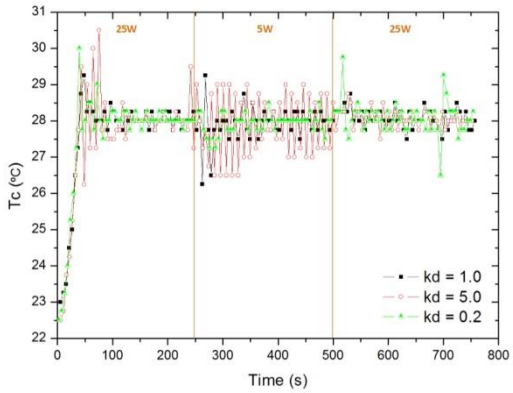

Figure 6.30 - Comparison of the derivative terms

6.3 Final Setup

Following the procedure described in section 5.5.3, several values for each gain of the PID controller were tested. The result presented in Figure 6.31 was obtained for the controller with the gains Kp=1.0, Ki=0.02 and Kd=1.0. The temperature reference set was 15ºC. As can be seen in the figure, the CPU load was changed so that oscillations were introduced to the system. The initial overshoot is of 1.5ºC and the highest overshot obtained when a variation occurred was 0.75ºC. The fact that the results were obtained in the final setup considering the same optimum values which were determined with the previous setup suggests that the controller was indeed properly tuned. Also the controller appears to be more stable with the CPU than with the resistance. The reason for this is that the Peltier cell is now cooling a surface that is at a temperature lower than with the resistance. The result is very satisfactory taking into account the requirements previously set.

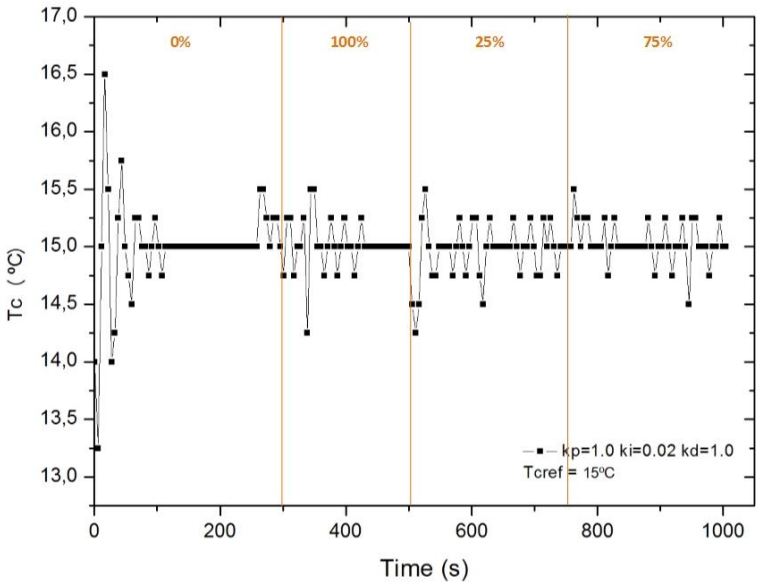

Figure 6.31 – PID Controller test with $T_{C_{ref}} = 15ºC$

As described in section 5.5.3 a final test was made that lasted for 72 hours under 100% of the CPU load, which is the worst case scenario for the condensation system. The results obtained show that the direct immersion cooling, using a boiling liquid, is a feasible technique. The controller was able to follow the temperature reference with minimal oscillations during the 72 hours as can be seen in Figure 6.32. Figure 6.33 is shown the current drawn by the Peltier cells which has an average of 2.55A with 9.5V. Finally in Figure 6.34 and Figure 6.35 it can be seen that the average temperature of the CPU was 64.1ºC for 72 hours and the minimum and maximum temperature achieved was 58ºC and 67ºC, respectively, which is quite within the safe working temperature range for the CPU. The difference in volume of the fluid used was $1mm^3$ of a total of $20mm^3$.

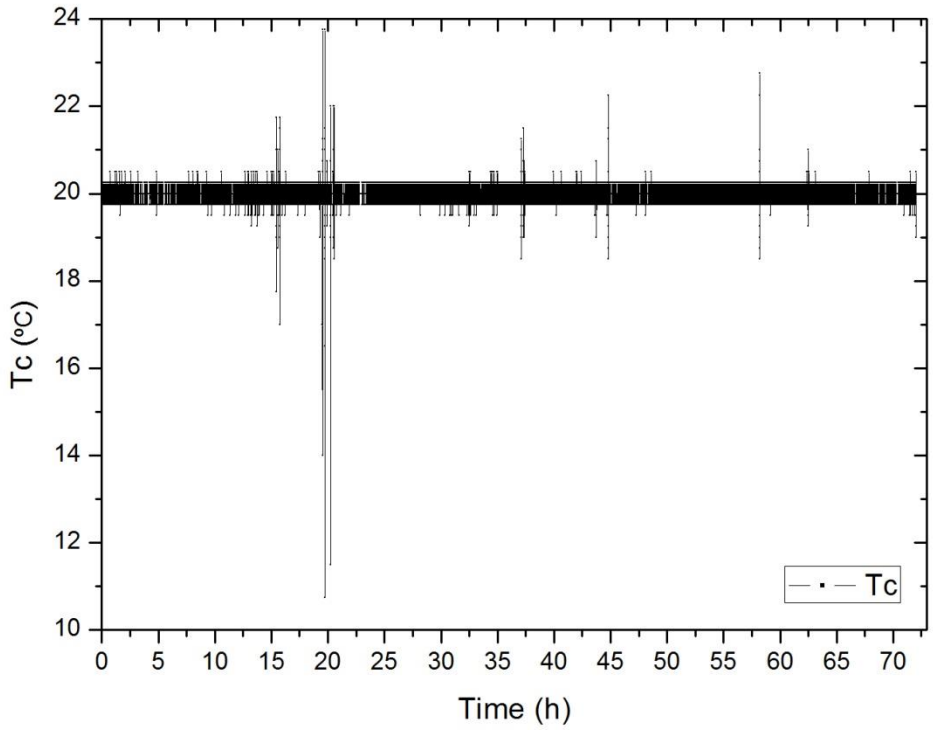

Figure 6.32 – Temperature measured during 72 hours under CPU full load

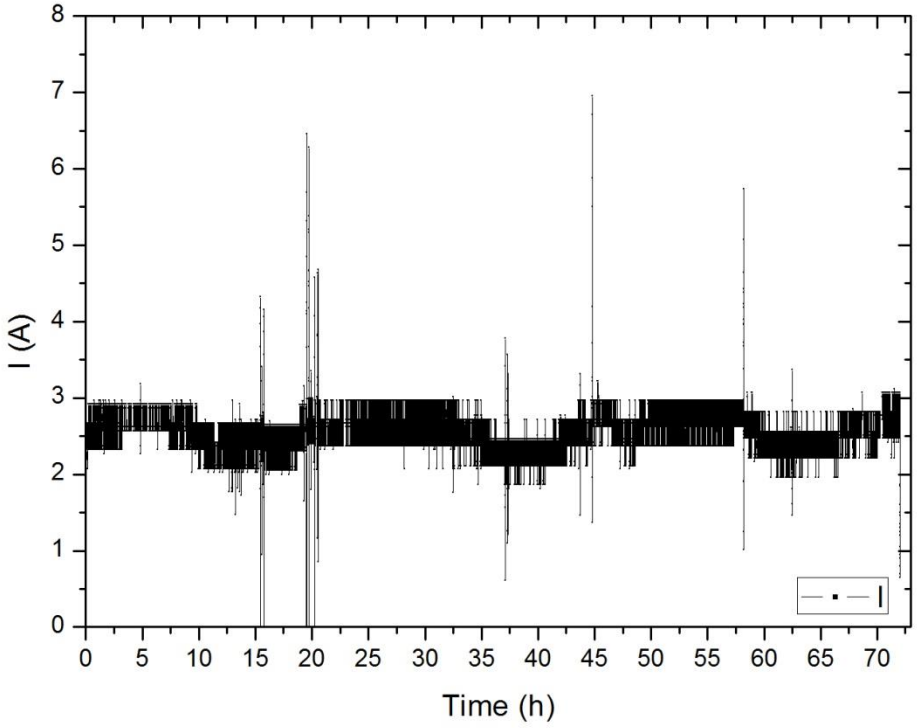

Figure 6.33 - Current drawn by the Peltier cell during 72 hours under CPU full load

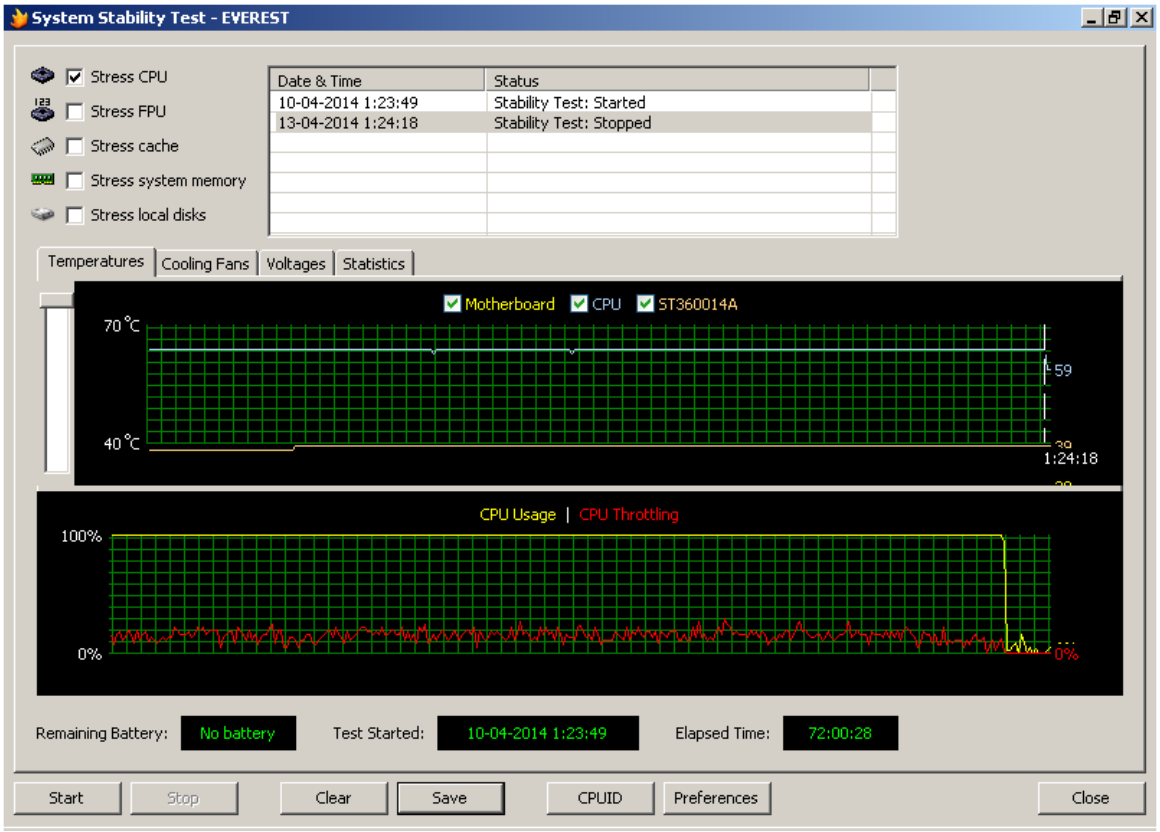

Figure 6.34 - CPU Temperature for the 72 hours

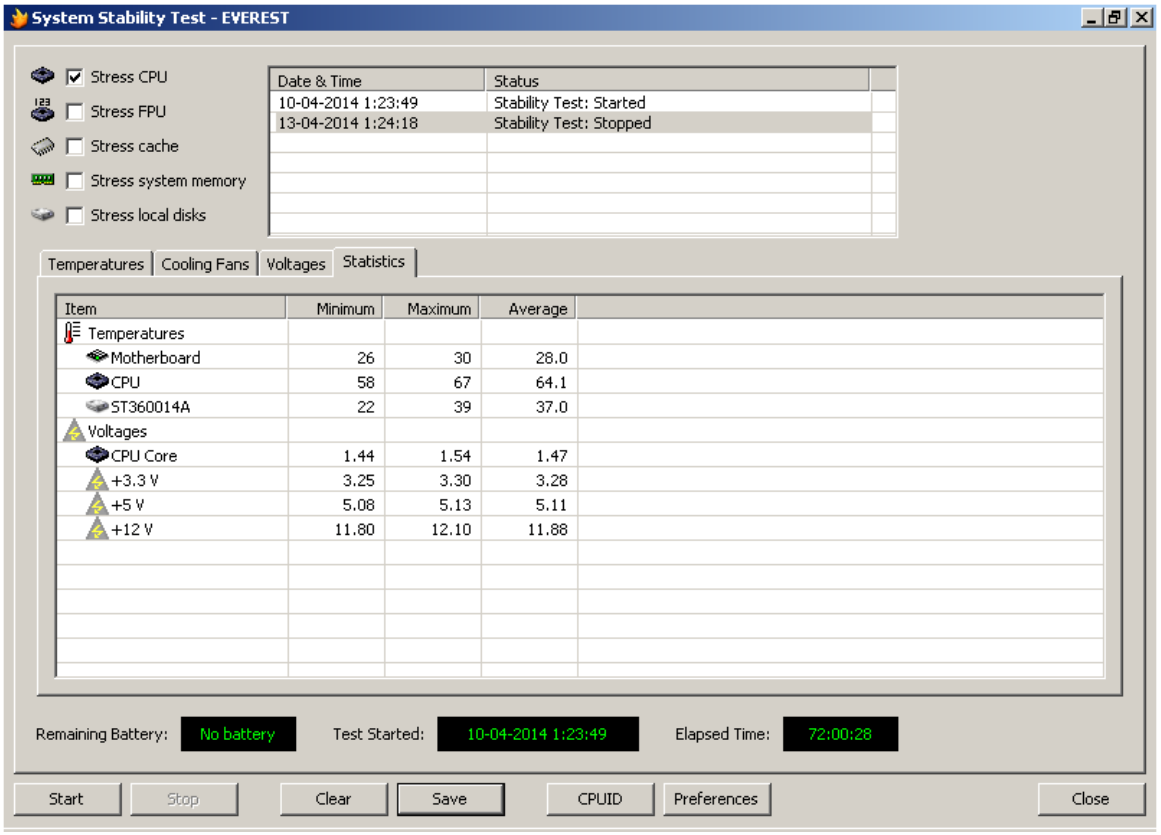

Figure 6.35 - CPU statistics for the 72 hours

Chapter 7

Conclusions

This chapter finalises this work, summarising conclusions and pointing out aspects to be developed in future work.

The present thesis reports the study of a controllable condensation system using Peltier cells, which was designed to be integrated in a direct immersion cooling system, with the boiling of a fluid, to cool a personal computer. In this context, several objectives were proposed to better understand the fundamental working principles of the Peltier cells and their main characteristics such as the internal physical parameters as well as its dynamic response. This whole analysis allowed understanding and characterizing the Peltier cells under real working conditions, which is vital to design a feasible system. In addition, the experimental characterization of the cells also allowed to propose a methodology to quantify these properties (e.g. the Seebeck coefficient and the thermal conductance) in practical studies, which is a hot topic currently debated in the literature.

Hence, in terms of the internal resistance one can conclude that the internal resistance of the Peltier cell decreases with increasing ΔT and increases with the power supplied to the Peltier cell, as described in the literature.

The dynamic response of the system (Peltier cell+cooling fan) in contact with a heated surface can be related to the variation of the temperature of the cold surface in time. In the condition in which any heat power is imposed to the cold surface, the difference in T_c is the result of the power removed by the cell and therefore the best performance of the system is related to an increase in this variation (the cell will act to decrease the temperature of the cold surface so the maximum ΔT_c is the ideal condition). On the contrary, as a heat power is imposed beneath the cold surface of the cell, the best performance is related to the capacity of the cell to respond in order to avoid that the temperature of the cold surface will increase. Hence in this case the desired performance leads to minimum variation of T_c. In this context, the thermal response of the system was evaluated in time. The results show that the response of the system is higher than expected (nearly 400s are required for the system to reach 2/3 of the temperature difference achieved in stationary state for any given current, for a given fixed current), due to the high thermal inertia associated to the entire system. However, when the condensation system was tested in the final setup, the Peltier cell response to heat flux variations was much faster in the order of about 20 to 30 seconds.

For the condensation to be controllable a PID controller was designed. Given that the system could not be modelled analytically the gains were determined experimentally, analysing the response of the system when the gains were varied, within determined ranges. The best results achieved were when the terms used were Kp=1.0, Ki=0.002 and Kd=1.0. The results were very satisfactory taking into account the requirements of the system to cool: after a temperature reference was defined, it was required that the value measured would not go above 1.5ºC of the reference for more than 10 minutes. When the PID controller was tested in the setup designed for the characterization of the Peltier cells with the terms previously mentioned, the maximum overshoot obtained was 0.75ºC and lasted for 15 seconds before settling back on the reference. When tested in the final setup, the maximum overshoot achieved was 0.5ºC when the CPU load changed from idle to full load which is the worst case scenario. Taking into account that the accuracy of the reading temperatures was 0.25ºC, the results were very satisfactory.

A final test of 72 hours with the computer under full load, which again, is the worst case

scenario was made to evaluate the feasibility of the system. The efficiency of the condensation system can be related to the volume of liquid that remains in the pool: the efficiency of the system is the highest for the lowest variation in the volume of liquid. In an ideal situation, the level is maintained, which means that under thermodynamic equilibrium all the liquid that is vaporized could be condensed in the system developed here. Hence the volume of the fluid in the pool was measured before and after the test and only a difference in the height of fluid of $1mm$ in a total of $20mm$ was registered after 72 hours of test. During this period the computer remained operational.

The fact that the control system was developed and tested under different conditions (and even different setup configurations) allowed an empirical optimization of the controller so that the cooling system designed and controlled here is flexible and robust enough to be used in other applications. This is so, since the controller is oblivious to the heat flux created by the surface. The temperatures read by the thermocouples are integrated in the Arduino Due, which outputs a reference voltage that directly controls the current supplied by the power supply to the Peltier cell. This way, the system can be easily transferred to any other surface with little or no redesign at all. This design also allows to system to be used in more powerful CPUs with little redesigned according to the dimensions and power dissipation. However, it is important to emphasize that the controller does not take directly into account the heat flux being created by the CPU. The variation of the temperature of the surface that the Peltier cell is controlling is a direct result of heat fluxes variation.

In future work, it is relevant to test the system in personal computers that dissipate more power and observe if all the fluid is properly condensed under higher heat fluxes. Depending on the TDP difference between the CPU tested here and the new CPU, a more powerful Peltier cell could be needed. This may affect the selection of the fan used and tuning of the PID controller terms. Another important test would be to increase the duration of time the CPU is continuously working, for example from 72 hours to a week.

Apart from the aforementioned adaptations of the controller which may be required when different processors are used, an important modification should be considered in a future work, in order to take a step ahead towards obtaining a commercial system. This is related the power supply used here, which is not viable from a commercial perspective. To achieve this, several requirements must be fulfilled. First, the power supply would have to be connected to the power grid. The 220VAC from the power grid would have to be rectified and stepped down to a desired maximum current output. For example, imagine one wishes a power supply that can output 50V and 20A in continuous current. The objective would be to transform the 220VAC from the power grid and rectify it for continuous current and step down to 50V and 20A. Then one would need a way to control the current output from 0-20A accordingly to a reference voltage (0-3.3V) produced by the Arduino Due. This way, if the Arduino outputs 0V, the power supply would output 0A and if the Arduino outputted 3.3V the power supply would output 20A. Following this procedure, a remotely controllable power supply would be designed which in this case would be remotely controlled by the Arduino but could be controlled by any other device that could generate the voltage reference. The idea is to replicate the power supply used, but with fewer functions as the power supply is considerably complex.

References

[1] G. E. Moore, “Cramming More Components onto Integrated Circuits,” 1965.

[2] CNET, “CNET,” [Online]. Available: http://news.cnet.com/New-life-for-Moores-Law/2009-1006_3-5672485.html.

[3] J. Hennesy and D. A. Patterson, Computer Architecture: A Quantitative Approach, Morgan Kaufmann, 2003.

[4] M. S. El-Genk and H. Bostanci, “Combined effets of subcooling and surface orientation on pool boiling of HFE-7100 from a simulated electronic chip,” *Experimental Heat Transfer,* vol. 16, pp. 281-301, 2003.

[5] B. Cohen, “State-of-the-art and trends in the thermal packaging of electronic equipment,” *ASME J. Electron,* vol. 114, pp. 254-270, 1992.

[6] S. S. Tonapsi, R. A. Fillion, F. J. Schattenmann, H. S. Cole, J. D. Evans and B. G. Sammakia, “An Overview of Thermal Management for Next Generation Microelectronic Devices,” in *IEEE/SEMI Advanced Manufacturing Conference*, 2003.

[7] P. Y. Paik, K. Chakrabarty and V. K. Pamula, “Adaptive Cooling of Integrated Circuits using Digital Microfluidics,” Artech House, 2007.

[8] T. Cader, L. J. Westra and R. C. Eden, “Spray Cooling Thermal Management for increased Device Reliability,” IEEE Transactions on Device and Materials Reliability, 2004.

[9] C. Lasance and R. Simons, “Advances in High Peformance Cooling for Electronics,” Electronics Cooling, 2005.

[10] P. Rodgers, V. Eveloy and M. Pecht, “Limits of Air-Cooling: Status and Challenges,” in *21st IEEE SEMI-THERM Symposium*, 2005.

[11] S. Kang, “Advanced Cooling for Power Electronics,” in *CIPS*, Nuremberg, Germany, 2012.

[12] S. Mohamed, El-Genk and H. Bostanci, “Combined effects of subcooling and surface orientation

on pool boiling of HFE-7100 from a simulated electronic chip," *Experimental Heat Transfer,* vol. 16, pp. 281-301, 2003.

[13] C. Amon, "MEMS-Based thermal management of high heat flux devices; EDIFICE: Embedded Droplet Impingement for Intregrated Cooling of Electronics," 2001.

[14] Bar-Cohen, M. Arik and M. Ohadi, "Direct Liquid Cooling of High Flux Micro and Nano Electronic Components," *Proceedings of the IEEE,* vol. 94, pp. 1549-1570, 2006.

[15] H. Seok Ahn, V. Sathyamurthi and D. Banerjee, "Pool Boiling Experiments on a Nano-Structured Surface," *IEEE Transactions on components and packaging technologies,* vol. 32, pp. 156-165, 2009.

[16] T. Harirchian and S. Garimella, "AN INVESTIGATION OF FLOW BOILING REGIMES IN MICROCHANNELS OF DIFFERENT SIZES BY MEANS OF HIGH-SPEED VISUALIZATION," *IEEE,* 2008.

[17] V. Silvério, A. Moreira and V. Semião, "Heat Transfer Investigations in micro-channel flows," in *15th Int Symp on Applications of Laser Techniques to Fluid Mechanics*, Lisbon, Portugal, 2008.

[18] A. Agarwal, *Micro-channels, Heat Transfer and Pressure Drop During Condensation of Refrigerants in,* Georgia Institute of Technology: Dissertation, 2006.

[19] Bertsch, "Review and Comparative Analysis of Studies on Saturated Flow Boiling in Small Channels," *Nanoscale and Microscale Thermophysical Engineering,* 2008.

[20] H. Bostanci, D. Rini, J. Kizito, Chow and Louis, "Spray Cooling with Ammonia on microstructured Surfaces: Performance Enhancement and Hysteresis Effect," *Journal of Heat Transfer,* vol. 131, 2009.

[21] I. Mudawar, "Assessment of High-Heat-Flux Thermal Management Schemes," *IEEE Transactions on Components and Packaging Technologies,* vol. 24, pp. 122-141, 2001.

[22] T. Shedd, "Next Generation Spray Cooling: High Heat Flux Management in Compact Spaces," *Heat Transfer Engineering,* vol. 28, pp. 87-92, 2007.

[23] J. Bierchenk and D. Johnson, "Latest Developments in Thermoelectric Enhanced Heat Sinks," *Electronics Cooling,* vol. 11, pp. 24-32, 1005.

[24] C. Master, "Cooler Master," 2014. [Online]. Available: http://www.coolermaster.com/cooling/cpu-air-cooler/v10/. [Accessed 6 4 2014].

[25] S. Riffat and X. Ma, “Thermoelectrics: a review of present and potential applications,” Applied Thermal Engineering, 2003.

[26] S. Haidar, *Thermodynamics of a Peltier cell,* 2007.

[27] Z. Luo, “Electronics Cooling,” 1 August 2008. [Online]. Available: http://www.electronics-cooling.com/2008/08/a-simple-method-to-estimate-the-physical-characteristics-of-a-thermoelectric-cooler-from-vendor-datasheets/. [Accessed 1 April 2014].

[28] B. Huang, C. Chin and C. Duang, “A design method of thermoelectric cooler,” *International Journal of Refrigeration,* vol. 23, pp. 208-218, 2000.

[29] D. Rowe, CRC Handbook of Thermoelectrics, CRC Press, 1995.

[30] R. Palacios, A. Arenas, R. Pecharromán and F. Pagola, “Analytical procedure to obtain internal parameters from performance curves of commercial thermoelectric modules,” *Applied Thermal Engineering,* vol. 29, pp. 3501-3505, 2009.

[31] J. Pérez-Aparicio, R. Palma, Taylor and R.L., “Finite element analysis and material sensitivity of Peltier thermoelectric cells coolers,” *International Journal of Heat and Mass Transfer,* vol. 55, pp. 1363-1374, 2010.

[32] O. Yamashita, “Effect of linear and non-linear components in the temperature dependences of thermoelectric properties on the cooling performance,” *Applied Energy,* vol. 86, pp. 1746-1756, 2009.

[33] C.-H. Cheng, S.-Y. Huang and T.-C. Cheng, “A three-dimensional theorectical model for predicting transient behavior of thermoelectric coolers,” *International Journal of Heat and Mass Transfer,* vol. 53, pp. 2001-2011, 2010.

[34] M.-J. Huang, R.-H. Yen and A.-B. Wang, “The Influence of the Thomson effect on the performance of a thermoelectric cooler,” *International Journal of Heat and Mass Transfer,* vol. 48, pp. 413-418, 2005.

[35] M. Deng, S. Wen and S. Bi, “Operator based network nonlinear control for a Peltier actuated thermal process with time-varying delays,” in *International Conference on Advanced Mechatronic Systems*, Zhengzhou, 2011.

[36] M. Deng, A. Yanou, Y. Tokuda and A. Wang, “Robust Fault Tolerant Thermal Control System Design of an Aluminum Plate with Peltier Device,” in *International Conference on Advanced Mechatronic Systems*, Tokyo, 2012.

[37] S. Maruyama, A. Komiya, H. Takeda and S. Aiba, “Development of Precise-temperature-controlled Cooling Apparatus for Medical Application by Using Peltier Effect,” in *International Conference on BioMedical Engineering and Informatics, IEEE*, 2008.

[38] H. Morimitsu and S. Katsura, “A Method to Control a Peltier device based on the Heat disturbance observer,” *IEEE,* 2010.

[39] H. Morimitsu and S. Katsura, “Frequency response analysis of Observer-based Thermal control system of Peltier device,” *IEEE,* 2011.

[40] “ovenind,” [Online]. Available: http://www.ovenind.com/bv/Products/5R6-900-Ramp-and-Soak-Benchtop-Temperature-Controller__5R6-900.aspx. [Accessed 2014 02 02].

[41] S. Nukiyama, “The maximum and minimum values of the heat Q transmited from metal to boiling water under atmospheric pressure,” *International Journal Heat Mass Transfer,* vol. 9, pp. 1419-1433, 1966.

[42] T. Drew and A. Muller, “Boiling,” *Transactions of the AIChE,* vol. 33, pp. 449-471, 1937.

[43] J. Leidenfrost, A Tract about some Qualities of Common Water, Carolyn S.E. Wares, 1964.

[44] M. N. Ozisik, Heat Transfer: A Basic Approach, McGraw-Hill, 1985.

[45] M. Arik, *Enhancement of pool boiling critical heat flux in dielectric fluids, Ph.D. Dissertation,* Univ. Minnesota, Minneapolis, 2001.

[46] E. Teodori, *Study of Pool Boiling Mechanisms in the context of cooling applications, MSc Thesis,* Universitá Degli Studi di Roma, 2011.

[47] H. Zicheng, G. Jiaqiang, S. Xinnan and W. Qian, “Pool Boiling Heat Transfer of Aqueous Surfactant Solutions,” in *Fourth International Conference on Intelligent Computation Technology and Computation, IEEE*, 2011.

[48] E. Teodori, A. Moita and A. Moreira, “Characterization of pool boiling mechanisms onver micro-patterned surfaces using PIV,” *International Journal of Heat and Mass Transfer,* vol. 66, pp. 261-270, 2013.

[49] G. Gamrat, M. Favre-Marinet and D. Asendrych, “Conduction and entrance effects on laminar liquid flow and heat transfer in rectangular micro-channels,” *International Journal of Heat and Mass Transfer,* vol. 48, pp. 2943-2954, 2005.

[50] M. Panão and A. Moreira, “Intermittent Spray Cooling: a new technology for controlling surface temperature,” *International Journal of Heat and Fluid Flow,* 2008.

[51] T. Moita, *Evaluation and Development of Advanced Cooling Systems for Microelectronics, MSc Thesis,* Instituto Superior Técnico, Lisboa, 2008.

[52] T. J. Seebeck, “Magnetic Polarization of metals and minerals by temperature differences,” 1822.

[53] V. Setia, “www.britannica.com,” [Online]. Available: http://www.britannica.com/EBchecked/topic/532358/Seebeck-effect. [Accessed 4 2 2014].

[54] “Ferrotec,” [Online]. Available: https://www.ferrotec.com/Technology/Thermoelectric/Thermalref04. [Accessed 2 4 2014].

[55] R. Chein and G. Huang, “Thermoelectric Cooler application in electronic cooling,” *Applied Thermal Engineering,* vol. 24, pp. 2207-2217, 2004.

[56] “Tellurex,” [Online]. Available: http://www.tellurex.com/technology/peltier-faq.php. [Accessed 4 2 2014].

[57] K. Skadron, “A computer-architecture approach to thermal management in computer systems: opportunities and challenges,” in *Proceedings of the 5th International Conference on Thermal and Mechanical Simulation and Experiments in Microelectronics and Microsystems*, 2004.

[58] “Arduino.cc,” [Online]. Available: http://arduino.cc/en/Main/arduinoBoardDue. [Accessed 2014 02 25].

[59] E. Morgado, Controlo de Sistemas Dinâmicos: uma introdução, IST, 2005.

[60] jkhax0r, “Code Project,” 22 2 2007. [Online]. Available: http://www.codeproject.com/Articles/17723/CPU-Load-Control. [Accessed 10 2 2014].

[61] V. D. Das and N. Soundararajan, “Size and temperature effects on the thermoelectric power and electrical resistivity of bismuth telluride thin films,” *The American Physical Society,* vol. 37, 1988.

[62] H. Zhang, Y. Mui and M. Tarin, “Analysis of thermoelectric cooler performance for high power electronic packages,” *Applied Thermal Engineering,* vol. 30, pp. 561-568, 2010.

[63] M. Dirmyer, J. Martin, G. Nolas, A. Sen and J. Badding, “Thermal and electrical conductivity of size-tuned bismuth-telluride nanoparticles,” *Wiley interScience,* vol. 8, pp. 933-937, 2009.